Mechanical characterization of wood plastic composite sandwich panels with foam core

Mémoire

Azam Kavianiboroujeni

Maîtrise en génie chimique

Maître ès sciences (M. Sc.)

Québec, Canada

Résumé

Le but de ce travail est de produire et de caractériser des structures sandwich à trois couches asymétriques avec ou sans cœur moussé. Pour ce faire, le travail est divisé en deux sections. Dans la première partie, l'effet de la variation des quantités d'agent de couplage et de fibres sont étudiés. La microscopie et la caractérisation mécanique sont utilisées pour évaluer l'effet du polyéthylène greffé d'anhydride maléique (MAPE) sur l'amélioration de la compatibilité entre les fibres de chanvre et le polyéthylène de haute densité (HDPE). Les résultats montrent que les propriétés mécaniques optimales (tension, flexion, torsion et impact) sont obtenues à 9% en poids de MAPE.

Dans la deuxième partie, des structures sandwich asymétriques à trois couches, avec ou sans cœur moussé, sont produites par extrusion suivi par un moulage en compression. Les effets de paramètres tels que la densité du cœur, la concentration en chanvre dans les peaux, les épaisseurs des couches et la séquence d'empilage sur leurs comportements en flexion et en impact sont étudiés. Les effets combinés de tous les paramètres mènent à contrôler les propriétés mécaniques (traction, torsion, flexion et impact) des structures sandwich asymétriques.

Abstract

The aim of this work is to produce and characterize asymmetric three-layer sandwich structures with and without foam core. In order to do so, the work is divided in two sections. In the first part, the effect of coupling agent and fiber content is investigated. Micrographs and mechanical characterizations are used to show that the addition of maleic anhydride polyethylene (MAPE) improved the compatibility between hemp and high density polyethylene (HDPE). It is found that the optimum mechanical properties (tension, flexion, torsion and impact) are obtained with 9% wt. of MAPE in the composite.

In the second part, asymmetric three-layer sandwich structures with and without foam core were produced using extrusion followed by compression molding. The effect of different parameters such as core density, skin hemp content, layer thickness, and stacking sequence on their flexural and impact behaviors are studied. The combined effect of all the parameters was found to control the mechanical properties (tension, torsion, flexion and impact) of asymmetric sandwich structures.

Table of content

List of tables

List of figures

Nomenclature

Abbreviations

ACA	Azodicarbonamide
APS	γ-aminopropyltriethoxysilane
CA	Coupling agent
CBA	Chemical blowing agent
CFC	Chlorofluorocarbon
EPR	Ethylene propylene rubber
ESCA	Electron spectroscopy for chemical analyses
FRC	Fiber-reinforced composites
FTIR	Fourier transform infrared spectroscopy
GFRP	Glass fiber-reinforced polymer
HDPE	High density polyethylene
HFC	Hydrofluorocarbon
HFRUPE	Hemp fiber reinforced unsaturated polyester composite
IFSS	Interfacial shear strength
LLDPE	Linear low density polyethylene
MA	Maleic anhydride
MA-g-SEBS	Maleated styrene-ethylene/butylene-styrene
MAH-SEBS	Maleic acid anhydride grafted styrene-ethylene/butylene-styrene block copolymer
MAPE	Maleic anhydride polyethylene
MAPP	Maleic anhydride polypropylene
MRPS	γ-mercaptopropyltrimethoxysilane
OPE	Oxidized polyethylene
PAS	Polyamides
PBA	Physical blowing agent
PMPPIC	Polymethylene polyphenyl isocyanate
PP	Polypropylene
PPE	Pure polyethylene
PS	Polystyrene
PU	Polyurethane
PVC	Polyvinyl chloride
SEM	Scanning electron microscope
SMA	Styrene-maleic anhydride
TGA	Thermal gravimetric analysis
WAXS	Wide-angle X-ray spectrometry
WPC	Wood polymer composite

Symbols

A	Hemp content in the skin (% wt.)
A	Foam area (cm^3)
B	Hemp content in the skin (% wt.)
b	Width (mm)
d	Depth (mm)
d	Impactor diameter (mm)
E	Flexural modulus (GPa)
E_T	Tensile modulus (MPa)
E_{tm}	Torsion modulus (MPa)
I_s	Charpy impact strength (J/m)
L	Support span (mm)
L_c	Core thickness (mm)
L_L	Lower skin thickness (mm)
L_U	Upper skin thickness (mm)
L/D	Length/Diameter
m	Slope in the initial linear part of the load-deflection curve (N/mm)
N_F	Cell density (number of cells/cm^3)
n	Number of cells
S	Maximum load supported by the beam (N)
S	Total area diffusing the impact energy in the sandwich structures with foam core (mm^2)
S'	Total area diffusing the impact energy in the sandwich structures without foam core (mm^2)
X	ACA content in core (% wt.)
y	Skin thickness (mm)
z	Skin thickness (mm)
σ_{max}	Flexural strength (MPa)
σ_t	Tensile strength (MPa)
ε_{max}	Strain at maximum stress (%)
ε_t	Elongation at break (%)

Very little grows on jagged rock.

Be ground.

Be crumbled,

so wildflowers will come up where you are.

"Rumi"

Acknowledgements

First and foremost, I wish to express my gratitude to my supervisor, Professor Denis Rodrigue. He was a great source of support and guidance during my research at Laval University. I will always be grateful for his help.

I would like to sincerely thank my co-supervisor, Professor Alain Cloutier, for his helps, supportive direction and scientific insight.

I would like to especially express my gratitude to my family for their never ending love, affection and inspiration. Without their kindness and support, I would not have made it this far.

I am thankful to all my office collaborators and technician Mr. Yann Giroux for their help and suggestions. My work would never be completed without their kind collaboration.

Finally, I acknowledge the support of the Natural Sciences and Engineering Research Council of Canada (NSERC), as well as Centre de Recherche sur les Matériaux Renouvelables (CRMR), Centre de Recherche sur les Matériaux Avancés (CERMA) and Centre Québécois sur les Matériaux Fonctionnels (CQMF) for technical and financial help.

Foreword

This master thesis consists of five chapters, including two articles. The first chapter includes a brief introduction on fibers, wood polymer composites (WPC), foams, sandwich structures and a literature review on multi-layer sandwich structures.

In the second chapter, different treatment, especially the use of coupling agents, in natural fiber composites are discussed. In addition, the effect of coupling agent (MAPE) concentration (0 to 11% wt.) and fiber content (0-40% wt.) on the morphological and mechanical properties (tensile, flexural, impact and torsion) of the composites are discussed. This chapter describes how the optimal MAPE concentration is found. I performed all experiments including sample preparation, mechanical tests and reported the results under the guidance of my supervisors. After completion with rheological experiments (future work), this chapter will be submitted as a paper:

> Azam Kavianiboroujeni, Alain Cloutier, Denis Rodrigue, *The effect of fibre and coupling agent content on the mechanical properties of hemp/polyethylene composites.*

Chapter 3 discusses the influence of different design parameters such as blowing agent content (0, 0.6 and 1.2% wt.), skin thickness (1 and 2 mm) and skins hemp content (10-40% wt.) on the flexural properties of multi-layer sandwich structures consisting high density polyethylene (HDPE) and hemp fibers. Moreover, the fabrication method of sandwich structures using compression molding is presented. I performed all experiments including sample preparation, mechanical tests and reported the results under the guidance of my supervisors. This article was accepted as:

> Azam Kavianiboroujeni, Alain Cloutier, Denis Rodrigue, *Mechanical characterization of asymmetric HDPE/hemp composite sandwich panels with and*

without a foam core, Journal of Sandwich Structures and Materials, accepted, July 2015, DOI: 10.1177/1099636215597667.

Chapter 4 investigates the influence of different design parameters such as blowing agent content (0, 0.6 and 1.2% wt.), skin thickness (1 and 2 mm) and skins hemp content (10-40% wt.) on the impact behavior of multi-layer sandwich structures made of HDPE and hemp with and without foam core. I performed all experiments including sample preparation, mechanical tests and reported the results under the guidance of my supervisors. Low-velocity falling weight and Charpy impact tests are performed in this chapter. This article was submitted as:

Azam Kavianiboroujeni, Alain Cloutier, Denis Rodrigue, *Low velocity impact behavior of asymmetric three-layer sandwich composite structures with and without foam core,* Submitted in Applied Polymer Composites Journal, October 2015.

The last chapter includes a general conclusion on the work performed and recommendations for future works.

Chapter 1

1.1. Introduction

More than 75 years ago, natural fibers were the main sources of materials for technical commodities and products such as paper, rope, canvas and textiles [1]. But, at the beginning of last century polymers were developed, produced and consumed in large quantities. Therefore, the natural fibers were substituted by polymers due to good technical performance and low prices of polymers and plastics. After several years, new concerns such as sustainable development of recyclable, renewable and biodegradable materials and reduction of human activities footprint on the environment shifted the attention to natural materials. Therefore, a new class of composites where the basic components are a fibrous material as filler and a polymer as binder have been developed [2]. The polymers provide good moldability, resistance to chemicals and corrosion, insulation and integrity [3]. On the other hand, fibrous materials such as cellulose, carbon, fiber and wood give mechanical reinforcement.

New progress in science and technology have introduced new demands for new materials, composites and structures with improved properties. Advanced fiber composites with very high strength and stiffness and multi-layer sandwich structures are two groups of advanced materials. In the following section, the properties, advantages and disadvantages are discussed in details.

1.2. Wood polymer composites

Wood polymer composites (WPC) are composite materials that contain a polymer (virgin or recycled) and wood flour or natural fiber. They are used mainly in outdoor deck floors, railing, fences, window or door frames, furniture, and landscaping timbers. These composites require less maintenance compare to metals or treated solid wood. The benefits of polymer composites over metals are presented in Table 1.1.

An important step in WPC processing is choosing the polymer matrix since there are a wide range of them and as the binder, they have an important role determining the mechanical and physical properties of the composite.

Table 1.1. Advantages of polymer composites over metals [4].

Better corrosion resistance
High specific strength and stiffness, Low thermal coefficient of expansion
Better fatigue resistance, Potentially lower component costs
Lower fabrication costs, Lower quality assurance costs
Minimal plies, Fewer joints
Increased impact resistance, Increased fracture toughness

The polymer matrix can be either a thermoset or a thermoplastic. Epoxy, polystyrene (PS), polyurethane (PU) and phenolic are most commonly used thermoset resins. Although their composites have better mechanical performance, particularly higher stiffness and strength but the increasing demand for recyclable materials encourages the substitution of thermoset by thermoplastics. A list of advantages and disadvantages of these polymers are presented in Table 1.2.

Table 1.2. Advantages and disadvantages of thermoset and thermoplastic matrix [4].

Property	**Thermosets**	**Thermoplastics**
Formulations	Complex	Simple
Melt viscosity	Very low	High
Fiber impregnation	Easy	Difficult
Processing cycle	Long	Short to long
Processing temperature/ Pressure	Low to moderate high	High
Fabrication cost	High	Low
Solvent resistance	Excellent	Poor to good
Damage tolerance	Poor to excellent	Fair to good
Prepreg stability	Poor	Excellent

These composites are accessible at low prices since different types of low cost fibers, agro-wastes or byproducts are available everywhere. The use of fiber in WPC industry has improved constantly. For an example, about 525000 tons of filler was consumed in the USA in 1967 which increased to 1.9 million tons in 1998 and 3.8 million tons in 2010 [5]. It is estimated that about 8% was bio-based fibers' share.

Table 1.3 clearly shows the growing trend of the WPC industry over the last five years. China has the highest production growth rate with 25%, while it has the second largest WPC industry after North America. Almost 50% of the global WPC market is produced by North America which is the leader in natural fiber composites consumption where the main applications are in building and construction sections, followed by Asia. The automotive industry is the biggest consumer of WPC in Europe.

Table 1.3. WPC Market development (http://news.bio-based.eu/, Key words: WPC, production, trend).

Region	2010 (Ton)	2015 (Ton)	Growth (%)	Global share in 2015 (%)
North America	900000	1300000	8	48
China	300000	900000	25	33
Europe	150000	250000	11	9
Japan	60000	120000	15	4
Russia	10000	70000	48	3
South East Asia	30000	55000	13	2
South America	10000	50000	38	2
India	5000	40000	52	1
Total	**1450000**	**2695000**	**13**	**103**

According to Eckert [5], the main markets for WPC, on a weight basis, can be summarized as: building products (70%), marine uses and infrastructure (13%), industrial consumer (10%), and automotive (7%).

The filler part in WPC is mainly derived from wood, but other natural fibers such as flax, wheat straw, hemp, cotton, sisal, bamboo, and kenaf are being commercially used in combination with polymers such as polypropylene (PP) in automotive industry [6].

Composites based on natural fiber have been welcomed in both developing countries to consume a local material resource and in developed countries to decrease the influence of human activities on nature by developing new materials. One of the main reasons why they are significantly used is that most of the polymers are not suitable for load-bearing applications due to low stiffness and strength, but natural fibers offer high stiffness and strength, good thermal properties and acoustic insulation. Besides, they are non-abrasive to mixing and processing equipment and they are cost effective because of high filling levels [7].

The inclusion of natural fibers in composites leads to weight reduction which is an important factor in transportation. Another advantage of natural fibers is that at the end of their life cycle, the amount of released CO_2 through combustion or decomposition equals to amount of CO_2 absorbed during their growth [1].

The reinforcement of polymers with natural fibers allows the combination of performance and cost to replace synthetic or mineral fibers conventionally used as filler [8]. Increasing concerns about the limited fossil energy resources and strict regulations to limit the emission of green gases besides the increasing demands for low weight and cost effective products have resulted in increasing consumption of natural fiber polymer composites in automotive and construction industries globally.

The natural fiber composites can be used for the following applications [9]:

- Building and construction industry: partitioning and ceiling, flooring, window and door frames, roof tiles.

- Storage devices: boxes, storage silos, containers.

- Furniture: chair, table, shower, patio deck.

- Electric devices: electrical appliances, pipes, etc.

- Everyday applications: lampshades, suitcases, helmets, etc.

- Transportation: automobile, plain and railway coach interior, boat, etc.

- Toys.

In Table 1.4, the WPC market in different industries is compared to the market of structural materials such as steel and aluminum. The marine industry widely uses WPC in a way that its share is about 68%. Although the WPC market in construction values more than other industries, it has just 4% of the market which is very low. Besides the advantages mentioned above, natural fiber composites also have some disadvantages which will be discussed in the following sections.

Table 1.4. WPC market production (www.Lucintel.com).

Market	WPC market (Billion $)	Structural material market (Billion $)	WPC share (%)
Transportation	2.7	75.7	3.6
Marine	0.5	0.7	68
Aerospace	2.0	19.1	10
Pipe & Tank	2.1	29.6	7
Construction	3.1	78	4
Wind Energy	2.0	5.4	38
Consumer Goods	1.1	7.7	14

1.3. Natural fibers

Since 3000 years ago, humankind has used cellulose which is considered as the most dynamic material in nature, to make the life better [2]. Over the last decades, cellulosic fibers have

been applied in load-bearing composites and their applications have grown due to their low cost, high specific strength and stiffness and low density compared to synthetic fibers such as glass and aramid. They act as reinforcement by supporting the stresses transferred from the weaker resin matrix. For good composites, the elongation of the fiber must be lower and its stiffness higher than the matrix. Besides fiber type, its dimension has an important role in maximizing stress transfer. Fibers with higher surface area per unit fiber weight improve significantly the stress transfer.

A list of the mechanical properties of the most popular reinforcing fibers is presented in Table 1.5.

Table 1.5. Mechanical properties of natural fibers compared to conventional composite reinforcing fibers [1].

Fiber	Density (g/cm^3)	Elongation @ break (%)	Tensile strength (MPa)	Young's modulus (GPa)
Cotton	1.5-1.6	7.0-8.0	287-597	5.5-12.6
Jute	1.3	1.5-1.8	393-773	26.5
Flax	1.5	2.7-3.2	345-1035	27.6
Hemp	1.2	1.6	690	88.0-90.0
Sisal	1.5	2.0-2.5	400-938	61.4-128
E-glass	2.5	2.5	2000-3500	70.0
S-glass	2.5	2.8	4570	86.0
Aramid	1.4	3.3-3.7	3000-3150	63.0-67.0

Natural fibers based on their origins and their sources can be categorized into: plants, animals or minerals fibers [10]. Natural fibers with plant origin are subdivided into different groups. A classification of the various non-wood natural fibers is presented in Figure 1.1.

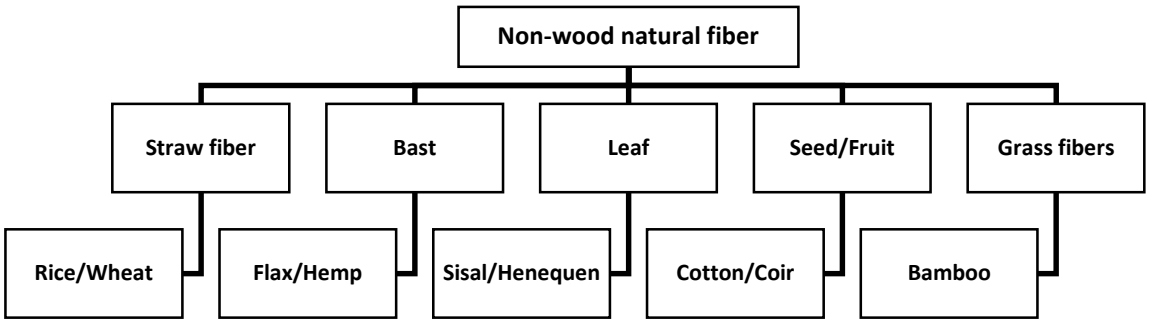

Figure 1.1. Classification of non-wood natural fibers [6].

The essential component of all fibers is cellulose. It is a linear condensation polymer consisting of D-anhydroglucopyranose units linked together by β1-4-glycosidic as shown in Figure 1.2. The intra-molecular hydrogen bonding is the essential cause of high stiffness and rigidity of cellulose and its tendency to crystallization [2].

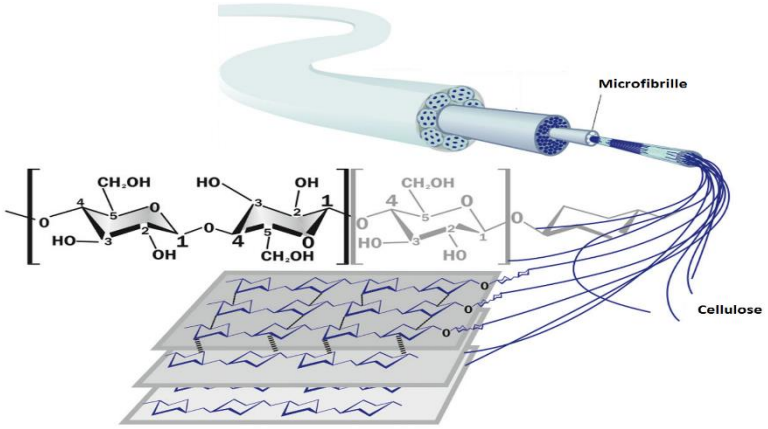

Figure 1.2. Structure of cellulose [11].

The linear structure of cellulose enhances its capability to form strong inter and intra-molecular bonds [14].

Fibers have a complex multi-layer structure consisting of the primary wall around a secondary wall as shown in Figure 1.3. The secondary layer has three distinct layers (S_1, S_2

and S_3). These layers consist of cellulose, hemicellulose and lignins in varying amounts to form of microfibrils. The S_2 layer is usually the thickest layer and determines the mechanical properties of the fibers.

Hemicelluloses are also found in all plant fibers and have a structural role in fiber walls. They are present in all layers of the cell wall, However, they can mainly be found in the primary and secondary layers in association with cellulose and lignins [12]. They are associated with cellulose microfibrils by hydrogen bonding, embedding the cellulose in a matrix and function as a cementing matrix in the microfibrils making a network of cellulose-hemicellulose. Hemicellulose are polysaccharides, bonded together by relatively short branching chains with a degree of polymerization of about 50-200 [13].

Hemicelluloses have a hydrophilic characteristic and have lower molecular mass compared to cellulose. Hemicellulose are biopolymers made of several monomers like mannose, arabinose, xylose, galactose and even glucose [14].

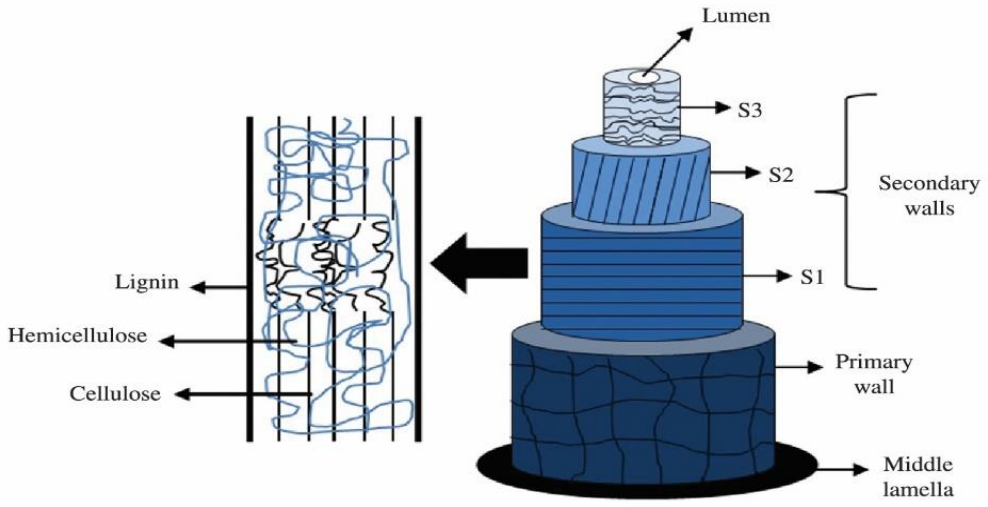

Figure 1.3. Schematic representation of plant fiber structure: S1-external secondary wall, S2-middle secondary wall and S3-internal secondary wall [15].

Two main types of hemicelluloses are xylans and glucomannans. The strength and hardness of the wood fibers are intrinsically linked with the amount and extent of monomers in the

polymers. However, the constituents of hemicellulose vary from one plant to another. About 20-30% (dry weight) of wood consists of hemicelluloses.

Lignin is another main component of natural fibers. It is a complex polymer, based on three monolignols: (a) p-coumaryl alcohol, (b) coniferyl alcohol and (c) sinapyl alcohol. It is a heterogeneous 3-D polymer, randomly branched polyphenol in an amorphous structure. About 30% (dry weight) of wood is made of lignin [14]. Cell wall rigidity is due to the presence of lignin. It is responsible for the impact and compression resistance of the structures. Moreover, it limits water penetration into wood products.

Pectin, waxes, water and water soluble substances are other fiber components. The hydrophobic lignin and pectin components act as coupling agents and improve the stiffness of the cellulose/hemicellulose part [14].

The proportion of cellulose, hemicellulose and lignin as the main constituents of natural fibers are dependent on age, fiber source and extraction conditions used to obtain the fibers [15]. Table 1.6 summarizes the average values of some vegetal fiber properties, including their chemical constituents.

Table 1.6. Chemical constituents for some vegetal fibers [1].

Fiber	Cellulose (% wt.)	Hemicellulose (% wt.)	Lignin (% wt.)	Ashes (% wt.)
Jute	60	22.1	15.9	1.0
Ramie	80-85	3-4	0.5	-
Kenaf	72	20.3	9	4.0
Flax	71	18.6-20.6	2.2	-
Hemp	72	10	3	2.3
Sisal	74-75	10-13.9	7.6-7.9	0.4

The mechanical properties of cellulosic fibers are influenced by cellulose degree of polymerization, type of cellulose, crystal structure and defects, degree of crystallinity, chain orientation, voids structure, interface and sizes [16].

1.3.1. Natural fiber limitations

WPC have attracted increasing interests due to their interesting mechanical and physical properties with their sustainable characters. However, it is important to have a perfect understanding of their limitations when developing end use applications in the automotive, building, appliance and other industries.

Some drawbacks such as low elongation, high fragility, low impact strength and high density (compare to polymers), their tendency to form aggregates, low thermal stability, low resistance to moisture and low compatibility between the fibers and the polymers limit their application as filler and reinforcing components [14]. The most important challenge is that the final mechanical and physical properties of the composites depend on the quality of the fiber-matrix interface which influences the stress transfer from the matrix to the fiber [17]. High mechanical properties of the composites are dependent on a strong fiber-matrix interface bond. But poor compatibility between the fibers and the polymers origins from high concentration of hydroxyl groups in cellulose and hemicellulose which gives the fibers hydrophilic and polar characteristics increasing the moisture capacity of the fibers [18], while most polymers are non-polar and hydrophobic. However, this drawback can be overcome by fiber treatment.

Another disadvantage of natural fibers is their high moisture absorption [7]. Fiber swelling is a direct consequence of moisture absorption. This problem cannot be ignored because it leads to dimensional instability, propagation of micro-cracks through the composites and degradation of mechanical properties. The complete elimination of moisture absorption is difficult but it can be minimized by encapsulation of the fibers by the matrix. The modification of the hydroxyl groups on the fiber via physical and chemical methods reduces moisture absorption. Moreover, methods improving the fiber-matrix bonding by using coupling agents reduce the rate and amount of absorbed moisture.

Dhakal et al. [19] studied the effect of high water absorption on the mechanical properties of a hemp fiber reinforced unsaturated polyester composites (HFRUPE). They showed that

increasing moisture uptake decreased the tensile and flexural properties of HFRUPE composites due to degradation of the interface. They reported that the tensile modulus of specimens with 3, 4 and 5 layers of hemp compared to dry specimens decreased by 61, 97, and 87%, respectively.

Figure 1.4 clearly shows that when a composite is exposed to water, the fibers started to swell leading to crack propagation through a thermoset resin. As more water penetrated through the micro-cracks and the fibers continued swelling, the composites failed due to swelling stresses.

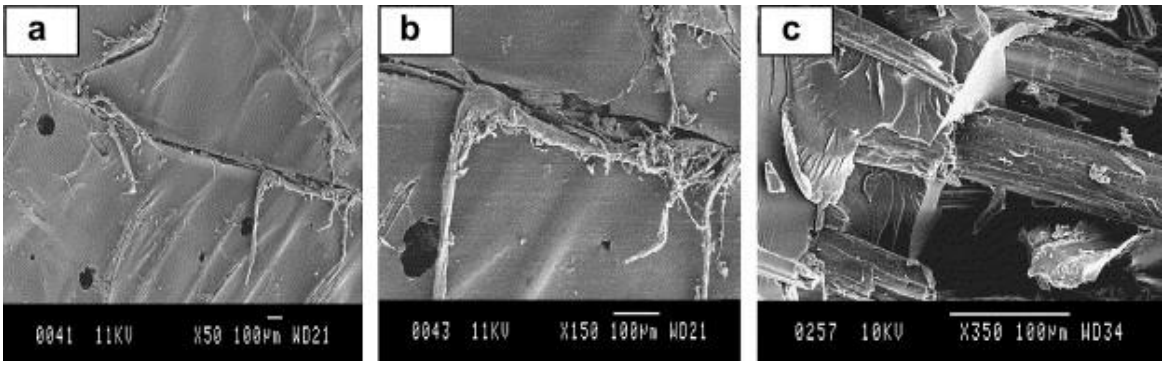

Figure 1.4. SEM micrographs of the failure steps: (a) matrix cracking, (b) fracture running along the interface, and (c) fiber-matrix debonding due to the presence of water molecules [19].

In another study, the effect of water absorption on dimensional stability and impact energy of jute fiber reinforced polypropylene was investigated [20]. The results showed that water absorption capacity and swelling increased linearly with fiber content. It was shown that the inclusion of a coupling agent reduced the effect of water absorption on swelling. On the other hand, it was shown that in specimens without coupling agent the water molecules resided in three regions: the lumen, the gap between the fibers and the matrix (Figure 1.5 (A)) and the cell wall, while in specimens with coupling agent water did not accessed the gap between the fibers and the matrix due to good interfacial adhesion (Figure 1.5 (B)) [20].

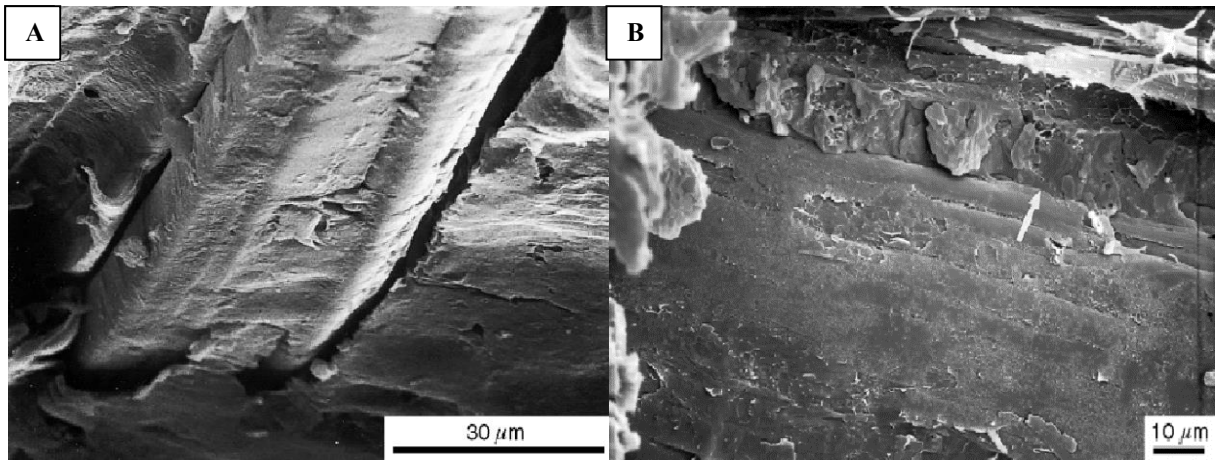

Figure 1.5. SEM micrographs of the fractured surface of a jute/polypropylene composite. A: without coupling agent, and B: with coupling agent [20].

However, the presence of a large amount of hydroxyl groups (-OH) on the surface of natural fibers has the advantage of being easily functionalized with chemical groups. This is why several teams worked on improving the fiber-matrix adhesion via different methods to change the polar/hydrophilic nature of natural fibers.

1.4. Surface modification methods

It is well known that the final mechanical and physical properties of composites are dependent on the properties of each constituent and the quality of interfacial adhesion [6]. In a composite, the fibers are the load bearing components and the polymer "simply" transfers the load to the fibers through interfacial bonding [21]. So, fiber-matrix interface plays an important role for load transfer. There is also an interphase which is a region between the bulk fibers and the matrix having different layers as shown in Figure 1.6.

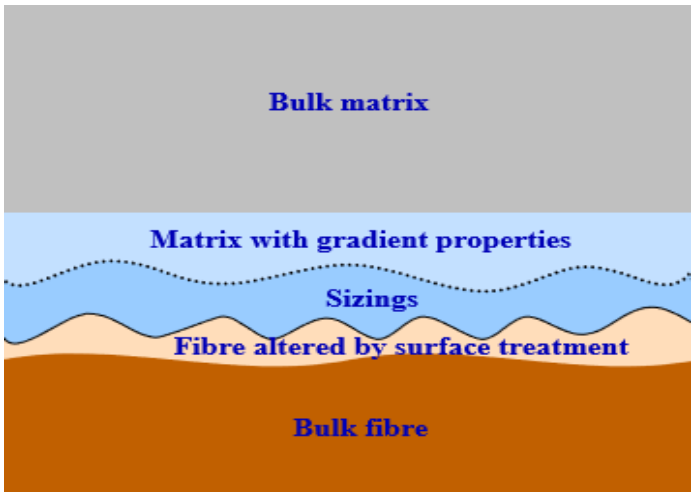

Figure 1.6. Schematic representation of a fiber-matrix interphase [21].

The nature of the interphase is dependent on the composite and it influences the mechanical performances of the composite [22]. Soft interphase leads to a composite with low stiffness and strength and high resistance to fracture, while stiff interphase results in stiff composite with low fracture resistance. Therefore, different modification methods have been developed to improve the quality of the fiber-matrix interface and increase compatibility between them.

1.4.1. Physical methods

Lignocellulosic fibers can be treated by physical methods. In this case, the structural and surface properties of the fibers are changed in a way that the mechanical bonding between the fibers and the matrix improves. In this method the chemical composition of the fiber is not changed [1]. Stretching, calendaring, thermo-treatment and yarn production are the most widely used physical treatment for fibers. Electric corona, cold plasma discharge, electron beam irradiation are other forms of physical treatments. These methods are known to be easy and versatile for surface activation of the fibers.

The most recently developed physical methods are plasma and corona treatments. In a plasma, an ionized gas containing ions, electrons and photons is used to modify the fiber

surface. In this method, different surface modifications such as changes in the surface energy, grafting of reactive free groups and surface cross-linking are possible depending on the gases used. Plasma treatment takes the fiber surface impurities away and increases the porosity of the fiber which improves the mechanical interlocking between the fibers and the polymer.

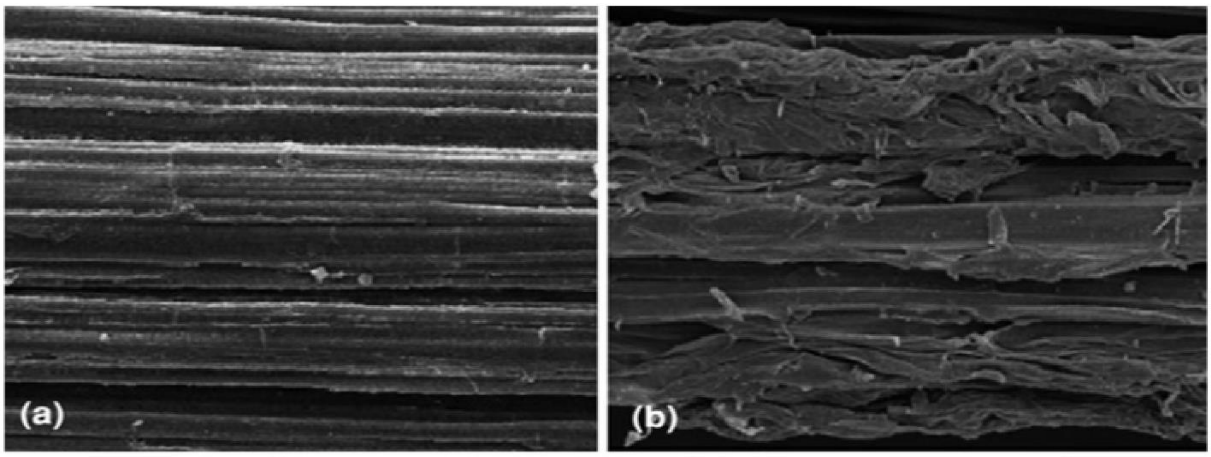

Figure 1.7. Surface morphology of a wood fiber: a) before and b) after plasma treatment [14].

Figure 1.7 shows the morphology of plasma treated wood fibers. Untreated wood fiber as shown in Figure 1.7(a) has a smooth surface which is the primary walls of wood fibers. Figure 1.7(b) shows a very rough surface consisting of large amounts of defects and cracks, pits, as well as corrugations after plasma treatment.

1.4.2. Chemical methods

The chemical treatment of fibers is aimed at improving the interfacial adhesion between the fibers and the matrix to improve the mechanical performance of composites and decrease their water absorption due to hydroxyl groups [23]. In these methods, the properties of the fiber surface, fiber strength, impurities content and fiber-matrix interaction are modified [24].

Chemical methods can be designed to eliminate weak boundary layers, produce a tough and flexible layer, or develop a cross-linked boundary layer between the fibers and the polymer.

They can also improve fiber wettability by the polymer or form covalent bonds between the polymer and the fibers. All the reactions take place based on the reaction of –OH with molecules with one or several active groups which are able of reacting with hydroxyl groups at the fiber surface to form a hydrophobic grafting on the surface.

Chemical treatments include alkali, silane, acetylation, and isocyanates. The most used, cost effective and common chemical treatment of natural fibers is alkaline treatment with sodium hydroxide (NaOH) [25]. In this method, an alkaline solution is used to treat the fibers and remove the majority of impurities such as hemicellulose, lignin, waxes and oils covering the fiber cell wall, making the interfibrillar region less dense and less rigid thereby increasing crystallinity. These changes improve surface tension, wettability, adhesion and compatibility of the fibers with the polymer. The reaction of NaOH with cellulose present in wood is shown as:

$$\text{Cell} - \text{OH} + \text{NaOH} \rightarrow \text{Cell} - \text{O} - \text{Na} + \text{H}_2\text{O} + \text{surface impurities} \qquad (1\text{-}1)$$

In this method, the surface of the treated fibers is more rough which improves the mechanical interlocking between the polymer and the fibers. The effectiveness of alkalization depends on the type of alkaline solution, treatment procedure and fibers. Several scientists reported improved mechanical properties after fiber treatment with NaOH. Prasad et al. [26] studied the alkali treatment of coir fiber by 5% NaOH for 72-96 hours at 28°C. The improvement of the tensile strength and Young's modulus of the fibers by 10-15% and 40%, respectively, were observed. The alkali treatment of the coir fiber increased the flexural strength of polyester resin composites by 40%. In another study, Mwaikambo and Ansell reported that the optimum NaOH concentration of a solution to treat kenaf and hemp was 6% [13]. Gassan and Bledzki reported that treating the fiber surface by 26% wt. NaOH for 20 minutes at 20°C improved the mechanical properties of unidirectional jute/epoxy composite up to 60% compared to untreated fiber composite, at a fiber content of 40% vol. [1].

In another study, the effects of chemical surface treatment with alkali and silane solutions on the fiber surface morphology and mechanical properties of hemp/PP composites were

investigated [27]. The results showed that the tensile and flexural strengths of the composites were not significantly affected by silane treatment, but alkali treatment of hemp with NaOH solutions improved the tensile and flexural strengths of the composite. Moreover, the 4% wt. NaOH treated fiber composite had maximum tensile and flexural strength values because this composite demonstrated the best interfacial bonding. The results were confirmed with a morphological study as some SEM observations are shown in Figure 1.8.

For composites based on thermoset matrices such as epoxy, polyester, phenol formaldehyde, etc., alkali treatment of natural fibers is one of the most common treatment methods [10].

Etherification is another common chemical treatment methods. Baiardo et al. [28] etherified flax fibers with ethyl iodide with the aim to decrease the natural hydrophilic character of cellulose. The results of Fourier transform infrared spectroscopy (FTIR) and wide-angle X-ray spectrometry (WAXS) verified that the chemically modified fibers were more thermally stable under composite processing conditions and the etherification treatment did not impair the thermal stability of flax.

In another study, trichloro-s-triazine was used to treat cellulose fibers in the form of paper sheets [29]. High-resolution electron spectroscopy for chemical analyses (ESCA) spectra was used to study the chemical characterization of the paper surface. The results verified that the treated surface contained some hydrocarbon-rich materials which meant that the surface properties were changed from hydrophilic to hydrophobic. Measuring the contact angle of the treated paper showed that it was increased from 0 to more than 120 degrees due to the treatment.

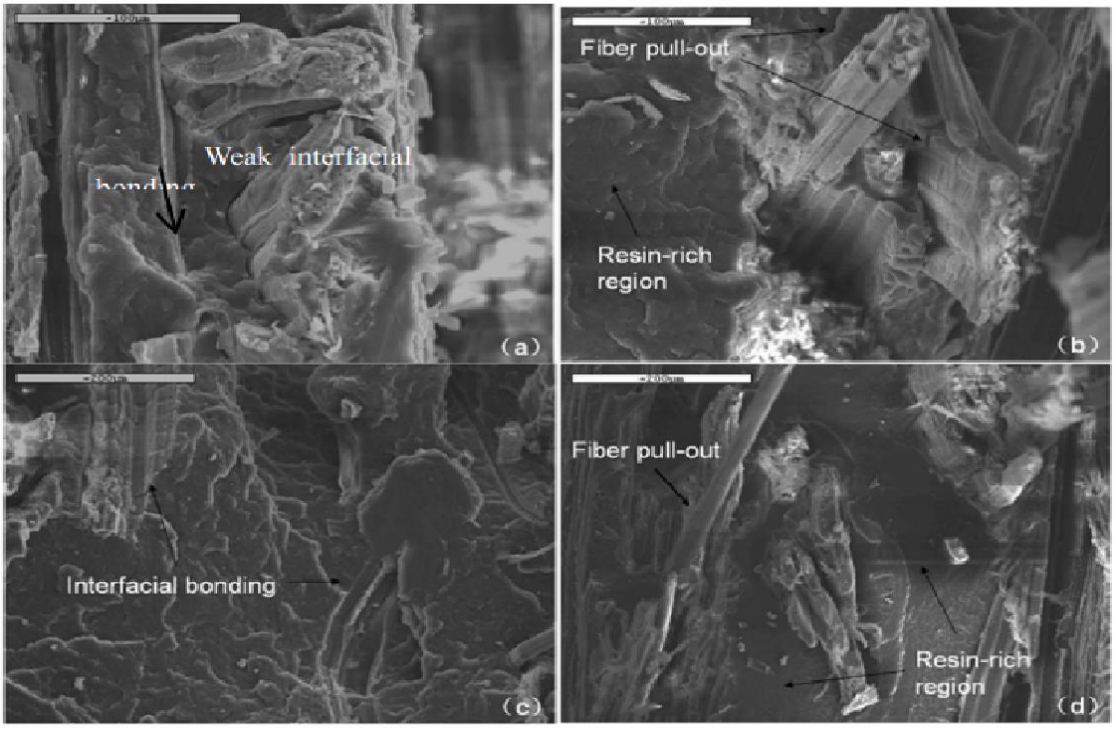

Figure 1.8. SEM observation of tensile fracture surfaces of the (a) untreated fiber composites, (b) 2% NaOH-treated fiber composites, (c) 4% NaOH-treated fiber composites, (d) 6% NaOH-treated hemp/PP composite [27].

The reduction of moisture capacity of the treated fibers with etherification can be explained by the reduction of the number of available –OH groups in cellulose, reduction of fiber surface polarity, and reduction in fiber swelling due to a cross-linked network between the matrix and the fibers based on covalent bonding [30].

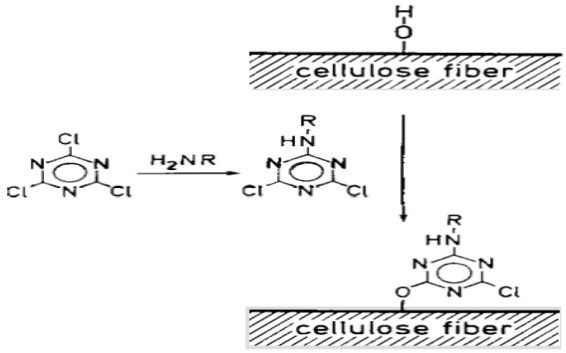

Figure 1.9. Reaction path of cellulosic fibers treated with trichloro-s-triazine [29].

In other chemical methods, acetic anhydride, alkyl ketene dimer, alkenyl succinic anhydride, and different fatty acids or their chlorides are commonly used for acetylation. As shown in Figure 1.10, acetylation of the C-OH decreases hydrogen bonding and fiber polarity while increasing the compatibility between the polymer and the fibers. The hydroxyl groups are replaced with acetyl groups in the fiber chemical modification with acetic anhydride. Therefore, the interlaminar adhesion properties are modified and improved due to less hydroxyl groups available.

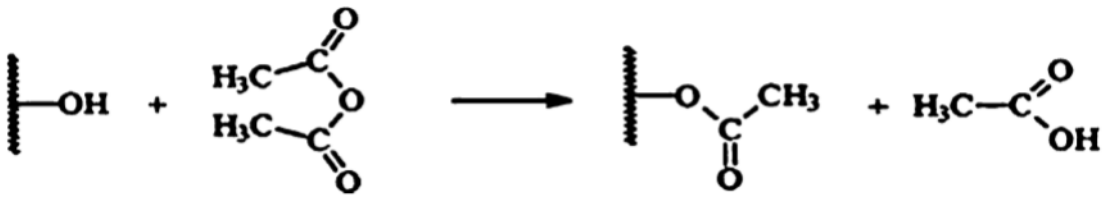

Figure 1.10. Esterification of fiber -OH groups with an acid donor [14].

The influence of acetylation on the thermal degradation of a blend of sisal with PP, HDPE and EPR was investigated [31]. The thermal stability of the composite with treated fibers was improved due to acetylation. The samples were characterized thermally through TGA to measure the activation energy. The results showed that the starting decomposition temperature remained constant for all samples. Moreover, it was reported that the stability of

acetylated fiber composites was improved due to substitution of hydroxyl groups by larger functional groups as shown in Figure 1.11. The alkali treatment restricted the segmental mobility and improved the main cellulose chain rigidity.

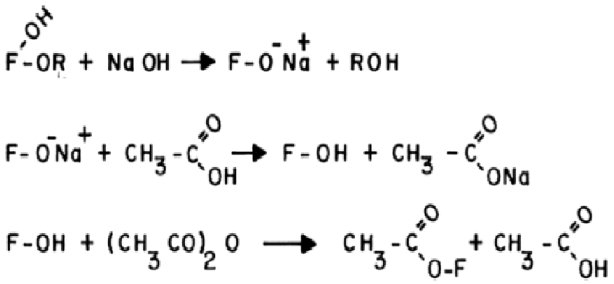

Figure 1.11. Chemical modification sisal fiber due to acetylation [31].

The properties of fiber composites based on polystyrene (PS) or polyvinyl chloride (PVC) can be enhanced by an isocyanate treatment [32]. It was reported that the extent of mechanical properties enhancement was a function of fiber weight content and isocyanate concentration. As shown in Figure 1.12, polymethylene polyphenyl isocyanate (PMPPIC) reacted with cellulose through covalent bonding, following by a strong interaction of delocalized π-electrons of the benzene rings. In this case, PMPPIC acted as a bridge at the interface between the fibers and PS providing a strong interfacial adhesion between them.

It has been shown that silanes are effective coupling agents for cellulosic fibers because of three advantages: a) they are commercially produced at large scale, b) they are able to react with OH-rich surface, and c) they can be tailored in a way to function effectively with the selected matrix for better reinforcement [33].

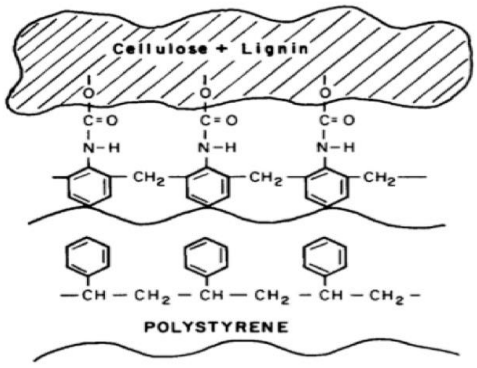

Figure 1.12. Hypothetical chemical structure of cellulose-PMPPIC polystyrene at the interfacial area [32].

Different researchers investigated the mechanisms and influences of silane treatment on the mechanical properties of different composites. Abdelmouleh et al. [34] reported that fiber treatment with silane coupling agents, which were able to react with epoxy and unsaturated polyester resins as shown in Figure 1.13, significantly improving the mechanical performance of the final composites of bleached soda pulp/PU and bleached soda pulp/epoxy which was attributed to covalent bond continuity at the fiber-matrix interface thereby enhancing stress transfer between them due to silane treatment.

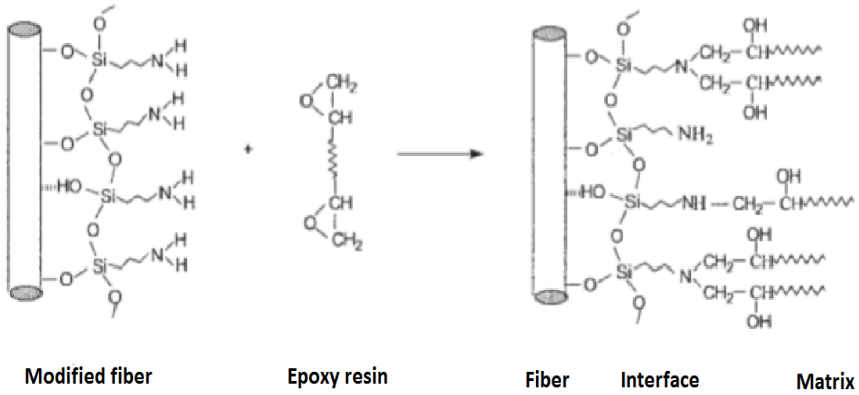

Figure 1.13. Schematic illustration of the interfacial zone of epoxy matrix in contact with silane-modified fibers [34].

For epoxy-based composites at 20°C, E' increased from 2.55 GPa, for composites with untreated fibers, to 2.93 and 3.2 GPa respectively, for composites made with γ-

mercaptopropyltrimethoxysilane (MRPS) and γ-aminopropyltriethoxysilane (APS) treated fibers. The moisture absorption of the composites was studied and showed that the silane treatment was not significant in reducing water uptake. The PS composites containing untreated fibers absorbed 8% of water, whereas the composites based on MRPS-treated fiber absorbed 6%. The same trend was reported for epoxy-based composites.

Gonzalez et al. [35] evaluated the deposition mechanism of a silane coupling agent on henequén fiber surface and the influence of the chemical treatment on the composite surface and mechanical properties. The chemical reactions between the fibers and silane was confirmed by FTIR. Moreover, it was reported that the tensile strength of a 80:20 v/v HDPE/henequén composite increased from 21 MPa for a untreated fiber to 27 MPa for a treated one.

1.4.3. Compatibilizing agents

Another method of increasing the interaction between the fibers and the polymer in a composite is by using compatibilizing agents. Compatibilizers can be defined as substances that are used in small quantities to treat a surface so that bonding occurs with other surfaces. Coupling agents are able to act as compatibilizers for hydrophilic fibers and hydrophobic polymer matrices. They can also improve the fiber dispersion in polymer matrices. They mainly reduce the interfacial energy at the fiber-matrix interface, thereby reducing fiber agglomeration to facilitate the formation of new interfaces.

Some compatibilizers are also used in WPC providing compatibility between polymers and natural fibers through interfacial tension reduction [14]. Some compatibilizers like acetic anhydride and methyl isocyanate are mono functional reactants lowering the surface energy of the fibers and reducing their polarity. Maleic anhydride polypropylene (MAPP), maleic anhydride polyethylene (MAPE), maleated styrene-ethylene/butylene-styrene (MA-g-SEBS) and styrene-maleic anhydride (SMA) can act as compatibilizers by forming chemical bonds between MA and –OH groups present on the fiber surface. Besides covalent bonding with

the fibers, polymer chain entanglement and strong secondary interactions such as hydrogen bonding are other mechanisms of action for compatibilizers.

One of the most common compatibilizer when HDPE is used as the matrix is MAPE. As shown in Figure 1.14, the interfacial interaction between the fibers and the polymer is likely both chemical (ester bond) and physical (hydrogen bond) interaction between maleic anhydride groups in MAPE and –OH groups on the fibers. Moreover, polyethylene chain of MAPE can diffuse into the HDPE matrix via entanglement. All these mechanisms lead to better interfacial adhesion between the fiber and the matrix.

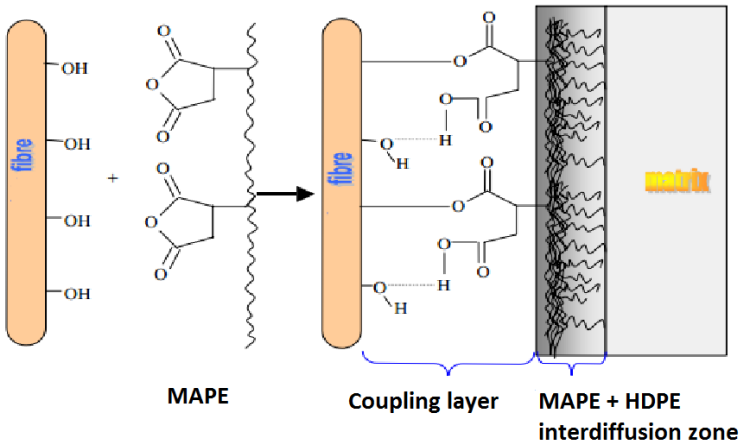

Figure 1.14. Hypothetical structure of MAPE coupling agent and cellulosic fibers at their interface [36].

The compatibilizing agent type and specification have important impacts on the interfacial adhesion between the fibers and the matrix. In a composite, improvement of interfacial bonding leads to better physical and mechanical properties depending on molecular weight (chain structure), concentration and acid number (maleic anhydride groups) [37]. A high compatibilizer concentration has a negative effect on interfacial adhesion. However, increasing the molecular weight of the compatibilizer directly influences the fiber-matrix bonding strength. Therefore, high molecular weight, moderate acid number and low concentration are optimum to improve interfacial bonding and composite properties.

A stress-relieving boundary layer between the fibers and the matrix with a coupling agent is created when the following conditions are satisfied [38]:

- The boundary region is firmly bonded to the fibers.
- The bulk polymer is efficiently wetted by the boundary layer preventing void formation.
- The boundary layer maintains contact between the fiber surface and the coupling agent interphase.

1.5. Polymer foams

Polymer foams are lightweight materials generally consisting of two phases: a solid polymer and a gaseous phase. They have attracted enormous attention because of their wide applications in insulation, cushion, absorbent, and weight-bearing structures [14].

The market value of foam applications in different industries in 2000 was about US $2 billion [39]. It is forecasted that the market will consume about 25.1 million tons polymers by 2019 [40]. This number is expected to rise considerably as diverse applications are growing.

Commercial foams are often based on a limited number of polymer matrices such as polyurethane (51%), polystyrene (29%), polyvinyl chloride (9%) and polyolefins (6%) [41].

The main challenges in foam applications are low mechanical strength, poor surface quality and low thermal and dimensional stability. Although they are widely used in thermal insulation, automotive, aerospace, marine, aircraft, construction, packaging and sport industries due to their light weight, impact absorption, thermal insulation, flotation, acoustic isolation and noise abatement are other important applications [42].

Since the 1980s, several developments have been made in foam manufacturing and processing [43]. Today, foaming of polymers can be carried out by various methods such as

mechanical, physical and chemical processes. The most common methods are summarized below [44]:

- Thermal decomposition of chemical blowing agents
- Volatilization of low boiling liquids such as fluorocarbons (physical blowing agent)
- Expansion of dissolved gas in a polymer
- Incorporation of gas-filled microspheres into a polymer system

The easiest method for polymer foaming is using a blowing agent in injection molding with conventional machines [45]. The materials used as blowing agent are based on the mechanism by which the gas is liberated and can be classified in two major groups [46]:

- **Chemical blowing agents**

  Chemical blowing agents (CBA) decompose during processing in a chemical reaction which is induced by heat. The decomposition can be exothermic or endothermic. Exothermic foaming agents release heat while decomposing, providing a fast and complete decomposition. The effective foaming gas released is mainly nitrogen. Ammonia carbonate, carbonates of alkali metals, as well as azo-and diazo compounds such as azodicarboxylic acid derivatives are some examples of chemical blowing agents. The most important exothermic foaming agents are azodicarbonamide (ACA) and the sulfonylhydrazides. The properties of commonly used chemical blowing agents are summarized in Table 1.7.

  The decomposition of endothermic foaming agents is heat-consuming. The speed of gas evolution is controlled through process temperature. These foaming agents are used in food contact applications because they are physiologically safe and nontoxic.

  As shown in Figure 1.15 the decomposition of azodicarbonamide in three different reactions produces a mixture of nitrogen, carbon monoxide and ammonia [47].

Table 1.7. Properties of common chemical blowing agent [46].

Compound	Gas yield (cc/g)	Decomposition temp. (°C)	Matrix
Benzene sulphonhydrazide	125	140-160	Low density polyethylene
Azodicarbonamide	200-230	170-230	PP, PS, HDPE
Proprietary Ammonia-free type	125	220-250	Polyamides, Polycarbonates
p-toluene sulphonyl semi-carbazide	146	216-260	Polyamides, Polycarbonates
Trihydrazinotria-zine	190	265-290	Polyamides, Polycarbonates

The following issues have to be considered when a chemical blowing agent for a polymer is chosen:

- Decomposition temperature has to be close to the polymer melting and hardening temperatures.
- Liberated gas must be noncorrosive, nontoxic and non-flammable.
- Rate of gas liberation must be high, but controllable.
- Gas liberation temperature range must be narrow.
- They must be available at low cost.

- Blowing agent and liberated gases **must** have high solubility and low diffusivity in the polymer.

- **Physical blowing agents**

Physical blowing agents (FBA) liberate gases due to physical processes such as evaporation or desorption at high temperature or low pressure. Low boiling-point liquids such as aliphatic, halogenated and aromatic hydrocarbons (CFC, HFC), alcohols and ethers fall in this category. Nitrogen, carbon dioxide, air and helium are the main gases that are widely used as physical blowing agents.

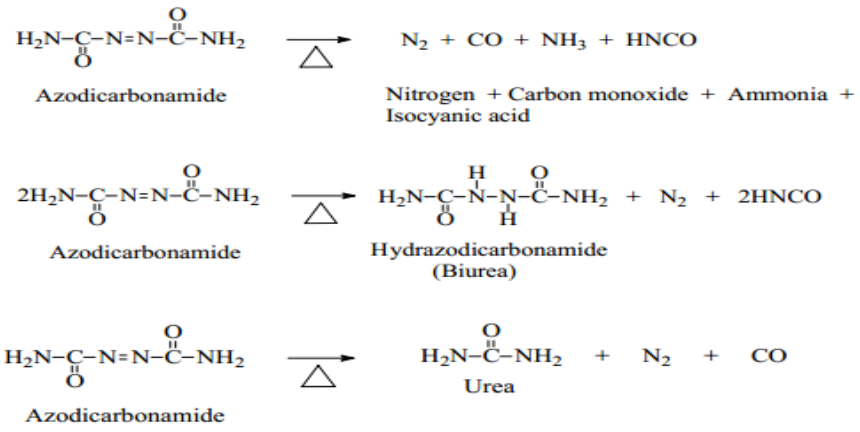

Figure 1.15. Azodicarbonamide decomposition reactions [47].

Polymers can be processed into rigid or flexible foams [46]. Rigid foams are generally used in building insulation, appliances, transportation, packaging, furniture, flotation and as container, while flexible foams are used in furniture, transportation, bedding, sports, shock and sound insulation [39].

Foams are also classified in two groups as open cell and closed cell based on their geometry. In open cell foams, the cells are interconnected and the foam structures have ribs and struts. This form has high absorption capability. In closed cell foams, the cells are completely isolated from each other by walls. This form is used for insulation applications due to its lower permeability.

Plastic foams are produced in a wide variety of densities ranging from 1.6 kg/m^3 to 960 kg/m^3 [48]. Since the mechanical properties are generally proportional to foam density, the final application determines the density to be used. Thus, for rigid foams, load-bearing applications require high densities reinforced foams, while low densities are usually used for insulation [49].

1.5.1. Principles of foam formation

The foaming process is controlled by physical and rheological properties such as blowing agent solubility and diffusivity, interfacial tension, shear and elongational viscosities, melt elasticity, blowing agent content, and processing variables such as temperature, pressure, and process type [40, 50]. Processing consists of three steps as shown in Figure 1.16:

- Bubble nucleation
- Bubble growth
- Bubble stabilization

The first step in foaming is nucleation when a gaseous phase (bubbles) is developed in the liquid polymer-gas system [46]. This process can be either a homogeneous process in a homogenous liquid or heterogeneous process with the presence of a second phase like fine solid particles such as nucleating agents [40]. The presence of small particles act as a catalyst by reducing the required activation energy to achieve a stable nucleus in the liquid system.

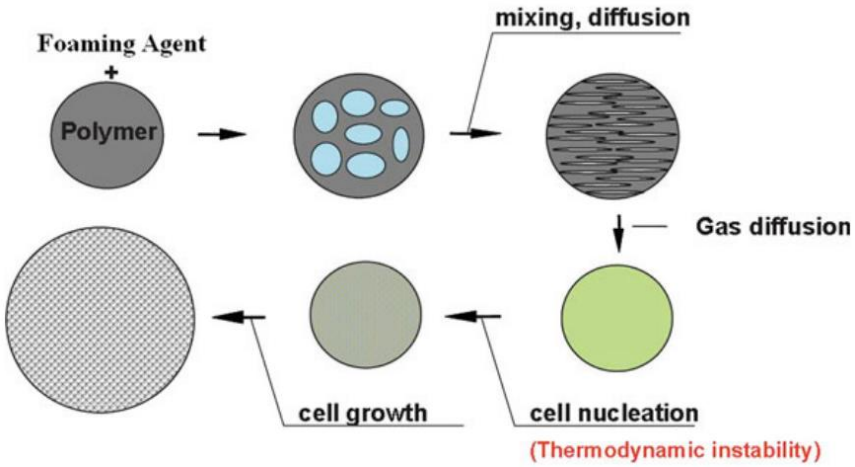

Figure 1.16. Foaming process diagram [14].

Bubble growth is the step when the nucleus grows due to the diffusion of the dissolved gases from the liquid polymer-gas system [40]. Bubble growth is mainly controlled by melt

viscosities, gas diffusion coefficient, gas concentration, temperature, pressure and the number of bubbles. Higher gas concentration gradient in the system enhances the gas diffusion and promotes the bubble growth.

Bubble stabilization usually takes place due to polymer cooling [51]. Cooling increases melt viscosities and decreases mobility to solidify the system completely and stabilize the cells. This step is important since cell morphology and geometry such as cell size, cell density, cell size distribution and foam density influence the mechanical properties of the foams.

It is known that a cellular structure with smaller cell sizes and higher uniformity leads to better mechanical, physical, and thermal properties, so achieving a high cell density system is desirable [52].

1.6. Structure design of composites (sandwich structure)

Typical three-layer composite sandwich structures are composed of two relatively dense, stiff and thin face sheets, commonly composite laminates and metals, enclosing a thick and light weight core in the form of a metallic and non-metallic honeycomb, cellular foams, balsa wood or lattice structures [53]. These materials have gained widespread acceptance as an excellent way to obtain very lightweight structures with high specific bending stiffness as well as high specific bending strength and improved fatigue properties [54, 55]. In these structures, the face sheets can be made of thermoplastic composites based on HDPE and PP because of their processability, high impact strength, low cost, high resistance to chemicals and long shelf life [56].

Although these structures offer some interesting advantages over other engineering structures such as steel and aluminum, they have some drawbacks such as low thermal capacity, poor fire resistance, high deformability at high temperature and sensitivity to impact loads [57].

In these structures, the main function of the skins is bearing the in-plane compressive and tensile stresses from bending moment, while the main functions of the low-weight core are

providing the resistance against the shear forces as the transverse forces, stabilizing the face sheets at a specific distance from each other, and supporting them against some failure modes such as buckling and wrinkling [58].

The design of sandwich structures is complex and needs comprehensive understanding of mechanical and deformation behaviors of components and structure under complex loading conditions, because the overall performance of sandwich structures is dependent on the properties of the face sheets and core, as well as dimensions and loading type [53]. Moreover, the properties of composite sandwich structures can be tailored by choosing the appropriate materials and volume fractions [57]. Modern sandwich structures can have three or more special-purpose layers for moisture, thermal or sound insulation, energy damping or protection against corrosive materials.

The failure behavior of sandwich structures has been investigated because any sudden failure can have castrophic consequences, especially in some industries such as buildings and aerospace. Moreover, their mechanical behavior has been studied and reported in several publications [53, 59-62].

Dyre et al. [62] investigated the effect of simple and complex cross-section design on the modulus of elasticity and toughness of fiber-reinforced composites (FRC) for prosthodontic applications. Two composites made of ultra-high-molecular-weight polyethylene fiber ribbon, woven E-glass fibers, or unidirectional R-glass fibers were used to make specimens with a range of fiber positions, orientations, or geometries.

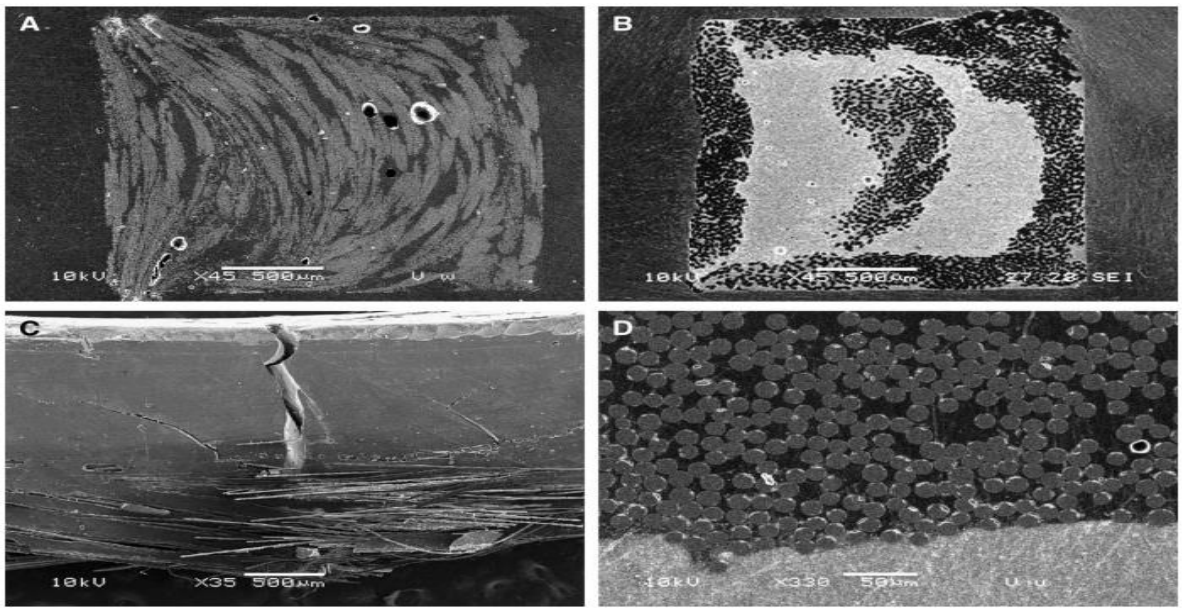

Figure 1.17. SEM micrographs of test specimens. A) five layers of UHMWPE woven fiber arranged into an I bar configuration, B) five layers of woven E-glass fiber arranged into laminate configuration with vertical orientation, C) one layer of unidirectional R-glass fiber placed in the compression side of the specimen, and D) one layer of unidirectional R-glass fiber placed in the tension side of the specimen [62].

They reported that the elasticity of FRC increases when glass fiber materials (one or more) are placed in the compression side of the sample. On the contrary, the results suggested that toughness increases when fibers were placed in the tension side. They also reported that, depending on the cross-section arrangment, the modulus can increase by up 200-300% and the toughness by up to 70 times.

In another study, the mechanical properties in terms of interfacial shear strength (IFSS) and flexural stiffness of a double wall panel consisting of an unreinforced thermoplastic polymer layer (LLDPE) and a thermoplastic composite layer (PP + E-glass fibers) were measured [56]. The results showed that the mechanical properties are dependent on the configuration of the beam structure. The structure with the composite layer at the intrados had higher strength, while the relative position of the layers did not influence the stiffness. Moreover, failure modes of the beam were studied by SEM as shown in Figure 1.18. As reported, the failure modes were dependent on load direction, processing conditions and beam

configuration. The results indicated that high physical adhesion between the layers was obtained due to some diffusion of LLDPE into the PP + E-glass fiber.

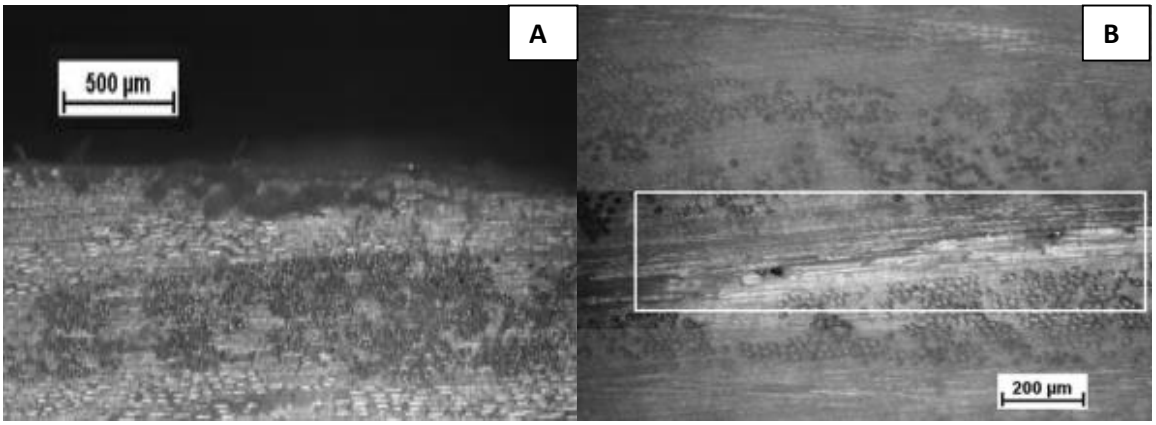

Figure 1.18. A) Damage at the load nose contact area during a short-beam test performed with PP + E-glass fiber at the intrados position, and B) interlaminar failure between the load nose and support with PP + E-glass fiber at the extrados [56].

Mechraoui et al. [63] studied the influence of skin thickness, core density and skin composition on the tensile and flexural properties of three-layer sandwich structures with foam core. It was found that increasing the skin ratio and fiber content increased both tensile and flexural moduli, while higher density reduction decreased the properties, as shown in Table 1.8. It was shown that the effect of the skins is more important on the flexural properties than for tensile properties.

Kazemi et al. [64] studied the failure modes of three layered sandwich structures with different stacking sequences and configurations. Moreover the influence of skin wood content, thickness of skins and stacking sequence on the impact and flexural properties of symmetric and asymmetric sandwich structures were studied. The results showed that the main failure mode was skin failure. Besides, it was reported that the flexural properties were mainly controlled by the skin layers. increasing overall wood content in the skins led to increasing flexural modulus for both symmetric and asymmetric structures. For instance, increasing skin wood content from 30% (30-0-30) to 40% (40-0-40), increased the flexural

modulus of the structures from 1628 to 1900 MPa. They showed that flexural modulus was independent of load direction. Thus, both skins affected the stiffness of the structures equally. As an example, the stiffness of 10-0-20 was reported as 1355 MPa compared to 1379 MPa for the 20-0-10 structure. For all the asymmetric structures, the reported flexural strength was dependent on load direction, while the core did not influence it signicantly. Moreover, it was shown that flexural deformability of asymmetric structures was higher when the load was applied to the skin with higher wood content. Impact results confirmed the negative influence of increasing overall wood content on the structures impact strength.

Table 1.8. Effect of CBA content and initial skin ratio on the flexural modulus of structural foams [63].

		Flexural modulus (MPa)				
CBA concentration (% wt.)	**Skin ratio (%)**	**11**	**23**	**30**	**42**	**57**
	1.5	41.5±0.1	43.1±0.1	50.4±0.1	53.5±0.2	66.8±0.3
	2.5	35.4±0.1	37.6±0.2	41.9±0.3	47.7±0.5	51.4±0.1

In another study, the behavior of sandwich panels with PVC foamed core and glass fiber reinforced epoxy face sheets under four point bending tests was investigated [65]. The main reported failure mode for these structures was compressive failure of the inner face which indicated that the compressive strength of the glass fiber reinforced epoxy skin controlled the strength of the sandwich structures. Figure 1.19 shows that the optimum core-to-face weight ratio for flexural strengh and stiffness are one and two, respectively. Comparing theoretical and experimental curves showed that the theoretical model provided good predictions. It was shown that at core-to-face ratios above the optimum value, increase in panel weight was relatively low. For example, a 100% increase in weight ratio led to 6% increase in structure weight. It was also mentioned that the structure of sandwich panels can be optimized with respect to desired characteristics and final applications.

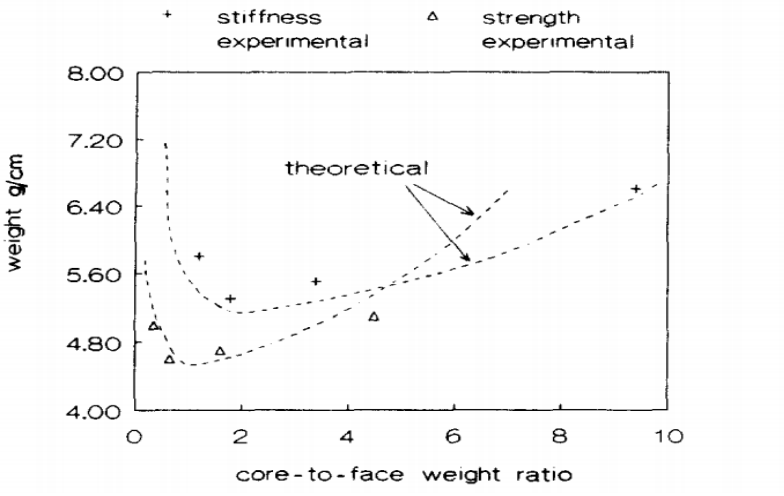

Figure 1.19. Sandwich structure weight as a function of core-to-face weight ratio [65].

The failure modes and their occurrence crieteria in sandwich structures with carbon/epoxy facings and aluminum honeycomb or PVC closed-cell foam cores under three and four-point bending tests, were studied experimentally [53]. A summary of the failure modes is shown in Table 1.9 which are compressive failure, adhesive bond failure, indentation failure, core failure and facing wrinkling. It was indicated that the type of loading, material properties and dimensions of the sandwich structure were the main parameters controlling the failure modes and their initiations.

Table 1.9. Failure modes in sandwich beams [53].

Mode	Criteria
Face sheet compressive failure	Composite failure criterion (e.g. maximum stress)
Face sheet debonding	Maximum shear stress of adhesive, or interfacial fracture toughness
Indentation failure	Core state of stress reaches failure condition; critical compressive stress in face under combined local and global bending
Core failure	State of stress in foam reaches failure condition
Face sheet wrinkling	Face sheet stress equals critical local buckling stress

Different scenarios were considered in this study. In one case, beams under three-point bending with different span length were studied to show the failure modes, their initiation, sequence and interaction were dependent on loading conditions. As shown in Figure 1.20, for short spans, core failure occurs before facing wrinkling. For long spans, facing wrinkling takes place before core failure.

As it was mentioned, one of the weak points of sandwich structures is their high sensitivity to foreign object impact which may be caused by a tool dropped during maintenance or runway debris [55]. The stiffness and strength of the composite can be significantly decreased by low-velocity impact as well. Therefore, the low-velocity impact behavior of sandwich structures has been investigated from three different aspects: (1) impact response, (2) damage characterization, and (3) post-impact parametric studies.

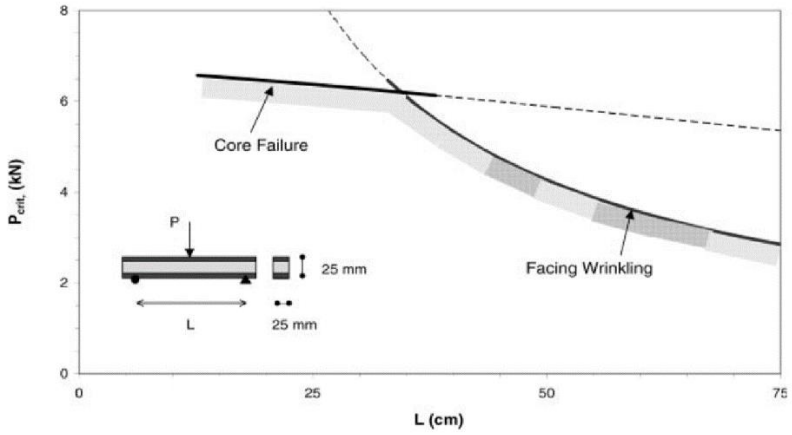

Figure 1.20. Critical load vs. span length for failure initiation in sandwich beams under three-point bending [53].

Wang et al. [66] studied the effect of impactor diameter, impact energy, and sandwich panel configuration parameters such as skin and foam core thickness on the impact behavior of a sandwich structure composed of a polyurethane foam core with plain weave carbon fabric laminated skins. The results showed that core thickness did not influence the impact response and sandwich structure failure mode. Moreover, it was shown that increasing skins thickness

increased the peak load and reduced the contact duration when larger impactors applied larger contact force. Also, increasing impact energy increased damage diameter and indentation depth increase with the impact energy. The following damage modes were reported for sandwich structures with foam core: permanent indentations, matrix crushing due to compression, delamination between layers, fiber fracture, foam core crushing under the skin, and overall residual deformation of the sandwich structure.

Rizov studied the low velocity behavior of a PVC foam with densities of 60 (H60) and 100 (H100) kg/m^3, respectively [67]. As reported in Table 1.10, impact energy, maximum deflection, and impact damages were dependent on foam density. Heavier foams showed higher maximum contact force and higher local rigidity due to the increase of elastic modulus. As impact energy was increased from 4.3 to 53.5 J by varying the drop height, the maximum deflection and thickness of the crushed zone were increased. The observations showed that the foam specimens had energy absorption with both crushing and cracking when the impact energy exceeded a threshold level due to a mixed energy absorption mechanism of the foam.

In another study, Mines et al. [68] investigated the low velocity behavior (static and impact) of two polymer composite sandwich panels: one with a foamed core and one with a honeycomb core to identify energy absorbing modes and capabilities. The results showed that the failure processes of sandwich panels did not change from impact test to static test. The results confirmed the influence of the core density on failure mode which was dominantly core crushing.

They also suggested a combination of core and skins which allowed the outer skin to deform easily to absorb energy when the core was under shear and supported multi-axial stresses and the face sheets could bear tension and bending, as effective ways to increase the energy absorption capacity of the structure. As another design option, they proposed a multi-layer sandwich structure with high energy dissipation capacity to delay perforation.

Table 1.10. Measured damage parameters for H60 and H100 foam beam and panel specimens at different energy levels [67].

Foam material	Specimen type	Impact energy (J)	Maximum deflection (mm)	Thickness of the crushed zone (mm)
H60	Beam	4.3	4.8-5.0	1-2
		8.2	6.4-6.9	2-3
		15.7	9.1-9.6	3-5
		22.4	10.9-11.3	6-7
		33.1	11.9-12.2	8-10
	Panel	4.3	4.3-4.5	1-2
		8.2	6.1-6.5	2-3
		15.7	8.8-9.3	3-5
		22.4	10.2-10.9	6-7
		33.1	11.3-11.5	8-9
H100	Beam	4.3	3.6-3.8	1-2
		8.2	4.4-4.7	3-3
		15.7	5.7-6.0	3-4
		22.4	6.6-6.8	4-6
		33.1	6.9-7.3	7-9
	Panel	4.3	3.5-3.7	1-2
		8.2	4.2-4.5	2-3
		15.7	5.5-5.8	3-4
		22.4	6.3-6.7	4-6
		33.1	6.7-6.9	6-7

Therefore, the optimization of perforation behavior of the sandwich panels would be possible with the right combination of materials and structures.

1.7. Problems and thesis objectives

Although the feasibility of sandwich structure production has been shown, it is worth to ask how the mechanical behavior of these composite sandwich structures with foam core and asymmetric structure produced by compression molding are affected by different structural parameters such as skin thickness, skin fiber content and core density. The answers would help developing new structures for sandwiches with foam core.

Therefore, the main objectives of this work include:

- Fabrication and characterization of composite materials using an industrial method.
- Finding the optimal MAPE (coupling agent) content in a composite.
- Production of different sandwich panels with and without a foam core.
- Mechanical characterization of sandwich panels with different configurations.
- Study the deformation and failure modes of sandwich structures depending on their configuration.
- Investigate the influence of cell density on the mechanical performances of sandwich panels.
- Study the effect of design parameters such as skin thickness, skin fiber content and core density on the mechanical performances of sandwich structures.

Based on the main objectives, this thesis is divided into five main chapters:

The first chapter presented a general overview, the main definitions and concepts related to WPC, foaming and sandwich structures with foam core. Then, a review of the literature dealing with the mechanical properties of composite sandwich structures with foam core was conducted.

The second chapter deals with the optimization of the compatibilizing agent and the characterization of HDPE/hemp composites. The effect of the compatibilizing agent content is investigated by studying the morphological and mechanical properties of the composites to find the optimal content. Then, composites with different fiber content are produced and characterized.

The flexural and morphological properties of asymmetric sandwich structures with and without foam core with different stacking and configurations is presented in the third chapter.

The fourth chapter investigates the influence of different parameters such as skin thickness, core density and skin fiber content on the impact behavior (Charpy and falling weight) of the sandwich structures with different configurations.

Finally, the fifth chapter includes general conclusions based on the main results and some suggestions for future studies and further developments of these structures.

Chapter 2

Effect of coupling agent and hemp content on the mechanical properties of polyethylene composites

2.1. Introduction

Wood polymer composites (WPC) have attracted a great deal of attention during the past decades. They have been used mainly in the construction industry in North America, while in Europe the automotive industry is the biggest consumer of agricultural fibers such as hemp and flax with recycled plastics. The construction industry has just begun to benefit of WPC.

Natural fibers are used mainly as filler in composites to decrease production costs, reduce final products weight and enhance mechanical properties such as strength and stiffness. Moreover, fibers are assumed to be renewable, recyclable and biodegradable resources with minimum CO_2 footprint and low energy consumption to grow and process. They also have high electrical resistance, as well as good thermal and acoustic insulation properties. Another advantage of using natural fibers is that their surface modification and grafting process is practical and easy. But, the main drawbacks of working with fibers as a filler in composites are their high moisture absorption, low degradation temperature, low fire resistance and incompatibility with most polymers.

Fibers, compared to thermoplastics such as HDPE, PP, have high Young's moduli which is contributing to high composite stiffness [69]. Improving composite Young's modulus is dependent on several parameters such as fiber content, fiber orientation, interaction and fiber-matrix adhesion. Mixing polar and hydrophilic fibers with nonpolar and hydrophobic matrices influences the quality of fiber dispersion in the matrix, as well as interfacial adhesion between them. Maximizing the adhesion between both phases significantly affects the mechanical properties of the composites and improves the reinforcing role of the fibers due to improved interfacial stress transfer.

2.2. Compatibilizing agent optimization

A low cost and effective method to improve the interfacial adhesion between the fibers and the matrix is using compatibilizing agents. These compounds are bonding agents and

surfactants, including compatibilizers and dispersing agents [14]. Bonding agents act like a bridge connecting wood fibers with the matrix by one or more of the following mechanisms: covalent bonding, polymer chain entanglement, and strong secondary interactions such as hydrogen bonding [70].

Several efforts have been made in the last two decades to improve the interfacial bonding strength between fibers and matrices in a composite using different methods [32, 37, 71]. Lu et al. [37] investigated the efficiency of seven coupling agents in wood-fiber/HDPE composite. They reported that interfacial bonding strength, flexural modulus and other mechanical properties were dependent on compatibilizer type, functional groups, molecular weight, concentration, and molecular structure. The results showed that maleic anhydride polyethylene compatibilizers (226D and 100D) performed better than the other compatibilizers such as oxidized polyethylene (OPE) and pure polyethylene (PPE). Overall, 3% wt. of maleic anhydride polyethylene was reported as the optimal for the composite studied. Moreover, the compatibilizers improved interfacial bonding strength and flexural storage modulus by about 140% and 29%, respectively. They also discussed different models for fiber-polymer interaction at the interface including: a) brush, b) switch, and c) amorphous as illustrated in Figure 2.1.

The brush structure is obtained when the compatibilizers have high acid number and low molecular weight. The compatibilizers with moderate acid number and high molecular weight prefer the switch configuration, while moderate acid number and low molecular weight results in an amorphous structure. Comparing the performance of the different compatibilizers, it was concluded that compatibilizers with high molecular weight, moderate acid number, and low concentration performed better in WPC.

In another study, the influence of four different isocyanate coupling agents, their chemical structures and mixing procedures on the mechanical properties of wood fiber/polystyrene composites was investigated [72]. The results showed that depending on isocyanate concentration, the coupling agent functioned either as an adhesion promoter or inhibitor. Thus, improved mechanical properties of the composite were obtained at moderate

concentration, while at high concentration lower properties were obtained. It was also reported that the chemical structure and molecular weight of isocyanates controlled the mechanical performance of the composites.

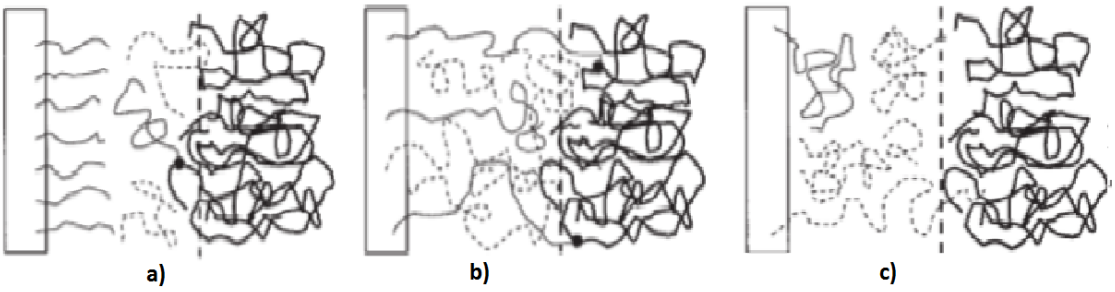

Figure 2.1. Schematic representation of wood fiber-polymer interactions: a) brush, b) switch, and c) amorphous [37].

The efficiency of nine different maleic anhydride polypropylene (MAPP) in a flax/PP composite was investigated in another work [73]. It was found that MAPP molecular weight substantially influenced the efficiency of MAPP compared to its content in the composite. The interfacial adhesion between flax and PP was controlled by the maleic anhydride content grafted per PP chain, MAPP molecular weight, and miscibility degree between MAPP and PP. The results showed that the molecular weight of the compatibilizer was more important compared to maleic anhydride content.

Adhikary et al. [74] investigated the mechanical properties of a wood flour (*Pinus radiata*)/HDPE (recycled and virgin) composite with MAPP. The composite made of recycled HDPE showed good water absorption compared to the composite with virgin HDPE, while tensile and flexural properties of both composites were almost equal. The specimens with MAPP showed higher tensile strength and stiffness which were attributed to improved interfacial bonding between the fibers and HDPE due to esterification. As an example, the tensile strength of the composite rHDPE with 50% wt. wood flour and 3% wt. MAPP was 60% higher than the same composite without MAPP. The flexural modulus and strength of the composite made of rHDPE, 40% wt. wood flour and 3% wt. MAPP were

reported 1.81 GPa and 24.9 MPa, respectively, higher than 1.13 GPa and 20.0 MPa for the composite without MAPP.

The stress-strain behavior of composites with recycled and virgin HDPE (represented as r and v, respectively), with and without MAPP (shown as CA) is presented in Figure 2.2.

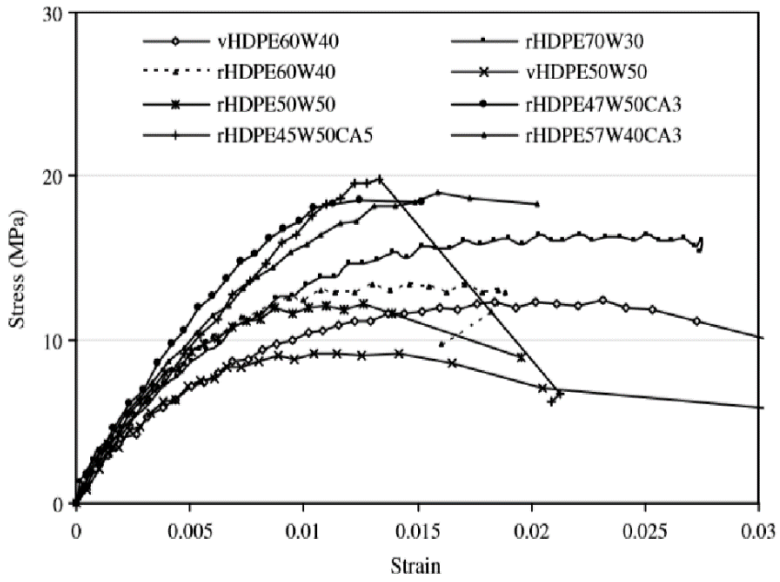

Figure 2.2. Tensile stress-strain curves of HDPE-wood flour composites [74].

The addition of wood increased the stiffness of composites, while the strain at break reduced. The composites without MAPP showed inferior mechanical properties in comparison to the composites with MAPP due to lack of bonding between the fibers and the matrix. The composites with compatibilizers showed higher maximum strength. They attributed this to improved interfacial bonding between wood and HDPE because of the formation of ester bonds.

The results showed that adding MAPP (3-5% wt.) affected water absorption. For example, in the composites made of recycled HDPE with 50% wt. wood flour + 3% wt. MAPP and 50% wt. wood flour + 5% wt. MAPP, water absorption was reduced to 1.31 and 1.18% for 24 h immersion, respectively.

Catto et al. [75] studied the feasibility of using MAPE as a compatibilizing agent in a recycled HDPE and eucalyptus fiber composite. The physical, mechanical and thermal properties of the composites with different concentration of MAPE were evaluated. The results showed that the optimal MAPE concentration was 3% wt. although the composites with 3 and 7% MAPE presented the best results for strength at break with 40 and 39 MPa, respectively. Young's modulus of the composite with 7% MAPE (695 MPa) showed the highest value indicating that the optimum compatibilizing content might be function of the property to optimize.

All treated composites showed superior thermal stability compared to HDPE with MAPE. The results were confirmed with lower contact angles and higher surface tension of the composites with MAPE in comparison with HDPE+MAPE, as shown in Figure 2.3.

The peak performance of MAPE in natural fiber composites was investigated by Keener et al. [76]. They reported that using Epolene™ G-3015 at 3% loading based on the total composite weight, agrofibre composites improved their flexural and tensile strengths by up to 60% and increased the impact properties by three times compared to composites without MAPE.

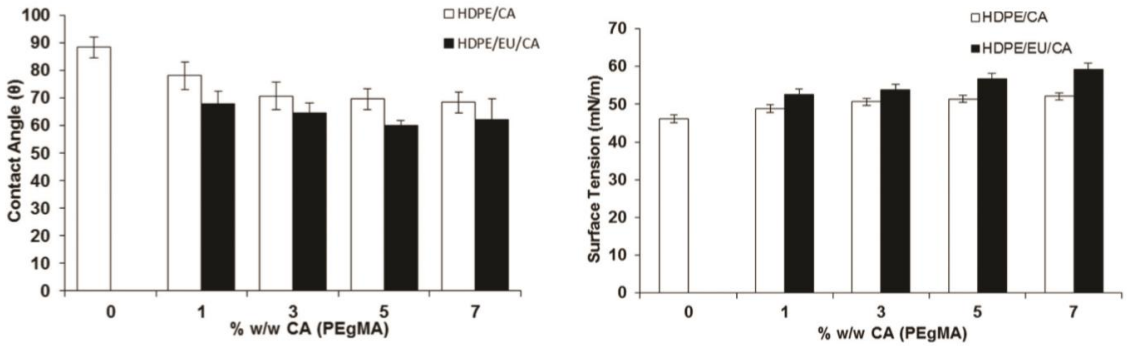

Figure 2.3. Contact angles and surface tension of HDPE and its composites [75].

In another study, the effect of MAPE on the mechanical and morphological properties of a wheat straw/HDPE composite was investigated [77]. The inclusion of compatibilizer

improved the tensile strength, tensile modulus, tensile energy absorption, failure strain, and notched Izod strength. It was shown that the use of 2% MAPE in the composite improved the tensile strength by 43%, the tensile modulus by 116%, and the impact strength (notched) by 12%.

Rana et al. [78] investigated the influence of MAPP (G-3002) on the mechanical properties and moisture absorption of jute/polypropylene composites. They reported that for composites with 60% wt. fiber, adding just 1% compatibilizer can increase the flexural strength by 100%, tensile strength by 120%, and impact strength by 175%. Moreover, using MAPP reduced moisture absorption of composites. This was attributed to bonding between the –OH groups of the fibers with the carboxyl groups of MAPE.

Another study showed that adding 2% MAPP to aspen/PP composites improved flexural strength, tensile strength and unnotched Izod impact strength compared to the composites without compatibilizer [7]. The impact test and different mechanism of energy absorption were studied as well. It was reported that for notched Izod impact test, crack propagation governs the energy absorption mechanism, while in unnotched Izod impact it is a combination of crack initiation and propagation. Crack initiation takes place at high concentrated stress points such as fibers end or at the fiber-matrix interface where the adhesion is low. The use of MAPP increased the adhesion at the interface thereby leading to higher energy to initiate cracks. Thus, the Izod impact strength of the composites with MAPP was increased. It was reported that the failure strain and tensile energy absorption of the composites with MAPP were increased due to covalent bonding between –OH groups of the fiber and MAPP, as well as entanglement between PP and MAPP. It was shown that the addition of 1.5% wt. MAPP led to maximum strain, while further increase of compatibilizer did not affect the failure strain. Adding MAPP influenced the tensile and flexural strength significantly due to improved adhesion between the fibers and the polymer combined with efficient stress transfer between them. As a result, the use of MAPP increased the tensile and flexural strength of the composites by 100 and 50%, respectively.

Hedenberg and Gatenholm studied the formation of covalent links between maleic anhydride functions in maleic acid anhydride grafted styrene-ethylene/butylene-styrene block copolymer (MAH-SEBS) and –OH groups of a fiber as shown in Figure 2.4 [79].

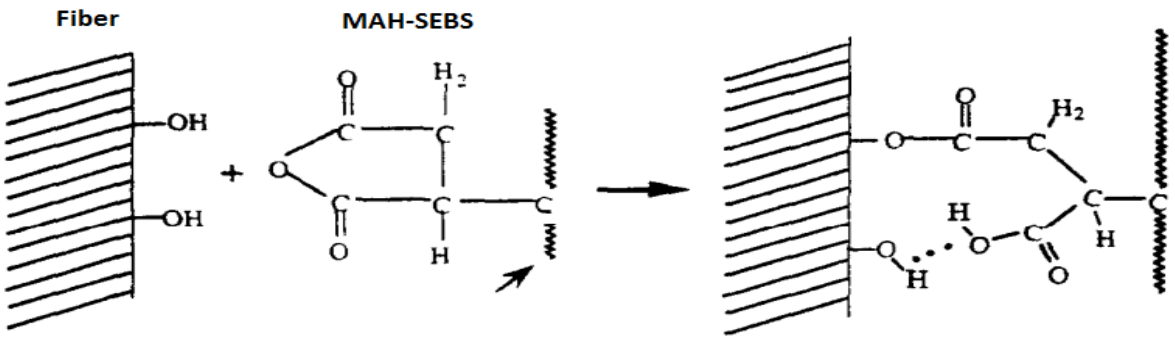

Figure 2.4. Proposed chemical reaction between MAH-SEBS and the cellulose surface [80].

FTIR spectroscopy confirmed the formation of ester linkage between the fibers and compatibilizer which resulted in enhanced mechanical properties of the composites with compatibilizers due to covalent bonding and improved fiber dispersion. Moreover, it is predicted that better fiber alignments in the composites and further improvement of fiber/matrix interfacial adhesion would increase the composite strength.

Based on the limited amount of information available on hemp/polyethylene composites, the objective of this study is to investigate the influence of compatibilizing agent content on the mechanical properties of compression-molded hemp/HDPE composites. Furthermore, the optimal MAPE content in terms of maximum mechanical properties in tensile, flexural, and impact is found. Finally, composites with different fiber content and optimum MAPE content are produced and characterized.

2.3. MAPE content optimization

2.3.1. Materials and method

2.3.1.1. Materials

High density polyethylene (HDPE) grade C-7525 with a melting temperature of 126°C, a melt index of 0.15 g/10 min (190°C, 2.16 kg) and a density of 0.930 g/cm^3, supplied by Petromont (Canada) was used as the matrix. Hemp fibers provided by the Canadian Hemp Trade Alliance (length between 1 and 1.2 mm) with a density of 1.34 g/cm^3 and maleic anhydride-grafted polyethylene (Epolene C-26) was supplied by Westlake Chemical Corporation (USA) with a density of 0.919 g/cm^3 and a melting point of 121°C.

2.3.1.2. Sample production

Composites with 10% wt. hemp and different MAPE content (0, 5, 7, 9 and 11% wt. based on total hemp weight) were prepared as described next.

In the first step, hemp fibers were dried overnight in an oven at 80°C to remove moisture. Then, HDPE/MAPE and hemp (10% wt.) were introduced in the first and fourth zone of a twin-screw extruder (Leistritz ZSE-27, L/D = 40) with a screw speed of 100 rpm. The temperature profile was set at: 180/185/195/195/195/195/195/195/200/200˚C. Then, the extruded composites were pelletized and dried at 80°C overnight in an oven to be dried completely. In the next step, compression molding was used to produce composite plates by a Carver laboratory press at 170°C and under a load of 3 tons. The compounds were first preheated for 3 minutes, then pressed for 5 minutes in molds with dimensions of 250x250x3 mm^3, and finally cooled down.

2.4. Characterization

2.4.1. Morphology

The morphology and interfacial adhesion of the fiber and matrix were studied by scanning electron micrographs (SEM). A JEOL model JSM-840A was used to study the structures exposed through cryogenic fracture and coated with a thin layer of Au/Pd prior to analysis.

2.4.2. Mechanical testing

Tension, torsion, flexion and impact tests were performed to evaluate the mechanical properties of the samples. All test specimens were cut from the 3 mm thick compression molded plates according to different test standards.

The tensile properties were determined using an Instron model 5565 universal testing machine with a 500 N load cell at a strain rate of 5 mm/min and at room temperature. The specimens were cut directly from the molded plates according to ASTM D638 (type V). Young's modulus (E_t), tensile strength (σ_t) and elongation at break (ε_t) values are reported based on a minimum of five samples.

Three-point bending flexural tests (60 mm span) were conducted on specimens with dimensions of 75×12.7×3 mm^3 according to ASTM D790. An Instron model 5565 with load cell of 50 N with a crosshead speed of 5 mm/min was used to measure the flexural modulus (E) and flexural strength (σ_{max}) of the samples at room temperature. The average and standard deviation results were based on five replicates. The flexural modulus and flexural strength were calculated experimentally via:

$$E = \frac{L^3 m}{4bd^3} \tag{2-1}$$

$$\sigma_{max} = \frac{3SL}{2bd^2} \tag{2-2}$$

where L, b, and d are the support span, width, and depth of the sample, respectively. Parameters m and S are the slope in the initial linear part of the load-deflection curve and the maximum load supported by the beam, respectively.

Charpy impact tests were conducted according to ASTM D6110 with a Tinius Olsen testing machine Model Impact 104 with a pendulum force of 22.76 N. Rectangular samples with dimensions of 120×12.7×3 mm^3 were V notched with an automatic notcher Dynisco model ASN. The average value of Charpy impact strength (I_s) with standard deviation is reported based on ten specimens tested at room temperature.

Torsion modulus (E_{tm}) was determined at room temperature using an ARES Rheometer with dynamic frequency sweeps between 0.1 and 300 rad/s in the linear viscoelastic regime (0.05% strain). The modulus was determined at a frequency of 1 rad/s for comparison purposes. Three rectangular specimens (75×11×3 mm^3) were tested and results were reported as the average and standard deviation of a minimum of 3 samples.

Density was measured using a gas (nitrogen) pycnometer model ULTRAPYC 1200e (Quantachrome Instruments, USA). The reported values are the average of at least three measurements.

2.5. Results and discussion

2.5.1. Morphology

The morphology of the composites was studied using SEM under various magnifications. Figure 2.5 presents typical micrographs of the hemp/HDPE composites with different MAPE content. As it can be seen, the quality of the adhesion and bonding between both phases of the composites were dependent on the compatibilizer content.

Figure 2.5(A) shows an image for the composite with 10% wt. hemp and 5% wt. MAPE. The low compatibility between the fibers and the matrix was recognizable due to the presence of

several gaps which confirmed the lack of mechanical and chemical bonding across the interface. As is seen in Figure 2.5(B), the gaps between the matrix and the fibers at 7% wt. MAPE decreased considerably, but some gaps were still observed. Figure 2.5(C) showed 9% completely wetted the surface of hemp fibers by the matrix. The elimination of gaps at the fiber-matrix interphase indicated the improvement in the adhesion at the interphase and confirmed the good load transfer from the matrix to the fiber. Polymer adhesion at the interface, as it is clear in Figure 2.5 (D). Both phases were not well-attached anymore with 11% wt.

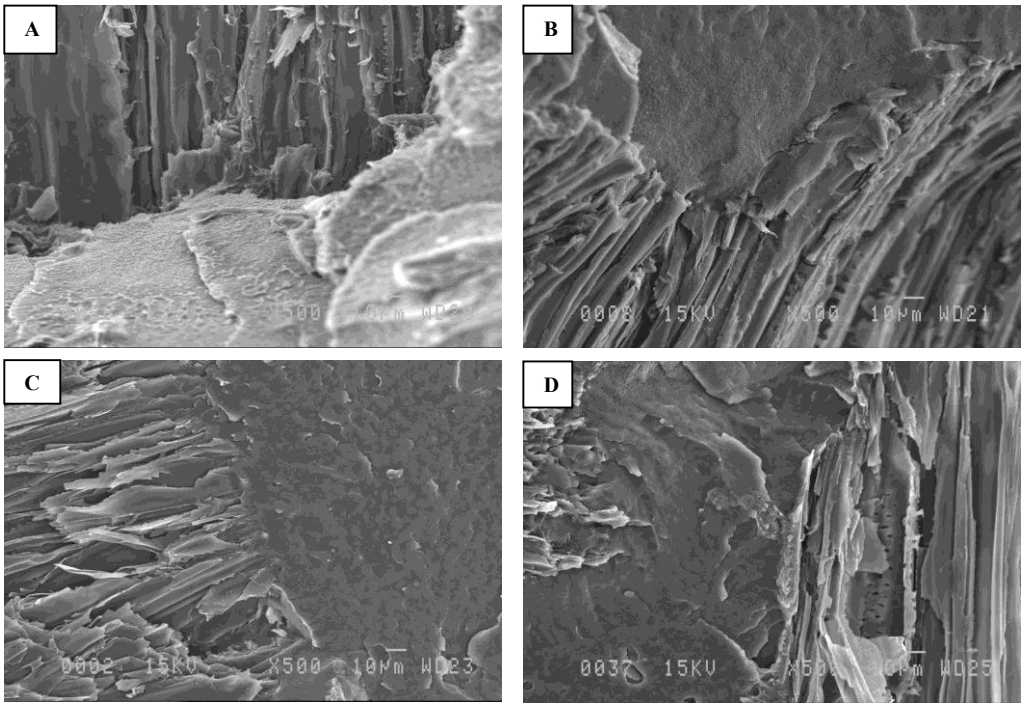

Figure 2.5. SEM microphotographs of composites with 10% wt. hemp fiber and: A) 5, B) 7, C) 9, and D) 11% wt. MAPE.

Increasing the content of compatibilizer did not affect positively the quality of the fiber-MAPE and clearly some voids were noticeable at the interphase. In this case (over-dosing), the compatibilizer did not act as a compatibilizer, but acted more as a plasticizer at higher content which limited stress interfacial transfer [81].

2.5.2. Mechanical characterization

The mechanical characterization (tensile, flexural and impact) of the composites with different MAPE contents are reported in Table 2.1.

As shown in Table 2.1, tensile modulus increased with MAPE content up to 9% with a maximum of 274 MPa which represents a 7% increase over the neat matrix. But increasing furthermore the MAPE to 11% decreased the tensile modulus to 266 MPa due to plasticizing effect of the compatibilizer. Tensile strength had a similar trend as tensile modulus, but the effect is more easily detected as the maximum value at 9% MAPE is 18.7 MPa, which is 48% higher than the neat matrix (12.6 MPa). Inclusion of the compatibilizer also enhanced the elongation of the composites. Again, the maximum is obtained at 9% MAPE.

Table 2.1. Mechanical properties of the composites with 10% wt. hemp with different MAPE content.

MAPE (% wt.)	E_t (MPa)	σ_t (MPa)	ε_t (%)	E (GPa)	σ_{max} (MPa)	I_s (J/m)
0	256 (22)	12.6 (0.6)	12.5 (0.9)	1.01 (0.01)	17.8 (1.1)	108 (6)
5	264 (10)	15.4 (0.7)	14.1 (1.8)	1.03 (0.01)	20.7 (0.8)	135 (13)
7	265 (15)	16.4 (0.3)	15.0 (0.8)	1.04 (0.03)	21.3 (1.2)	148 (5)
9	274 (11)	18.7 (0.9)	16.4 (0.5)	1.11 (0.04)	23.4 (0.9)	154 (15)
11	266 (25)	15.6 (0.1)	14.9 (0.7)	1.07 (0.07)	21.3 (0.7)	160 (13)

Numbers in parenthesis denote standard deviations.

Similar results were obtained for flexural modulus and strength, but a slight difference, which might be negligible within experimental uncertainty, can be seen for impact strength. Nevertheless, all the mechanical results seem to confirm the results of the morphological analysis: the optimum MAPE content for this system (10% wt. hemp) is 9% wt. under the processing selected. Therefore, the next step is to prepare composites with different hemp content with 9% MAPE and characterized them to evaluate the effect of hemp content on the mechanical properties of these composites.

2.5.3. Density

Results of density for the composite with 10% wt. hemp and different concentration of MAPP are given in Table 2.2.

Table 2.2. Density of the composites with 10% wt. hemp with different MAPE content.

	MAPE content (% wt.)				
	0	**5**	**7**	**9**	**11**
Density (g/cm^3)	0.969	0.970	0.970	0.971	0.966

The standard deviation of all reported data is ±0.001.

It was found that even density was influenced by MAPE concentration. Moreover, the quality of fiber/matrix adhesion was recognizable by studying density changes of samples. The density of the sample without MAPE was 0.969 g/cm^3. Interestingly, increasing the MAPE content did not affect the density for the samples with 5 and 7% wt. MAPE. Although increasing the MAPE content with density of 0.919 g/cm^3 from 5 to 7% wt., should decrease the density because HDPE with higher density (0.930 g/cm^3) was replaced with MAPE with lower density (0.919 g/cm^3). But it seemed that the voids and gaps in the composite with 5% wt. were replaced with composite due to the improved adhesion which led to the same density for both composites which was 0.970 g/cm^3. Increasing MAPE to 9%, increased the density of the composite to 0.971 g/cm^3, which was the maximum for all the composites with different MAPE.

2.6. Mechanical characterization

The tensile properties of the composites with different hemp content are presented in Table 2.3. It is clear that tensile modulus increased with fiber content, but the modulus increased more rapidly than fiber content: i.e. adding 20% wt. hemp increased Young's modulus by 54%. On the other hand, a general trend was observed that composites tensile strength and elongation were decreased by increasing fiber content. Similar trends were reported for

different composites [82, 83]. For instance, the tensile strength of 40% wt. hemp was 14.7 MPa which was about 22% less than the tensile strength of the composite with 10% wt. hemp (18.7 MPa).

As expected, tensile elongation decreases with increasing hemp content because hemp fibers have much lower elongation (about 1.6%) compared to the matrix (about 25%) and restricted the polymer chains flowing past one another [20, 84]. As an example, the elongation at 10% hemp was 15%, while the sample with 40% hemp showed an elongation at break of only 6%.

Table 2.3. Tensile properties of the composite with 9% wt. MAPE.

Hemp content (% wt.)	Tensile modulus (MPa)	Tensile strength (MPa)	Elongation (%)	Torsion modulus (MPa)
0	226 (10)	19.6 (1.0)	24.8 (0.7)	433 (15)
10	322 (11)	18.7 (0.9)	15.3 (0.3)	497 (25)
20	348 (2)	17.1 (0.2)	12.3 (0.2)	630 (11)
30	395 (22)	15.8 (1.4)	8.4 (0.7)	838 (35)
40	425 (46)	14.7 (0.8)	6.0 (0.4)	936 (22)

Numbers in parenthesis denote standard deviations.

The torsion properties of the HDPE/hemp composites are presented in Table 2.3. Inclusion of hemp fibers in the composite enhanced the torsion modulus (E_{tm}) that is attributed to higher modulus of the hemp fibers [83]. For instance, at a frequency of 1 rad/s the torsion modulus of neat HDPE was 433 MPa and it was increased by 15, 45, 94 and 116% with the addition of 10, 20, 30 and 40% hemp, respectively.

Table 2.4 presents the effect of fiber content on the flexural and impact properties of the composites. The flexural modulus was found to increase with fiber content. As an example, the flexural modulus at 40% hemp (1.94 GPa) is 123% higher than neat HDPE (0.87 GPa). Flexural strength of the composite was influenced by the fiber content. As the fiber content was increased in the composites, the flexural strength also increased. This behavior was due

to high strength and modulus of fibers and increasing the adhesion at the fiber-matrix interface which led to more uniform stress distribution [71]. For instance, the flexural strength of the composite with 30% hemp is 31.6 MPa, about 30% higher than the composite with 10% hemp (24.4 MPa).

Table 2.4. Properties of the composite with 9% wt. MAPE.

Hemp content (% wt.)	Flexural modulus (GPa)	Flexural strength (MPa)	Charpy impact (J/m)	Density (g/cm^3)
0	0.87 (0.04)	19.5 (0.5)	288 (24)	0.930 (1)
10	1.15 (0.09)	24.4 (0.2)	154 (11)	0.963 (1)
20	1.31 (0.06)	26.6 (0.5)	105 (6)	0.997 (1)
30	1.68 (0.06)	31.6 (0.9)	87 (3)	1.050 (1)
40	1.94 (0.04)	33.8 (0.6)	73 (5)	1.079 (1)

Numbers in parenthesis denote standard deviations.

Charpy impact strength showed a completely different trend compared to flexural properties. Increasing hemp content led to reduced impact strength of the composites. In fact, incorporation of solid fibers in the matrix provides points of stress concentration [85]. Thus, these points serve as crack initiation sites and ease crack propagation, thus reducing the impact strength. But this effect highly depends on interface quality in the composite. It is also related to fiber dispersion as fiber agglomeration influence the impact strength of polymer composites.

The density of the composites is also presented in Table 2.4. As reported in the literature, increasing fiber content in the composite increased the density because the density of hemp (1.34 g/cm^3) is higher than HDPE (0.930 g/cm^3) [82, 83].

2.7. Conclusion

In this study, high density polyethylene/hemp fiber composites were prepared by a combination of extrusion and compression molding. A special focus was made on the effect

of coupling agent (0, 5, 7, 9, 11% wt.) and fiber (0, 10, 20, and 30% wt.) contents. From the samples produced, morphology, density and mechanical properties in tension, flexion, torsion and impact were reported.

In the first step, composites with 10% wt. hemp were prepared with different MAPE concentration. Based on the morphological and mechanical results, it was found 9% wt. MAPE was the optimum content. This was attributed to increased adhesion and stress transfer at the interface between hemp and HDPE without having extra MAPE present at the interface acting as plasticizers.

In the second step, the effect of the hemp content in the composite was determined with the optimum MAPE concentration determined in the first step (9% wt.). In all cases, the stiffness and modulus were found to increase substantially with fiber addition due to the reinforcement effect of the fibers. For example, Young's and flexural moduli increased by about 70 and 120% respectively, with the addition of 40% wt. hemp.

From our results, it is clear that hemp fibers are good reinforcement for HDPE composites and these materials can now be used as skins to improve the performance of all polymer multilayer sandwich structures (panels) by enclosing a foam core.

Chapter 3

Mechanical characterization of asymmetric HDPE/hemp composite sandwich panels with and without a foam core

Azam Kavianiboroujeni, Alain Cloutier, Denis Rodrigue, Journal of Sandwich Structures and Materials, accepted, July 2015.

Résumé

Ce travail étudie les effets de différents paramètres de conception tels que le taux de chanvre dans les peaux (10-40% en poids), l'épaisseur des couches (1 et 2 mm) et la quantité d'agent moussant (0, 0,6 et 1,2% en poids) sur les propriétés en flexion des structures sandwich à trois couches constituées de chanvre et de polyéthylène de haute densité produits par moulage en compression. Les résultats montrent que le taux de chanvre est le paramètre le plus important pour les propriétés en flexion de ces structures. De plus, il est constaté que le module et la résistance spécifique (par unité de poids) augmentent respectivement de 30% et 36% après l'utilisation d'un cœur moussé. Enfin, la conception de structures sandwich avec ou sans cœur moussé pour les configurations asymétriques permet de produire une large gamme de propriétés en flexion.

Mots-clés: Mousse; Composite plastique; Moulage en compression; Flexion; Chanvre; Structure sandwich.

Abstract

This work investigates the effects of different design parameters such as hemp content in the skins (10-40% wt.), layer thickness (1 and 2 mm), and foaming agent content (0, 0.6 and 1.2% wt.) on the flexural properties of three layer sandwich panels of hemp and high density polyethylene produced by compression molding. The results show that hemp content was the most significant parameter for the flexural properties of these panels. In addition, it was found that specific modulus and strength (per unit weight) were 30% and 36% higher when using a foam core. Finally, sandwich panel design with or without a foam core for asymmetric configurations were shown to produce a wide range of flexural properties.

Keywords: Foam; Wood plastic composite; Compression molding; Flexion; Hemp; Sandwich panel.

3.1. Introduction

Recently, the demand for structural elements with lower weight, higher specific strength and lower environmental impact, has increased. Among all the promising candidates, sandwich panels (multi-layer structures) based on wood plastic composites (WPC) were developed and received great deals of attention. These structures are generally composed of two stiff skins and a light weight core. They are designed to be used in applications requiring high bending stiffness and low density [86]. In these structures, the main role of the skins is to bear bending loads and improve flexural stiffness, while the role of the core is to keep the skins apart and carry parts of the load, mostly shear [87, 88]. Multi-layer structures with rigid cellular core were shown to have higher specific stiffness and strength properties compared to structures without a cellular core. The cellular structure allows them to sustain large deformation while having better energy absorption capacity.

Gibson and Ashby investigated the general ideas of cellular materials and sandwich panels for different applications ranging from packaging to low weight building structures [89]. Other investigations focused on the effects of design parameters and material selection on the overall performance of multi-layer structures. The results showed that core density and thickness of the face materials were highly important. Moreover, it was possible to control the mechanical performance, especially specific strength [90, 91].

Sandwich structures have been used in packaging and material handling, aerospace, marine and automotive applications because light structures lead to weight reduction and better insulation. Moreover, less fuel consumption and CO_2 emission to the environment are other important aspects. But, recently these structures were used in civil engineering for building and construction industries. This is why several investigations focused on part design to develop and optimize multi-layer fiber composite structures to increase mechanical properties and long term properties [64, 92]. For example, Kazemi et al. [64] studied the effects of different parameters such as wood content, layer thickness and configuration (symmetric and asymmetric) of three-layered structural composites made from post-consumer waste plastics and wood flour. They showed that flexural properties were

controlled mainly by the skins. Moreover, the results clearly showed that layer configuration influenced flexural properties and asymmetric structures show a higher potential to optimize strength and weight. Manalo et al. [93] studied the flexural behavior and failure mechanisms of composite sandwich beams based on glass fiber-reinforced polymer (GFRP) skins and modified phenolic cores. They showed that beams loaded in the edgewise direction failed at a higher load with less deflection compared to specimens tested in the flatwise position. Daniel and Abot investigated the effect of GFRP skin thickness on flexural stiffness and core shear modulus of sandwich panels made of polyurethane foam cores with two different span lengths (200 and 400 mm) [94]. The results showed that stiffness was highly dependent upon skin thickness and the use of inserts.

In another investigation, the mechanical behavior of panels made of wood veneers of Aleppo pine as face sheets and cork agglomerate as core, was evaluated [59]. The final results revealed that multi-layer sandwich panels had higher strength and increasing the number of layers from 1 to 4 improved the mechanical performance of the structures. Fam and Sharaf studied the flexural properties of sandwich panels based on low density polyurethane foam core and GFRP skins with different rib configurations [95]. They showed that depending on rib configuration, strength and stiffness increased by 44-140% compared to sandwich panels without ribs. Moreover, they reported that the ultimate strength of the panels was similar to concrete panels reinforced with heavy steel of equal size, but the sandwich panels were 9-14% lighter.

Sharaf et al. [96] studied the influence of polyurethane foam core density on the flexural strength and stiffness of sandwich panels. The results showed that increasing core density enhanced the structural performance, while having negative effects on insulation properties. Styles et al. [97] investigated the influence of core thickness on failure mechanisms of an aluminum foam core/thermoplastic composite faces sandwich structure. They showed that skin wrinkling and skin fracture, as well as core cracking were dominant failure modes in thinner samples, while core indentation occurred mainly in thicker samples. Moreover, they showed that increasing skin thickness eliminated the problem of core indentation, but increased the occurrence of core shear cracking.

To pursue on the mechanical optimization of sandwich structures, this study focusses on the effect of design parameters such as hemp content, foaming agent concentration and skin thickness on the flexural properties and failure mode of three layer sandwich panels with and without a foam core. In particular, asymmetric structures are investigated.

3.2. Materials and methods

3.2.1. Materials

High density polyethylene (HDPE) with a melting temperature of 126°C, a melt index of 0.15 g/10 min (190°C, 2.16 kg) and a density of 930 kg/m^3 was supplied by Petromont Canada and used as the matrix. Hemp fiber (length between 1 and 1.2 mm) with a density of 1.34 g/cm^3 was kindly supplied by the Canadian Hemp Trade Alliance. Maleic anhydride-grafted polyethylene (Epolene C-26, Westlake Chemical Corporation) was used as a coupling agent to improve compatibility, dispersion and adhesion between HDPE and hemp fibers in the composite. This coupling agent has a density of 919 kg/m^3 and a melting point of 121ºC. Azodicarbonamide (Celogen AZ 150, Lion Copolymer) with a decomposing temperature range of 190-220°C and gas yield of 220 cm^3/g was used as chemical foaming agent.

HDPE composites with different hemp content (0, 10, 20, 30 and 40% wt.) and HDPE with different azodicarbonamide (ACA) content (0, 0.6 and 1.2% wt.) were prepared as described below to produce the skin and core layers, respectively.

3.2.2. Processing

Sample production can be summarized in three steps: 1) Skin production, 2) Core production, and 3) Sandwich panel production. The production of the skins started with hemp drying overnight in an oven at 80°C to remove humidity. Then, HDPE/MAPE (9% wt. based on total hemp weight) and hemp (0, 10, 20, 30 and 40% wt.) were introduced in the first and fourth zone of a co-rotating twin-screw extruder (Leistritz ZSE-27, L/D = 40), respectively. The screw speed was 100 rpm and the temperature profile for the 10 zones was set at:

180/185/195/195/195/195/195/195/200/200˚C. The extruded compounds were pelletized and dried at 80°C overnight in an oven. Then, composite layers with different hemp content and thickness were produced by compression molding at 170°C and under a load of 3 ton by a Carver laboratory press. In this step, the compounds were first preheated for 3 minutes and pressed for 5 minutes in molds with dimensions of 250×250 mm^2 with 1-2 mm thickness.

To produce the core, HDPE and ACA (0, 0.6 and 1.2% wt.) were introduced in the first zone of the same extruder with a screw speed of 100 rpm and a lower temperature profile for the 10 zones to limit ACA thermal decomposition in compounding: 160/165/165/165/165/165/165/160/160/155˚C. Then, the layers of HDPE with 0% ACA (4 mm thick) and layers of HDPE with 0.6 and 1.2% ACA with (1 mm thick) were produced by compression molding using a Carver press at 160°C under a load of 3 ton. The temperature was again selected to limit foaming during core compression molding.

In the last step, according to the desired final configuration, a core layer was sandwiched between two skins and transferred to a mold with dimensions of 250×250×7 mm^3. The sandwich structures were preheated at 225°C for 2 minutes and then 3 ton load was applied on the mold. Due to the high temperature, ACA decomposition started and pressure increased inside the mold. As soon as the pressure started to decrease (gas dissolution and gas loss), the pressure over the mold was removed and the sandwich panel was cooled down to stabilize the formed bubbles (foam expansion).

For sandwich panels with 0% ACA in the core, the skins and HDPE core were transferred to the same mold. Then, the mold was preheated for 3 minutes and pressed for 5 minutes under a load of 3 ton at a temperature of 170°C. Finally, the sandwich panel was cooled down and removed from the mold for analysis.

3.2.3. Sample coding

The three layer structures are presented with respect to their stacking configuration as: A(y)-X-B(z) where A and B represent the hemp content in the skin (% wt.) and X represents the

ACA content (% wt.) in the core, while y and z represent the thickness of the layer (mm). For flexural testing, the first letter in the sample coding represents the layer in extrados. For example, the sample 10(2)-1.2-40(1) represents a sandwich panel with 10% hemp and 2 mm thick skin in the extrados, a foam core with 1.2% wt. ACA, and 1 mm thick with 40% hemp skin in the intrados. A schematic representation in presented in Figure 3.1.

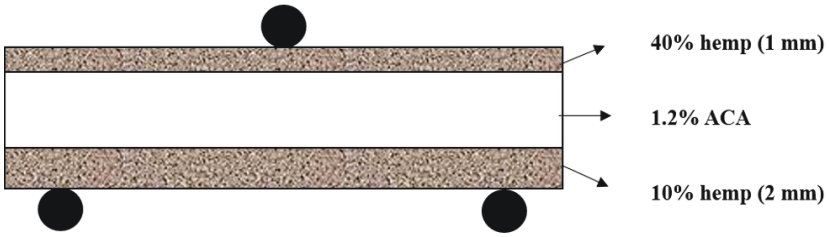

Figure 3.1. Example of sample coding: 10(2)-1.2-40(1).

3.2.4. Apparent density

Density measurements were performed with a gas (nitrogen) pycnometer model Ultrapyc 1200e (Quantachrome Instruments, USA). The reported values are the average of at least three measurements.

3.2.5. Microscopy

Scanning electron microscopy (SEM) was used to investigate the composite morphology, state of interfacial adhesion between each component, interlaminar adhesion and foam core morphology. A JEOL model JSM-840A was used to take micrographs at different magnifications. The samples were fractured in liquid nitrogen, coated with a thin layer of gold/palladium alloy and then examined at 15 kV. Also, a stereo-microscope (Olympus, SZ-PT) was used to measure the thickness of each layer and study the state of interlaminar adhesion between each layer. All images were analyzed via Image-Pro Plus 4.5 (Media Cybernetics, USA).

SEM pictures of ten different samples with the same foaming agent content were investigated to report the average cell size and cell density. Assuming an isotropic distribution of spherical cells, the cell diameter was obtained directly from the software. Cell density (N_F), defined as the number of cells (n) per cubic centimeter of foam, was calculated using [98, 99]:

$$N_F = (n/A)^{3/2} \tag{3.1}$$

where A is the area analyzed [100].

3.2.6. Mechanical testing

3.2.6.1. Flexural test

Three-point bending flexural tests (support span to overall thickness ratio of 16:1) were conducted at room temperature using a crosshead speed of 3 mm/min on an Instron model 5565 with a 500 N load cell at room temperature according to ASTM D790. Samples with dimensions of 120x15x7 mm^3 were cut from the molded sandwich panels. At least five samples were tested to report the average flexural modulus (E), flexural strength (σ_{max}) and strain at maximum stress (ε_{max}). The flexural modulus and strength were calculated as:

$$E = \frac{L^3 m}{4bd^3} \tag{3.2}$$

$$\sigma_{max} = \frac{3SL}{2bd^2} \tag{3.3}$$

where L, b, and d are support span, width, and depth of the sample, respectively. Parameters m and S are the slope in the initial linear part of the load-deflection curve and the maximum load supported by the beam.

3.3. Results and discussion

3.3.1. Density

Panel density is listed in Table 3.1. As expected, density increases with hemp content, but decreases with ACA content.

Table 3.1. Structures density (±0.001 g/cm^3).

Sample	0% ACA	0.6% ACA	1.2% ACA	Sample	0% ACA	0.6% ACA	1.2% ACA
10(1)-X-10(2)	0.946	0.768	0.684	**10(2)-X-10(1)**	0.946	0.768	0.684
10(1)-X-20(2)	0.955	0.776	0.691	**10(2)-X-20(1)**	0.950	0.772	0.688
10(1)-X-30(2)	0.970	0.788	0.704	**10(2)-X-30(1)**	0.958	0.778	0.694
10(1)-X-40(2)	0.981	0.797	0.713	**10(2)-X-40(1)**	0.963	0.783	0.698
20(1)-X-10(2)	0.950	0.772	0.688	**20(2)-X-10(1)**	0.955	0.776	0.691
20(1)-X-20(2)	0.959	0.779	0.695	**20(2)-X-20(1)**	0.959	0.779	0.695
20(1)-X-30(2)	0.974	0.791	0.707	**20(2)-X-30(1)**	0.967	0.785	0.701
20(1)-X-40(2)	0.985	0.801	0.716	**20(2)-X-40(1)**	0.972	0.790	0.706
30(1)-X-10(2)	0.958	0.778	0.694	**30(2)-X-10(1)**	0.970	0.788	0.704
30(1)-X-20(2)	0.967	0.785	0.701	**30(2)-X-20(1)**	0.974	0.791	0.707
30(1)-X-30(2)	0.981	0.797	0.713	**30(2)-X-30(1)**	0.981	0.797	0.713
30(1)-X-40(2)	0.993	0.807	0.723	**30(2)-X-40(1)**	0.987	0.802	0.718
40(1)-X-10(2)	0.963	0.783	0.698	**40(2)-X-10(1)**	0.981	0.797	0.713
40(1)-X-20(2)	0.972	0.790	0.706	**40(2)-X-20(1)**	0.985	0.801	0.716
40(1)-X-30(2)	0.987	0.802	0.718	**40(2)-X-30(1)**	0.993	0.807	0.723
40(1)-X-40(2)	0.998	0.811	0.727	**40(2)-X-40(1)**	0.998	0.811	0.727

For example, the structures 40(1)-0-40(2) and 40(2)-0-40(2) have the highest density (0.998 g/cm^3), while samples 10(1)-1.2-10(2) and 10(2)-1.2-10(1) have the lowest density (0.684 g/cm^3). On average, the density of the structures with 0.6% and 1.2% ACA are about 18% and 27% lower than neat HDPE (0.930 g/cm^3).

3.3.2. Morphology

Morphology and interfacial interaction between layers were investigated using scanning electron microscopy (SEM). Figure 3.2 presents SEM pictures of samples 10(2)-1.2-10(1) and 30(1)-0-30(2).

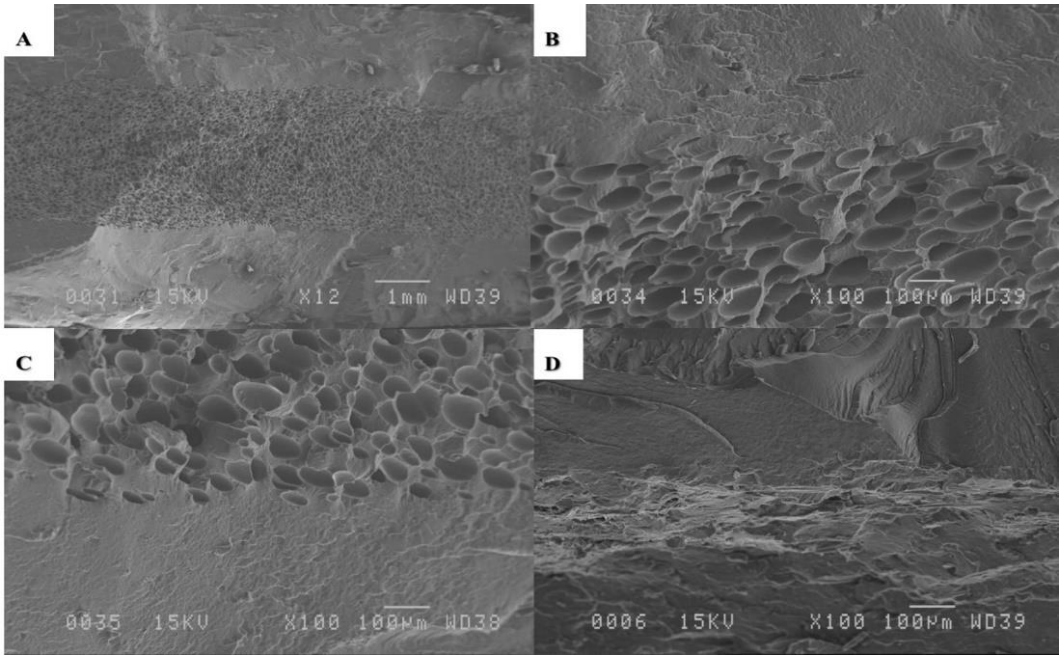

Figure 3.2. Typical SEM micrographs of the sandwich panels produced. A) SEM picture of a sandwich panel cross-section for sample 20(2)-1.2-20(1). B) and C) 10(2)-1.2-10(1). D) 30(1)-0-30(2). In all cases, good interlaminar adhesion between the skins and the foam core is observed (no void or gap).

The results show that increasing the foaming agent content in the core led to higher cell density and lower average cell diameter [46]. For example, when the foaming agent content increased from 0.6 to 1.2%, cell size decreased from 387 to 156 μm, but cell density increased from 4.26×10^3 to 8.88×10^4 cells/cm^3.

In addition, SEM pictures show that good interlaminar adhesion between the skins and the core was achieved. As seen in Figure 3.2, no distinct boundary between each layer was observed which indicates that good adhesion was achieved. These good melt weld-lines were

the reasons for low occurrence of skin-core debonding and core shear failure which are generally the main failure modes in multi-layer structures under loads [54, 101]. These failure modes cause serious problems and decrease the load-bearing capacity of these structures [102]. In our case, during the flexural tests, no skin-core debonding, compression buckling or core shear failure was observed. The main failure mode was tensile skin failure, especially for the skin layers under load with high hemp content because composites (skins) with lower hemp content have higher deformability and can withstand loads better. On the contrary, increasing the hemp content decreased skin elasticity leading to premature failure and crack propagation towards the core as observed in Figure 3.3 for two samples with and without a foam core. To postpone skin failure and improve deformability, asymmetric structures were developed where the lowest hemp content is placed in the extrados layer [103].

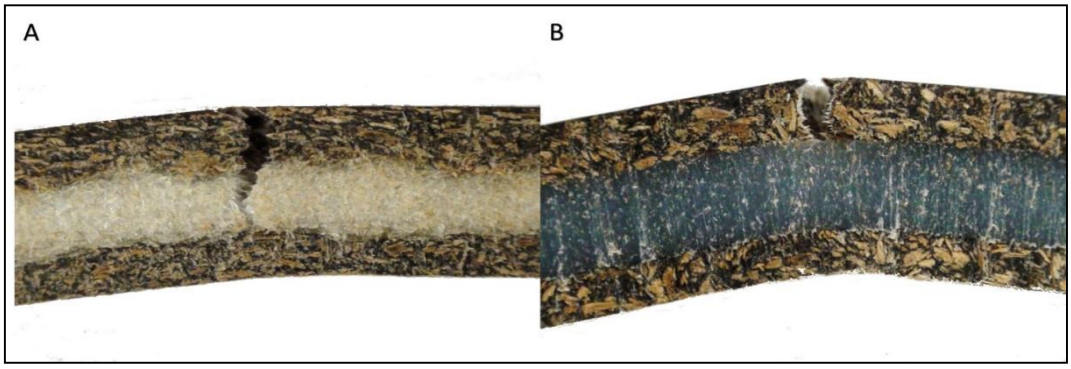

Figure 3.3. Three-point bending of multi-layer sandwich panels: A) 40(2)-1.2-40(1) and B) 40(2)-0-40(1). It can be seen that the main failure mode of the sandwich panels is skin failure (no delamination).

3.3.3. Flexural properties

3.3.3.1 Multi-layer structures without foam core

Flexural properties of three-layer sandwich panels such as flexural modulus (E), strength (σ_{max}), and strain at maximum stress (ε_{max}) were measured. Flexural properties of structures without a foam core are presented in Table 3.2.

Table 3.2. Mechanical properties of the panels with HDPE core.

Sample	E (MPa)	σ_{max} (MPa)	ε_{max} (%)	Sample	E (MPa)	σ_{max} (MPa)	ε_{max} (%)
10(1)-0-10(2)	1124 (96)*	20.2 (0.2)	18.6 (0.4)	**10(2)-0-10(1)**	1205 (39)	20.5 (0.3)	19.3 (0.3)
10(1)-0-20(2)	1191 (209)	19.7 (0.3)	18.4 (0.2)	**10(2)-0-20(1)**	1301 (77)	20.1 (0.2)	18.5 (0.4)
10(1)-0-30(2)	1278 (25)	19.4 (0.4)	17.3 (0.5)	**10(2)-0-30(1)**	1386 (47)	19.8 (0.7)	17.9 (0.3)
10(1)-0-40(2)	1338 (167)	19.2 (0.7)	16.4 (0.2)	**10(2)-0-40(1)**	1405 (22)	19.3 (0.9)	17.7 (0.5)
20(1)-0-10(2)	1209 (101)	21.1 (0.7)	17.6 (0.1)	**20(2)-0-10(1)**	1300 (143)	21.5 (1.1)	18.0 (1.2)
20(1)-0-20(2)	1285 (62)	20.6 (0.2)	17.3 (0.2)	**20(2)-0-20(1)**	1326 (56)	21.2 (0.1)	17.4 (0.1)
20(1)-0-30(2)	1333 (73)	20.2 (0.3)	16.1 (0.5)	**20(2)-0-30(1)**	1377 (25)	20.6 (0.8)	16.8 (0.5)
20(1)-0-40(2)	1394 (18)	19.9 (0.6)	15.0 (1.4)	**20(2)-0-40(1)**	1468 (22)	20.3 (0.4)	16.4 (0.1)
30(1)-0-10(2)	1297 (29)	22.2 (0.5)	14.6 (1.4)	**30(2)-0-10(1)**	1334 (121)	22.7 (0.2)	15.6 (0.8)
30(1)-0-20(2)	1336 (42)	21.7 (0.6)	14.1 (1.2)	**30(2)-0-20(1)**	1409 (49)	22.2 (0.5)	15.0 (1.0)
30(1)-0-30(2)	1421 (52)	21.4 (0.3)	13.0 (1.0)	**30(2)-0-30(1)**	1494 (72)	21.9 (0.7)	14.2 (1.0)
30(1)-0-40(2)	1553 (49)	20.9 (0.8)	12.6 (0.7)	**30(2)-0-40(1)**	1623 (139)	21.5 (0.2)	13.7 (0.8)
40(1)-0-10(2)	1413 (25)	23.3 (0.5)	12.0 (0.4)	**40(2)-0-10(1)**	1466 (66)	23.6 (0.4)	13.3 (0.8)
40(1)-0-20(2)	1520 (189)	22.8 (0.8)	10.6 (1.0)	**40(2)-0-20(1)**	1627 (132)	23.2 (0.5)	12.2 (0.5)
40(1)-0-30(2)	1585 (121)	22.2 (0.5)	9.4 (0.6)	**40(2)-0-30(1)**	1747 (110)	22.9 (1.0)	11.1 (0.5)
40(1)-0-40(2)	1676 (17)	21.7 (0.6)	9.0 (0.8)	**40(2)-0-40(1)**	1812 (48)	22.6 (1.2)	10.3 (0.9)

All reported numbers in parenthesis for mechanical properties are standard deviation.

Increasing the total amount of hemp content in both skins led to higher flexural modulus. For example, increasing hemp content in a structure from 10% (10(1)-0-10(2)) to 40% (40(1)-0-40(2)) increased flexural modulus from 1124 to 1676 MPa (49% improvement). Moreover, increasing hemp content in the extrados layer was more effective in comparison to the intrados layer. For instance, flexural modulus increased from 1205 MPa for 10(2)-0-10(1) to 1405 MPa for 10(2)-0-40(1) which is an increase of 17%, but compared to 40(2)-0-10(1) with a flexural modulus of 1466 MPa, the improvement was 22%.

Furthermore, the effect of skin thickness was investigated by comparing the flexural modulus of A(1)-0-B(2) and A(2)-0-B(1) in Table 3.2. Comparing the values of flexural modulus for both structures by applying the load on skins with different thickness showed when the load was applied on the thicker skin, higher flexural modulus were obtained [49, 104]. For instance, the flexural modulus of 40(2)-0-40(1) was 1812 MPa which was 8% higher than the flexural modulus of 40(1)-0-40(2) with a flexural modulus of 1676 MPa.

For all the structures without a foam core, the results showed that increasing hemp content in the skins had a small effect on flexural strength. This behavior was reported by Kazemi et al. [64], who explained that two mechanisms are controlling the flexural properties of multi-layer panels: rigidity with reinforcing content and deformability with decreasing reinforcement content. As shown in Table 3.2, higher hemp content in the extrados and lower hemp content in the intrados increased the flexural strength of the structures. For instance, the flexural strength of 40(1)-0-10(2) was 23.2 MPa and about 7% higher than 21.7 MPa for 40(1)-0-40(2). Moreover, the results showed that the flexural properties of the sandwiches are function of skin thickness. When the thicker skin is in the extrados, the sandwich panel had higher flexural strength. For instance, flexural strength of 40(2)-0-40(1) is 22.6 MPa and about 4% higher than 40(1)-0-40(2).

Increasing total hemp content in both skins decreased the strain at maximum stress. Sample 10(1)-0-10(2) with 19.2% has the highest strain at maximum stress, while sample 40(2)-0-40(1) with 9% has the lowest. Furthermore, comparing the structures with the same hemp content showed that sandwich panels with higher hemp content in the extrados skin have lower ε_{max}. As an example, ε_{max} of 40(1)-0-20(2) is 10.6%, while ε_{max} of 20(1)-0-40(2) is 15% which is about 42% higher. Moreover, increasing skin thickness in the extrados affected ε_{max}. As an example, the structure 40(1)-0-30(2) had a ε_{max} of 9.4%, while ε_{max} of 40(2)-0-30(1) was 11.1% which represents about 18% increase.

3.3.3.2 Multi-layer structures with foam core

Flexural properties of the panels with a foam core are presented in Tables 3.3 and 3.4.

Table 3.3. Mechanical properties of the panels with 0.6% ACA.

Sample	E (MPa)	σ_{max} (MPa)	ε_{max} (%)	Sample	E (MPa)	σ_{max} (MPa)	ε_{max} (%)
10(1)-0.6-10(2)	1051 (92)*	19.7 (0.3)	17.0 (0.7)	**10(2)-0.6-10(1)**	1093 (37)	20.2 (0.2)	18.0 (0.2)
10(1)-0.6-20(2)	1113 (33)	19.4 (0.3)	15.6 (0.5)	**10(2)-0.6-20(1)**	1162 (92)	19.9 (0.3)	17.0 (0.4)
10(1)-0.6-30(2)	1143 (52)	19.0 (1.0)	14.9 (0.5)	**10(2)-0.6-30(1)**	1225 (32)	19.5 (0.2)	16.1 (0.3)
10(1)-0.6-40(2)	1188 (36)	18.8 (0.5)	13.9 (1.0)	**10(2)-0.6-40(1)**	1258 (27)	19.1 (0.5)	15.7 (0.5)
20(1)-0.6-10(2)	1126 (42)	20.5 (0.5)	15.2 (0.8)	**20(2)-0.6-10(1)**	1149 (57)	20.9 (0.3)	16.3 (0.7)
20(1)-0.6-20(2)	1178 (102)	20.2 (0.6)	14.2 (0.7)	**20(2)-0.6-20(1)**	1193 (114)	20.6 (0.3)	15.2 (0.2)
20(1)-0.6-30(2)	1222 (128)	19.8 (0.7)	13.1 (1.2)	**20(2)-0.6-30(1)**	1256 (25)	20.2 (0.3)	14.9 (0.3)
20(1)-0.6-40(2)	1249 (106)	19.2 (0.4)	12.9 (0.3)	**20(2)-0.6-40(1)**	1287 (114)	19.9 (0.5)	13.8 (0.1)
30(1)-0.6-10(2)	1242 (109)	21.5 (0.3)	13.2 (0.2)	**30(2)-0.6-10(1)**	1278 (102)	22.1 (0.6)	13.9 (1.2)
30(1)-0.6-20(2)	1289 (117)	21.2 (0.8)	12.4 (0.9)	**30(2)-0.6-20(1)**	1389 (101)	21.7 (0.9)	12.8 (0.5)
30(1)-0.6-30(2)	1375 (53)	20.9 (0.5)	11.2 (0.4)	**30(2)-0.6-30(1)**	1417 (48)	21.2 (0.6)	10.8 (0.6)
30(1)-0.6-40(2)	1419 (83)	20.3 (0.7)	10.4 (0.8)	**30(2)-0.6-40(1)**	1472 (66)	20.8 (0.4)	10.3 (0.3)
40(1)-0.6-10(2)	1365 (95)	22.5 (1.3)	10.8 (0.3)	**40(2)-0.6-10(1)**	1500 (50)	23.0 (0.7)	11.9 (0.8)
40(1)-0.6-20(2)	1435 (61)	22.0 (0.3)	10.4 (0.2)	**40(2)-0.6-20(1)**	1555 (50)	22.4 (0.6)	10.3 (0.6)
40(1)-0.6-30(2)	1499 (113)	21.7 (0.7)	9.2 (0.8)	**40(2)-0.6-30(1)**	1618 (83)	22.1 (1.1)	9.7 (0.5)
40(1)-0.6-40(2)	1523 (136)	21.4 (1.0)	9.0 (0.3)	**40(2)-0.6-40(1)**	1634 (150)	21.6 (0.5)	8.8 (0.3)

All reported numbers in parenthesis for mechanical properties are standard deviation.

Flexural modulus values for both 0.6 and 1.2% ACA foam core increased with increasing total hemp content in both skins.

For the sandwich panels with 0.6% ACA, the flexural modulus increased by 45% from 10(1)-0.6-10(2) to 40(1)-0.6-40(2) and 50% from 10(2)-0.6-10(2) to 40(2)-0.6-40(1). Similarly, the same trends were observed for sandwich panels with 1.2% ACA.

Table 3.4. Mechanical properties of the panels with 1.2% ACA.

Sample	E (MPa)	σ_{max} (MPa)	ε_{max} (%)	Sample	E (MPa)	σ_{max} (MPa)	ε_{max} (%)
10(1)-1.2-10(2)	1030 (92)*	19.6 (0.5)	16.8 (1.0)	**10(2)-1.2-10(1)**	1082 (67)	20.2 (0.3)	17.0 (0.2)
10(1)-1.2-20(2)	1084 (49)	19.3 (0.5)	15.6 (0.3)	**10(2)-1.2-20(1)**	1145 (111)	20.0 (0.8)	16.1 (0.7)
10(1)-1.2-30(2)	1116 (63)	19.1 (0.2)	14.9 (0.2)	**10(2)-1.2-30(1)**	1191 (74)	19.4 (1.1)	15.2 (0.3)
10(1)-1.2-40(2)	1160 (92)	18.8 (0.3)	13.9 (1.0)	**10(2)-1.2-40(1)**	1226 (22)	18.9 (0.7)	14.4 (0.4)
20(1)-1.2-10(2)	1108 (122)	20.6 (0.3)	15.2 (1.0)	**20(2)-1.2-10(1)**	1138 (104)	20.8 (1.5)	15.8 (0.7)
20(1)-1.2-20(2)	1135 (52)	20.1 (0.2)	14.2 (0.2)	**20(2)-1.2-20(1)**	1179 (27)	20.5 (0.5)	14.6 (0.6)
20(1)-1.2-30(2)	1174 (35)	19.7 (0.6)	13.1 (0.2)	**20(2)-1.2-30(1)**	1206 (67)	20.4 (0.7)	13.5 (0.2)
20(1)-1.2-40(2)	1220 (57)	19.4 (1.4)	12.9 (0.2)	**20(2)-1.2-40(1)**	1247 (109)	20.1 (1.4)	13.3 (0.5)
30(1)-1.2-10(2)	1203 (113)	21.4 (0.7)	13.2 (0.8)	**30(2)-1.2-10(1)**	1265 (72)	21.8 (0.2)	13.9 (0.6)
30(1)-1.2-20(2)	1259 (57)	21.3 (1.0)	12.4 (0.9)	**30(2)-1.2-20(1)**	1318 (113)	21.5 (0.5)	13.0 (0.3)
30(1)-1.2-30(2)	1319 (120)	20.8 (0.9)	11.2 (1.0)	**30(2)-1.2-30(1)**	1336 (79)	21.0 (1.6)	12.3 (0.8)
30(1)-1.2-40(2)	1344 (53)	20.1 (0.2)	10.4 (0.9)	**30(2)-1.2-40(1)**	1371 (101)	20.6 (0.5)	11.0 (0.9)
40(1)-1.2-10(2)	1277 (106)	22.4 (0.8)	10.8 (0.6)	**40(2)-1.2-10(1)**	1327 (113)	22.8 (0.5)	11.2 (0.6)
40(1)-1.2-20(2)	1324 (92)	22.2 (0.3)	10.4 (0.3)	**40(2)-1.2-20(1)**	1353 (89)	22.3 (0.2)	10.8 (0.6)
40(1)-1.2-30(2)	1396 (127)	21.5 (0.9)	9.2 (0.3)	**40(2)-1.2-30(1)**	1414 (82)	21.6 (0.7)	10.0 (0.4)
40(1)-1.2-40(2)	1423 (92)	21.2 (0.9)	9.0 (0.3)	**40(2)-1.2-40(1)**	1456 (96)	21.5 (0.4)	9.6 (0.3)

All reported numbers in parenthesis for mechanical properties are standard deviation.

In addition, when the thicker skin is in the extrados, flexural modulus were higher. Increasing the thickness of the skin under tension by up to 2 times, improved the flexural modulus of the sandwich panels by up to a maximum of 10%. On the other hand, increasing the total hemp content in both skins by up to 2 times, increased the flexural modulus by 25%. For example, flexural modulus of 20(1)-0.6-20(2) increased from 1178 MPa to 1747 MPa (30% increase) for 40(1)-0.6-40(2). Consequently, increasing total hemp content in both skins was more effective to improve the flexural modulus compared to increasing the skin thickness.

The flexural strength results for sandwich panels with a foam core are presented in Tables 3.3 and 3.4. Comparing the flexural strength of sandwich panels with 0.6 and 1.2% ACA showed that the core did not influence the flexural strength of the sandwich panels which was mainly controlled by the skins. For example, the flexural strength of 30(1)-0.6-30(2) was 20.9 MPa compared to 20.8 MPa for 30(1)-1.2-30(2).

The effect of skin layers was investigated by comparing the results of flexural strength for different structures. The flexural strength increased with hemp content in the extrados. But, when the hemp content in the intrados was increased, the flexural strength decreased. This means that higher flexural strength could be obtained when the skin with the highest modulus (hemp content) was placed in the extrados and the intrados had the highest elasticity (lower hemp content). For instance, flexural strength of 30(2)-1.2-10(1) (21.8 MPa) was 6% higher than 30(2)-1.2-40(1) with a flexural strength of 20.6 MPa. Moreover, depending on loading direction, different flexural strengths were obtained for a structure. For instance, flexural strength of 40(1)-0.6-10(2) (22.5 MPa) was 16% higher than 10(2)-0.6-40(1) (19.1MPa) which confirmed the dominant role of the skins on flexural strength of sandwich panels [56].

Similar to structures without a foam core, the strain at maximum stress of the structures with foam core decreased as hemp content increased. For instance, 10(2)-0.6-10(1) has a ε_{max} of 18.0%, while sample 40(2)-0.6-40(1) has a ε_{max} of 8.8%. The structure with a lower hemp content skin in extrados had higher ε_{max}. This behavior shows that the elastic properties of the skin in the extrados are controlling the ε_{max} of the whole structure. The ε_{max} of 10(1)-1.2-40(2) was 13.9%, while sample 40(2)-1.2-10(1) had a ε_{max} of 11.2% which was 24% lower. Higher elasticity of the extrados skin played a dominant role in controlling ε_{max} of the structure. Furthermore, comparing ε_{max} of the structures with the same skin in extrados, but different skin in intrados showed that this skin had a small role in controlling deformability. For instance, ε_{max} of 20(2)-1.2-10(1) (15.8%) compared to 20(2)-1.2-40(1) (13.3%) was slightly reduced. Comparing the ε_{max} of structures with different skin thickness showed that thicker skin in extrados led to higher ε_{max}. For instance, ε_{max} of 30(2)-1.2-30(1) is by 10% higher than ε_{max} of 30(1)-1.2-30(2).

Comparing ε_{max} of structures with different core density (0, 0.6 and 1.2% ACA) showed that core properties had a minor influence on the deformability of the sandwich structures because in a flexural test the core carries less load compared to the skin layers [56]. But the structures with higher foaming agent content had lower ε_{max}. For example, the structure 30(1)-0.6-20(2)

had a ε_{max} of 12.4%, while the ε_{max} of 30(1)-1.2-20(2) was 12.1% (6% decrease). Accordingly, the structures without a foam core had higher ε_{max}. For example, the ε_{max} of 20(2)-X-30(1) without a foam core was 16.8%, while ε_{max} of structures with 0.6 and 1.2% ACA foam core decreased to 14.9 and 13.5%, respectively.

Furthermore, the effect of foam core was investigated by comparing the results for specific flexural strength (flexural strength divided by density) in Figure 3.4 and Figure 3.5. The results showed that structures with a foam core have much higher specific flexural strength. Comparing the results for foamed structures, the sandwich panels with 1.2% ACA core showed higher specific properties compared to 0.6% ACA foam core structures.

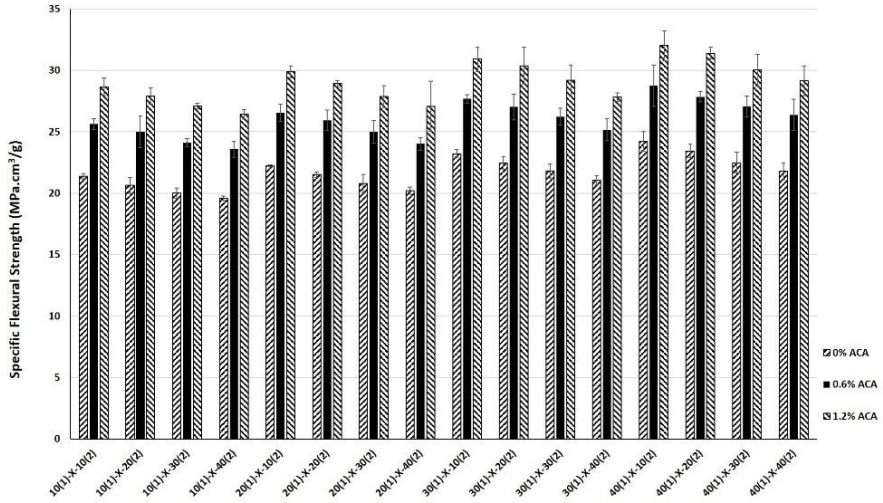

Figure 3.4. Specific flexural strength of structures with A(1)-X-B(2) configuration.

Although the sandwich panels with foam core had similar flexural strength, the main difference was final density. As an example, the specific flexural strength of 20(2)-0-40(1) was 20.9 MPa.cm^3/g, which is 21% lower than 20(2)-0.6-40(1) with 25.2 MPa.cm^3/g and 36% lower than 20(2)-1.2-40(1) with 28.5 MPa.cm^3/g. This was the most noticeable feature of foam core structures. Although, the foam core did not increased the flexural strength of the structures, it produced superior specific flexural strength.

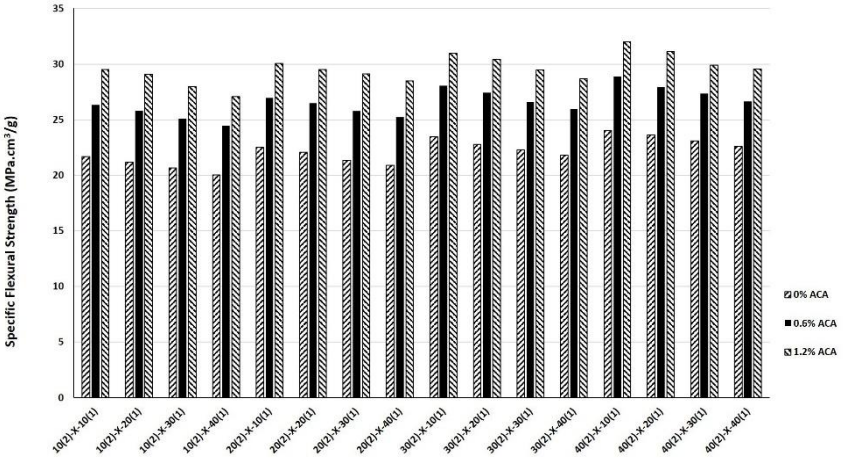

Figure 3.5. Specific flexural strength of structures with A(2)-X-B(1) configuration.

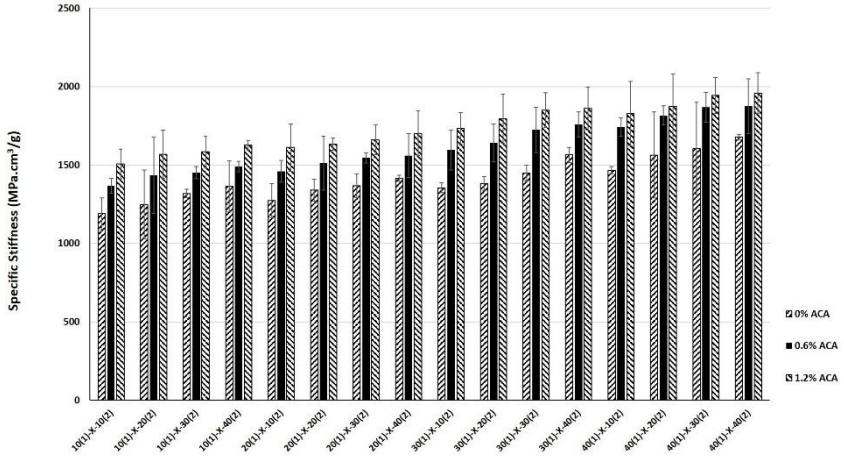

Figure 3.6. Specific stiffness of structures with A(1)-X-B(2) configuration.

In addition, the influence of core type was studied by comparing the specific flexural modulus of the sandwich panels. As observed in Figure 3.6 and Figure 3.7, foaming also increased the specific flexural modulus of the sandwich panels. For instance, the specific flexural modulus of 30(1)-1.2-20(2) and 30(1)-0.6-20(2) are 30% and 19% higher than 30(1)-0-20(2). In the case of 30(2)-X-20(1), the results followed the same trend and the specific flexural modulus

of sandwich panels with 1.2 and 0.6% ACA were 1864 and 1755 MPa.cm^3/g, which were 29 and 21% higher than 1447 MPa.cm^3/g for 30(2)-0-20(1).

Figure 3.8 is presented to better understand the flexural stress-strain behavior of some sandwich panels with different configurations. It can be seen that sandwich panels with higher total hemp (both skins) have higher flexural stress.

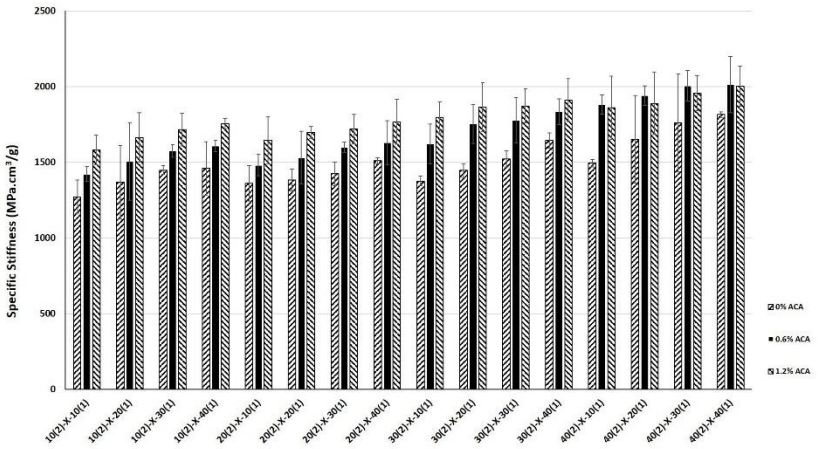

Figure 3.7. Specific stiffness of structures with A(2)-X-B(1) configuration.

For 40(2)-0-40(1), 40(1)-0-40(2), 40(2)-1.2-40(1) and 40(1)-1.2-40(2), the maximum flexural stress were 22.6, 21.7, 21.5 and 21.2 MPa compared to 20.5, 20.2, 20.2 and 19.6 MPa for 10(2)-0-10(1), 10(1)-0-10(2), 10(2)-1.2-10(1) and 10(1)-1.2-10(2). On the other hand, lower amount of hemp content in the sandwich panels gave them higher strain.

Samples 10(2)-0-10(1), 10(1)-0-10(2), 10(2)-1.2-10(1) and 10(1)-1.2-10(2) have ε_{max} of 19.3%, 18.6%, 17% and 16.8% compared to 10.3%, 9.0%, 9.6% and 9% for 40(2)-0-40(1),40(1)-0-40(2), 40(2)-1.2-40(1) and 40(1)-1.2-40(2), respectively. Moreover, comparing the curves showed that thicker skin in extrados improved the flexural stress and ε_{max} of sandwich panels with the same core.

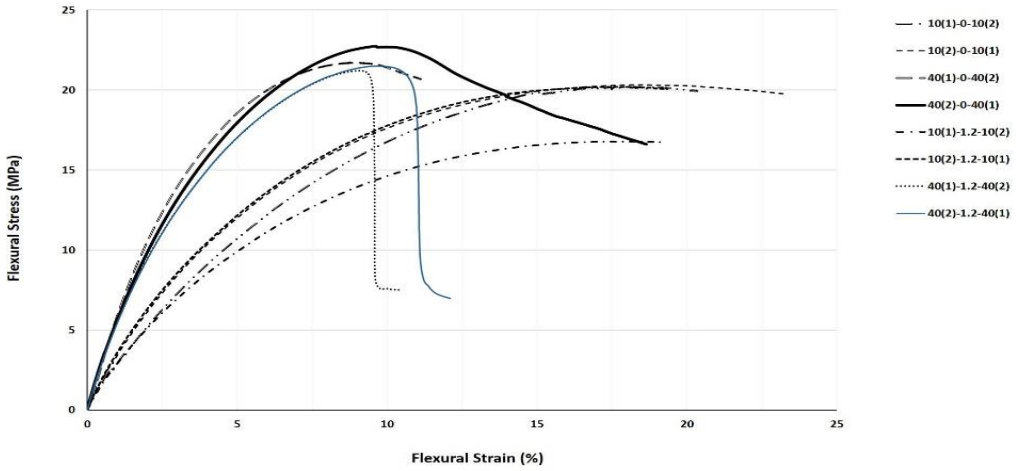

Figure 3.8. Typical flexural stress-strain curves for different sandwich panels with or without foam core.

The optical micrographs of some samples under 5% and 20% strain are presented in Figure 3.9. As it can be seen, at 5% strain all samples remained unbroken, but by increasing strain sample with higher hemp content and foam core started breaking and the fractures penetrated through the thickness of sandwich panels.

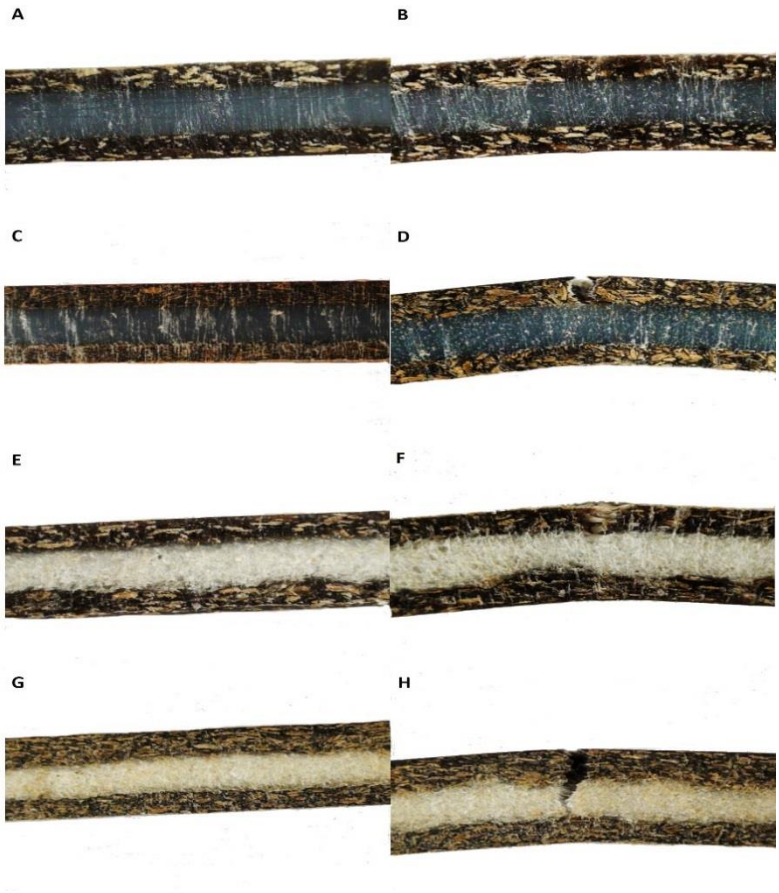

Figure 3.9. Optical micrographs of different samples under 5% (left column) and 20% (right column) flexural strain. A) and B): 10(2)-0-10(1), C) and D): 40(2)-0-40(1), E) and F): 10(2)-1.2-10(1), G) and H): 40(2)-1.2-40(1).

3.4. Conclusion

In this work, three-layer sandwich panels with and without a foam core were produced based on HDPE and hemp fiber via compression molding. The effect of fiber content, layer thickness and blowing agent content on the physical and flexural properties was studied. Morphological characterization of the structures was also discussed.

The morphological properties of the foam core (cell size and cell density) as well as overall density were affected by the foaming agent content. Increasing foaming agent concentration increased cell density, reduced cell size and decreased the density of the structures. Addition

of 1.2% of ACA reduced the overall density of the sandwich panels by 27%. Moreover, the SEM results confirmed that perfect interlaminar adhesion between the skins and the core for both foamed and unfoamed structures was achieved. In all cases, the main failure mode was tensile failure of the skin in extrados.

For all the sandwich panels, with or without a foam core, flexural modulus and flexural strength depend on the skin fiber content and their thickness. On the other hand, deformability of the structures decreased with increasing hemp content. It was also observed that the skin layers have more influence on the flexural properties compared to core properties.

Based on the results obtained, the specific flexural strength was mainly controlled by the core density. The results showed that the specific flexural strength structures with 0.6 and 1.2% ACA foam core were 21 and 36% higher than for an unfoamed one (0% ACA). Similar results were obtained for the specific flexural modulus; i.e. the values are mainly controlled by core density. The addition of 0.6% or 1.2% ACA in the core increased the specific flexural modulus by 21 and 29% compared to structures without a foam core.

Based on the samples produced, it can be concluded that a wide range of physical and flexural properties can be covered by selecting different panel design, especially when asymmetric structures are studied. Nevertheless, more work would be needed to study other mechanical properties like impact strength or sandwich panels based on more than three layers.

Acknowledgements

The authors acknowledge the financial support of the Natural Sciences and Engineering Research Council of Canada (NSERC). The technical help of Mr. Yann Giroux was also much appreciated.

Chapter 4

Low velocity impact behavior of asymmetric three-layer sandwich composite structures with and without foam core

Azam Kavianiboroujeni, Alain Cloutier, Denis Rodrigue, submitted in Applied Polymer Composites Journal, October 2015.

Résumé

Cet article présente une étude expérimentale des propriétés en impact des structures sandwich multicouches, avec ou sans cœur moussé, et constituées de polyéthylène de haute densité (HDPE) et de chanvre. Les tests de poids tombant à faible vélocité et Charpy sont réalisés pour étudier l'influence de la concentration de chanvre, de l'épaisseur de peau et de la densité du cœur moussé. La résistance, la force, l'énergie absorbée et le profil de déflexion sont enregistrés et analysés. Les échantillons endommagés sont ensuite inspectés afin de déterminer les modes de rupture. Les résultats des tests Charpy montrent que les structures avec un cœur moussé ont une capacité d'absorption d'énergie plus élevée comparés à leurs homologues sans cœur moussé. De plus, les résultats des tests de poids tombant à faible vélocité montrent que les structures sandwich sans cœur moussé dissipent mieux l'énergie que les structures avec un cœur moussé. Cette propriété est aussi fortement influencée par la concentration de fibre, l'épaisseur de la peau et la configuration de la structure.

Mots-clés: Mousse; Composite plastique; Comportement au choc; Chanvre; Structure sandwich.

ABSTRACT

This paper presents an experimental investigation of the impact behavior of three layer sandwich structures made of high density polyethylene (HDPE) and hemp with and without a foam core. Low-velocity falling weight and Charpy impact tests are performed to investigate the influence of hemp content, skin thickness, and core density. The strength, load, absorbed energy, and deflection histories are recorded and analyzed and the damaged specimens are then inspected to determine the failure patterns. Based on the Charpy impact results, the structures with foam core had higher energy absorption capability compared to their counterparts without foam core. In addition, based on the falling weight impact results the energy dissipation properties of sandwich structures without foam core are superior to the structures with foam core. This property is also greatly influenced by skin fiber content, skin thickness, and structure configuration.

Keywords: Foam; Plastic composite; Impact; Hemp; Sandwich structures

4.1. Introduction

Over the last decades, structural composite sandwich panels with foam core were widely used in several fields such as aerospace, marine and automobile industries due to their superior stiffness and strength per unit weight compared to engineering materials such as metals and alloys. Improved stability, high energy absorption, as well as improved fatigue properties and corrosion resistance are other benefits of sandwich structures. High energy absorption is due to large voids leading to cell wall collapse by bending and buckling [105-108]. Parameters such as core type, layer thickness and face sheet material control the properties of sandwich materials [109-111]. However, these structures have some limitations such as sensitivity to localized impact loading (low-velocity impact) which degrades the stiffness, strength and load-bearing of the structures due to limited plastic deformation. Tool drop, debris, bird strikes and ballistic loading can induce undetected damages to the composite structures [55, 108]. In this case, characterization of post-impact load-bearing properties of damaged structures is difficult [112]. In some industries such as aerospace and marine, such damages can have serious consequences. Therefore, a significant amount of studies have been done to investigate and predict the impact response of sandwich panels. To simulate the loading conditions to which a sandwich panel is subjected, the impact test fixture can be designed into two forms: low velocity impact by a large mass which can be a falling weight or a swinging pendulum, and high velocity impact by a small mass such as debris which are simulated by a gas gun or ballistic launcher [55].

Some experimental results can be found in the literature. Anderson and Madenci evaluated the low-velocity impact response of sandwich structures with graphite/epoxy faces combined with foam or honeycomb cores [113]. They reported that high-density foam-core and thicker face sheet increased the amount of energy required to generate damages. Park et al. [114] reported that the impact

resistance of sandwich structures with honeycomb core was affected by core thickness and face type. They showed that the main type of impact damage was face delamination. In another study, Mines et al. [115] showed that the energy absorbing capabilities and failure mechanisms of polymer composite sandwich constructions with honeycomb core were controlled by the core and impact velocity. Bernard and Lagace experimentally investigated the impact resistance of graphite-epoxy face sheet sandwich panels with different cores such as foam and honeycomb [116]. They determined the extent of internal delamination damages in sandwich panels by X-ray. In another study, Shih and Jang investigated the impact response of various sandwich panels with PVC foam cores [117]. They showed that the absorbed energy by the sandwich panels with foam cores was 15-100% greater than the sum of the absorbed energy by each constituent alone. Zhou and Hill undertook research on the influence of skin thickness on damage development and energy absorption of sandwich structures [118]. They reported that the sandwich structure rigidity and the mechanism of load transfer among the layers was a function of skin thickness. Foo et al. [106] reported the failure response of aluminum sandwich panels under low-velocity impact. They showed that honeycomb core density influenced the impact response. Hazizan and Cantwell studied the low-velocity impact response of sandwich structure with foam cores [119]. The results showed that the failure modes were dependent on core materials. Wang et al. [111] studied experimentally and numerically the behavior of foam core sandwich panels under low-velocity impact. They investigated the effects of impactor diameter and energy, foam core, and face sheet thickness on the impact behavior and concluded that the impact response was independent of the foam core, while increasing the face sheet thickness decreased the absorbed energy and contact duration. Hitchen and Kemp studied the effect of stacking on impact damage of carbon fibre/epoxy composites. They reported that the stacking sequence influenced the absorbed energy, total delamination area, as well as pre- and post-impact compression strength, while the delamination pattern was affected by fibre fracture. Lee et al. [120] studied the

dynamic response of a composite plate impacted by a ball. They reported that the transverse shear and transverse normal strain were transmitted by the core. They found that the impact velocity determined the contact force between the impactor and the plate. Zhang et al. [121] studied the low-velocity impact response of pyramidal lattice core sandwich panels with polyurethane foam. The results showed that the energy absorption efficiency of sandwich panels filled with higher density foam was lower than unfilled sandwich panels since the influence of the added weight is more important than the improvement given by the filled core. Mohan et al. [122] investigated the impact response and failure modes of aluminum foam with different face sheets. They reported that the impact performance of sandwich structure was mainly affected by the mechanical properties of the face sheets. In another study, Kazemi et al. [123] investigated the effect of stacking sequence and layer thicknesses on Charpy impact of a three-layer structural composite. It was reported that for symmetric configurations, increasing wood content decreased Charpy impact strength, while for asymmetric configuration, Charpy impact strength was independent of layer stacking and wood content.

Although several investigations have been performed on the influence of different parameters (configuration and material properties) on the impact response of sandwich panels, more investigations are necessary to completely understand their effect on the impact response and damage behavior.

In this work, the low-velocity impact behavior of three layer sandwich structures with foam core is studied to determine the effect of core density, skin thickness, and skin composition. Sandwich panels without a foam core are also produced and tested for comparison purposes. The findings in terms of energy/force, load-deflection response, and failure mode are discussed to enable a better understanding of their impact responses. This report is actually a continuous effort to understand the mechanical response of polymer sandwich panels where the morphology, density, and flexural properties of these structures were previously

measured and discussed [124]. These results are used here to explain the impact response observed.

4.2. Materials and methods

High density polyethylene (HDPE) with a melting temperature of 126°C, a melt index of 0.15 g/10 min (190°C, 2.16 kg) and a density of 930 kg/m^3 was supplied by Petromont Canada (C-7525) and used as the matrix. Hemp fiber (sieved larger than 1 mm) with a density of 1.34 g/cm^3 was kindly supplied by the Canadian Hemp Trade Alliance. Maleic anhydride-grafted polyethylene (Epolene C-26, Westlake Chemical Corporation, USA) was used as a coupling agent to improve compatibility, dispersion, and adhesion between HDPE and hemp fibers in the composite. This coupling agent has a density of 919 kg/m^3 and a melting point of 121^{o}C. Azodicarbonamide (Celogen AZ 150, Lion Copolymer, USA) with a decomposing temperature range of 190-220°C and a gas yield of 220 cm^3/g was used as the chemical foaming agent.

HDPE composites with different hemp content (0, 10, 20, 30, and 40% wt.) and HDPE with different azodicarbonamide (ACA) content (0, 0.6, and 1.2% wt.) were prepared as described below to produce the skin and core layers, respectively.

4.2.1. Processing

Sandwich structures were produced in three steps: 1) skin production, 2) core production, and 3) sandwich panel production. The production of the skins started with hemp drying overnight in an oven at 80°C to remove humidity. Then, HDPE/MAPE (9% wt. based on total hemp weight) and hemp (0, 10, 20, 30, and 40% wt.) were introduced in the first and fourth zone of a co-rotating twin-screw extruder (Leistritz ZSE-27, L/D = 40), respectively. The temperature profile for

the 10 zones was set at: 180/185/195/195/195/195/195/195/200/200˚C and the screw speed was controlled 100 rpm. Then, the extruded compounds were pelletized and dried at 80°C overnight in an oven. The composite layers with different hemp content and different thickness were manufactured using compression molding at 170°C under a load of 3 tons by a Carver laboratory press. The composite compounds were first preheated for 3 minutes, then pressed for 5 minutes in molds with dimensions of 250×250×1 or 2 mm^3.

HDPE and ACA (0, 0.6, and 1.2% wt.) were introduced in the first zone of the same extruder with a temperature profile for the 10 zones of 160/165/165/165/165/165/165/160/160/155˚C to limit ACA thermal decomposition in extruder. The layers of HDPE with 0% ACA (4 mm thick) and layers of HDPE with 0.6 and 1.2% ACA (1 mm thick) were produced by compression molding using the same Carver press at 160°C under a load of 3 tons. The temperature was again selected to limit foaming during core compression molding.

As the last step, according to the desired final configuration for sandwich structure with foam core, a core layer with 0.6 or 1.2% ACA was placed between two skins in a mold with dimensions of 250×250×7 mm^3. The sandwich structure was preheated at 225°C for 2 minutes and then 3 tons of load was applied on the mold. Because of high temperature, ACA started to decompose and pressure increased inside the mold. As soon as the pressure started to reduce (ACA decomposition completed), the pressure over the mold was removed and the sandwich panel was cooled down to stabilize the bubbles (foam stabilization).

For sandwich panels with 0% ACA in the core, the skins and HDPE core were transferred to the same mold. Then, the mold was preheated for 3 minutes at a temperature of 170°C and pressed for 5 minutes under a load of 3 tons. Finally, the sandwich structure without foam core was cooled down and removed from the mold.

4.2.2. Specimen coding

The three layer structures are presented with respect to their stacking configuration as: A(y)-X-B(z) where A and B are associated to the hemp content in the skin (% wt.) and X represents the ACA content (% wt.) in the core, while y and z are the layer thickness (mm). For falling-weight impact testing, the first letter in the sample coding represents the top layer. For example, the sample 20(2)-0.6-30(1) represents a sandwich panel with 20% hemp and 2 mm thick skin in the top layer, a foam core with 0.6% wt. ACA, and 1 mm thick with 30% hemp skin in the bottom layer. A schematic representation is presented in Figure 4.1.

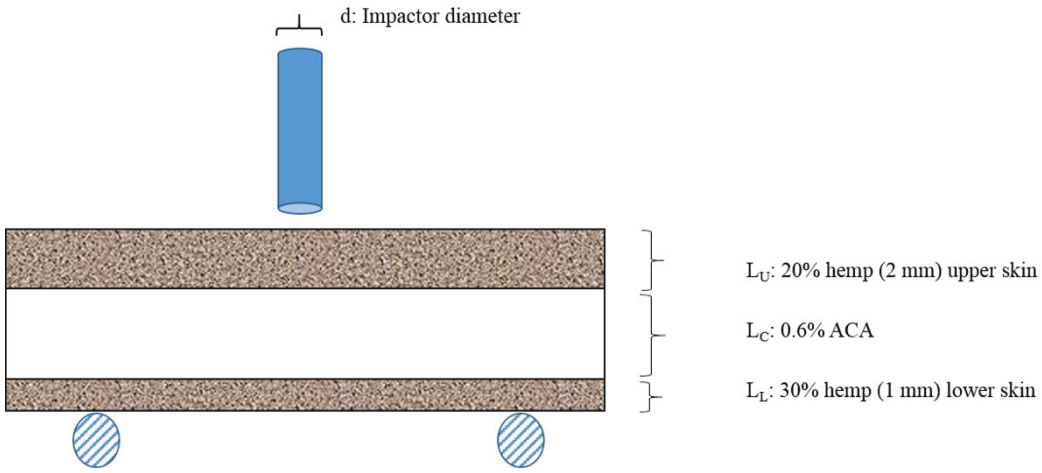

Figure 4.1. Example of sample coding: 20(2)-0.6-30(1).

4.2.3 Mechanical tests

4.2.3.1. Charpy impact test

Charpy impact tests were performed using a Tinius Olsen (model Impact 104) impact tester, according to ASTM D6110. The samples (120×12.7×7 mm^3) were

notched edgewise with a Dynisco model ASN 120m. Ten specimens were tested for each sandwich panel.

4.2.3.2. Falling-weight impact test

Low-velocity impact tests with the same range of energy for all specimens were performed with a drop weight instrumented impact tower, Instron CEAST (Model 9340) according to ASTM D3763. The CEAST DAS 8000 Junior was used as the high speed data acquisition and impact processing system. Response of the impact test was recorded from the data acquisition system in terms of load, time, energy, and displacement.

The test specimens were positioned between two steel plates (support fixtures) with a circular window having a diameter of 76.0 mm in the center of the plates. The steel plates applied enough force to prevent specimen slippage in the clamps. The energy and mass of the impactor were kept constant at 60 J and 5 kg for all specimens to obtain a complete perforation. In this work, the impactor was released from a chosen height and dropped freely along the guide columns. The specimens were impacted at the center of the test section by the hemispherical impactor with a diameter of 12.7 mm and a speed of 3.51 m/s. For each case, at least three specimens were tested.

4.2.3.3. Damage characterization

During the drop-weight impact test, the sandwich panels were damaged internally or externally. These damages can be in the skins, in the core or at the skin-core interface in terms of delamination, elastic cavity formation through the sandwich panels or cavity formation through them by crushing of all layers. After the impact tests, the damage type was evaluated visually using a stereo-microscope (Olympus, SZ-PT).

4.3. Results and discussion

4.3.1. Pendulum impact test

The Charpy impact strength of the sandwich structures with and without foam core is plotted in Figure 2. As expected, the sandwich structures with foam core presented better energy absorption properties because the cellular structure hinders the propagation of the cracks and improves the energy absorption [125]. For example, the impact strength of sample 10(1)-1.2-10(2) is 131 J/m compared to 109 and 99 J/m for samples 10(1)-0.6-10(2) and 10(1)-0-10(2).

Figure 4.2 shows that increasing the total fiber content in the skins reduced the impact properties of all samples because the fibers acted like stress concentration points and provided sites for crack initiation.

Also, strong bonding between the fibers and the matrix due to coupling agent addition increased the stiffening of polymer chains [126]. For instance, the impact strength of sample 20(1)-0-10(2) is 89 J/m compared to 76 J/m for sample 20(1)-0-40(2) which is a 10% decrease. Sandwich structures with similar total fiber content (fixed core), had similar impact strength. For example, the impact strength of 20(1)-0-40(2) and 40(1)-0-20(2) are 83 J/m.

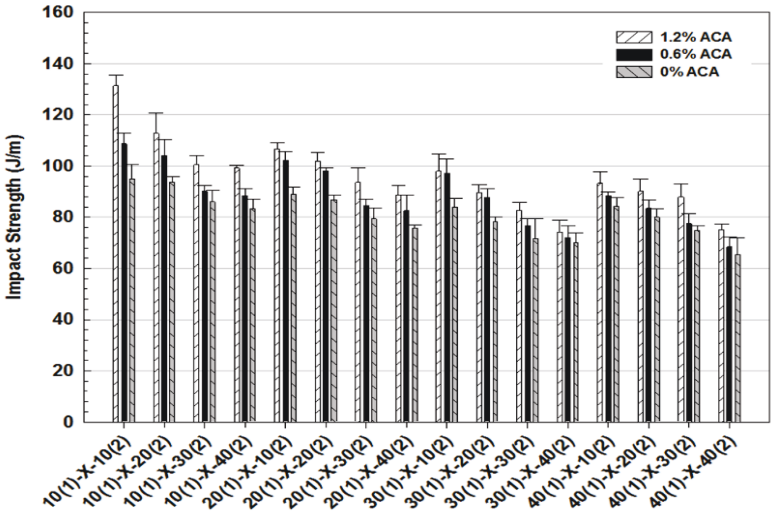

Figure 4.2. Impact strength of the sandwich structures.

The specific impact strength (impact strength divided by density) is plotted in Figure 4.3. It can be seen that sandwich panels with foam core have higher specific impact strength compared to structures without foam core. For instance, the specific impact of 30(1)-1.2-20(2) and 30(1)-0.6-20(2) are 128 and 112 $J.cm^3/m.g$ which are 60% and 40% higher respectively, than the specific impact strength of 30(1)-0-20(2) which is 81 $J.cm^3/m.g$.

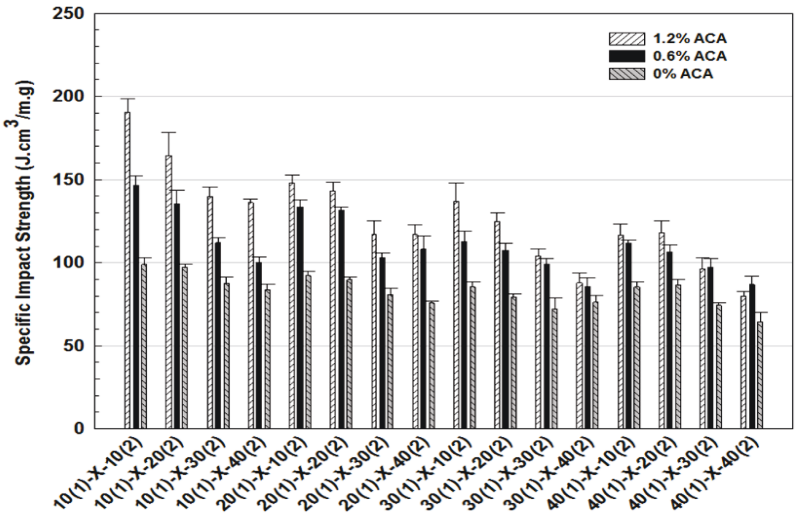

Figure 4.3. Specific impact strength of the sandwich structures.

4.3.2. Falling weight impact test

Falling weight drop impact tests were carried out on sandwich panels with and without foam core. The impactor energy was selected at 60 J to completely perforate the structures.

The response of a sandwich structure to impact test can be characterized by a load-deflection curve. The shape of this curve is influenced by the shape of the impactor, stacking sequence, and layer thickness. In this curve, the maximum force is defined as the maximum force a sandwich panel can sustain and the contact duration is the total contact time between impactor and sandwich panel up to perforation [127]. Figure 4.4 shows typical force-deflection curves of the perforated sandwich structures with and without foam core.

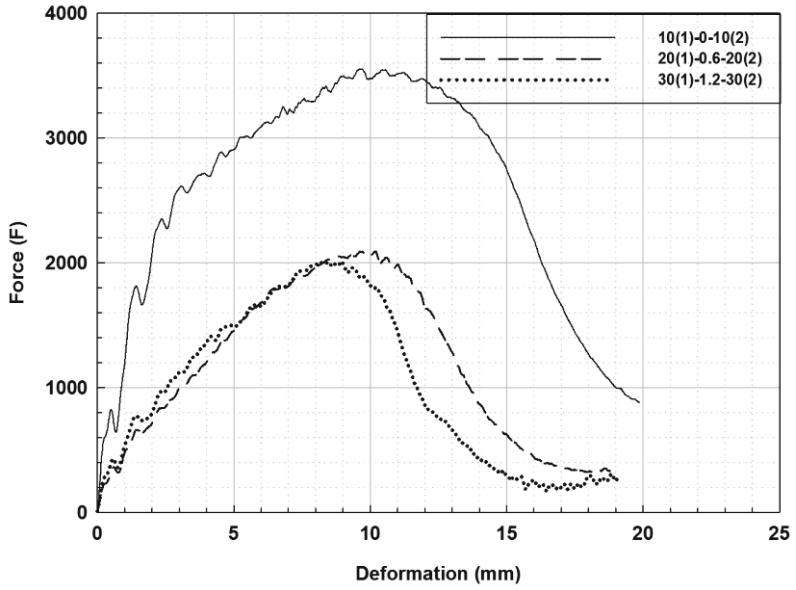

Figure 4.4. Typical force-deformation curves for selected samples.

As it can be seen in Figure 4.4, all the curves have similar shapes. In the loading or stiffening section the force increases with deformation, while in the unloading or softening section the force decreases with deformation. All the curves are open curves ending at nearly constant value which is called the pure friction zone showing that the impactor completely perforates the sandwich panels and loses contact [128].

The failure of the sandwich structures is characterized by a variety of changes in the load-displacement curve. Two thresholds are identified in the load-deformation responses. The first one is called Hertzian failure and takes place when the force increases to a peak, then falls suddenly and continues oscillating [113, 129, 130]. Hertzian failure denotes the first initial damages in the structures which can be in the form of layer delamination [128, 129, 131]. The sharp drop of force and change in the curve slope after Hertzian failure are related to stiffness reduction of the structure by delamination [114]. The second threshold or the

maximum force corresponds to the driving force for the first structure failure in the form of fiber breakage and skin failure. It determines the load carrying capacity and integrity of the structure.

The total absorbed energy by the structures, which includes elastic and plastic contributions, is a measure of dissipated energy by different damage phenomena occurring through the structure [55]. Energy absorption can be calculated using the force history. In this work, the mechanical response of low-velocity impacted sandwich panels is characterized in terms of peak load, deflection at peak load, and total absorbed energy.

4.3.2.1. Sandwich structures without foam core

The mechanical responses of structures without foam core are presented in Table 4.1. According to the results, increasing the total amount of hemp in the skins led to higher peak load that determined the load bearing capacity of the structures. This behavior may be associated with the skins stiffness; i.e. as the stiffness increased, so did the peak load. For instance, increasing hemp content in both skins from 10% (10(1)-0-10(2)) to 40% (40(1)-0-40(2)), improved the peak load from 3518 to 4459 N which is an increase of 27%. This can be associated with the stiffness of 10(1)-0-10(2) and 40(1)-0-40(2) which were reported to be 1124 and 1676 MPa, respectively [124].

Moreover, the effect of increasing hemp content in the top skin to improve the peak load is more pronounced than for the bottom skin. As an example, the peak load value of 10(2)-0-10(1) is 3236 N, while the value increased to 3751 N for 40(2)-0-10(1) and to 3474 N for 10(2)-0-40(1) which are about 16% and 7% improvement, respectively. This is directly related to structure stiffness for 10(2)-0-10(1), 40(2)-0-10(1) and 10(2)-0-40(1) which were 1205, 1466, and 1405 MPa, respectively [124].

Table 4.1. Mechanical response of low-velocity impacted sandwich panels without a foam core.

Sample	Max. force (N)	Deflection @ max. force	Energy (J)	Sample	Max. force (N)	Deflection @ max. force	Energy (J)
10(2)-0-10(1)	3236 (232)	10.2 (0.2)	23.8 (2.1)	**10(1)-0-10(2)**	3518 (139)	10.3 (0.5)	25.3 (1.5)
10(2)-0-20(1)	3316 (178)	9.9 (0.7)	23.2 (1.9)	**10(1)-0-20(2)**	3555 (78)	10.0 (0.6)	24.7 (1.6)
10(2)-0-30(1)	3386 (203)	9.2 (0.5)	22.5 (0.8)	**10(1)-0-30(2)**	3600 (302)	9.5 (0.8)	24.2 (0.8)
10(2)-0-40(1)	3474 (213)	8.9 (0.9)	22.1 (1.5)	**10(1)-0-40(2)**	3671 (199)	9.0 (0.1)	24.0 (1.9)
20(2)-0-10(1)	3347 (180)	9.6 (0.4)	22.4 (2.0)	**20(1)-0-10(2)**	3581 (241)	9.8 (0.7)	24.3 (2.0)
20(2)-0-20(1)	3425 (53)	9.1 (0.7)	21.5 (1.1)	**20(1)-0-20(2)**	3722 (277)	9.3 (0.6)	23.9 (1.3)
20(2)-0-30(1)	3522 (276)	8.9 (0.5)	20.9 (0.9)	**20(1)-0-30(2)**	3818 (168)	9.1 (0.5)	23.2 (0.8)
20(2)-0-40(1)	3645 (64)	8.5 (0.6)	20.3 (1.4)	**20(1)-0-40(2)**	3890 (315)	8.8 (0.4)	22.6 (0.5)
30(2)-0-10(1)	3499 (207)	9.0 (0.3)	20.5 (1.7)	**30(1)-0-10(2)**	3770 (63)	9.1 (0.5)	23.1 (1.1)
30(2)-0-20(1)	3587 (154)	8.6 (0.2)	19.9 (0.5)	**30(1)-0-20(2)**	3921 (98)	8.8 (0.7)	22.2 (1.6)
30(2)-0-30(1)	3690 (320)	8.3 (0.5)	19.5 (1.2)	**30(1)-0-30(2)**	4103 (170)	8.4 (0.6)	21.3 (1.2)
30(2)-0-40(1)	3801 (104)	8.0 (0.4)	19.2 (0.8)	**30(1)-0-40(2)**	4218 (261)	8.1 (0.5)	21.0 (0.9)
40(2)-0-10(1)	3751 (298)	8.3 (0.3)	19.2 (1.3)	**40(1)-0-10(2)**	4151 (307)	8.6 (0.7)	21.5 (1.3)
40(2)-0-20(1)	3960 (195)	7.9 (0.3)	18.7 (1.7)	**40(1)-0-20(2)**	4285 (281)	8.2 (0.1)	20.4 (2.0)
40(2)-0-30(1)	4146 (330)	7.6 (0.5)	17.5 (0.6)	**40(1)-0-30(2)**	4383 (365)	7.8 (0.2)	19.5 (0.4)
40(2)-0-40(1)	4305 (256)	7.4 (0.6)	17.0 (0.7)	**40(1)-0-40(2)**	4459 (255)	7.6 (0.6)	19.0 (0.8)

Numbers in parentheses are standard deviations.

Furthermore, the peak load is dependent on the sandwich panel configuration and different results for peak load are obtained depending on load direction. As the thicker skin is placed as the bottom skin, the peak load increased [111]. This can be seen by comparing the values for series A(1)-0-B(2) and A(2)-0-B(1). For instance, the peak load of 30(1)-0-30(2) is 4103 N which is 11% higher than the peak load of 30(2)-0-30(1) with a peak load of 3690 N.

The deflection of the structures is affected by the total hemp content in both skins. As the total hemp content increased in the structures, the deflection at peak load decreased. Samples 10(1)-0-10(2) with 10.3 mm and 40(2)-0-40(1) with 7.4 mm have the highest and lowest deflections at peak load. Comparing the structures with similar skins show that higher deflections at peak load are obtained when the top skin has higher deformability. For example, the deflection of the structure

10(2)-0-40(1) is 8.9 mm, while the deflection of 40(2)-0-10(1) is 8.3 mm. The flexibility of the structures is slightly influenced by the thickness of the skins. As the thicker skin is placed as the bottom skin, the deformability of the structure is improved. For instance, the deflection of 40(1)-0-40(2) is 8.3 mm compared to 8.6 mm for 40(2)-0-40(1) (4% increase).

In the case of absorbed energy, different results are obtained depending on the sandwich panel structures and load direction. For all structures, the absorbed energy of the structure with thicker bottom skins is higher. As an example, the absorbed energy by 40(1)-0-40(2) is 19.0 J, which is 12% higher than 40(2)-0-40(1) with 17.0 J. The dependence of the absorbed energy to the load direction can be attributed to the fracture pattern difference between foamed and unfoamed cores, as well as the total surface area which diffused the impact energy [132]. Moreover, the absorbed energy is dependent on the total hemp content. As the total hemp content increased, the total absorbed energy decreased. As the total hemp content of a structure increased, the energy dissipation capacity is reduced because of lower deformability and absorbed energy in terms of elastic energy.

The absorbed energy of structure 10(1)-0-10(2) is 23.8 J, while samples 10(1)-0-40(2) and 40(1)-0-40(2) absorb 22.1 and 17.0 J, respectively. The results of Table 1 indicates that the energy absorption capacity of the structures is affected by the direction of applied load and skin thickness. The total absorbed energy of the structures are improved when the top skin has more deformability (lower fiber content) and the bottom skin is thicker. The maximum value of absorbed energy for the structures without foam core belongs to 10(1)-0-10(2) with 25.3 J, while structure 40(2)-0-40(1) has the least energy absorption capacity with 17.0 J. Changes in the total absorbed energy confirm that the properties of the skins influence the mode of energy absorption [133].

4.3.2.2. Sandwich structures with foam core

The mechanical response of low-velocity impacted sandwich panels with foam core are presented in Tables 4.2 and 4.3.

Table 4.2. Mechanical response of low-velocity impacted sandwich panels with a 0.6% ACA foam core.

Sample	Max. force (N)	Deflection @ max. force	Energy (J)	Sample	Max. force (N)	Deflection @ max. force	Energy (J)
10(2)-0.6-10(1)	1856 (127)	10.7 (0.8)	15.9 (1.1)	**10(1)-0.6-10(2)**	1934 (115)	10.6 (0.8)	16.8 (1.2)
10(2)-0.6-20(1)	1888 (51)	10.0 (0.5)	15.3 (0.9)	**10(1)-0.6-20(2)**	2000 (189)	10.2 (0.5)	16.5 (1.1)
10(2)-0.6-30(1)	1929 (18)	9.9 (0.6)	14.6 (0.8)	**10(1)-0.6-30(2)**	2056 (71)	10.0 (0.3)	16.3 (0.8)
10(2)-0.6-40(1)	1958 (43)	9.6 (0.3)	14.1 (0.9)	**10(1)-0.6-40(2)**	2101 (129)	9.8 (0.6)	15.7 (0.5)
20(2)-0.6-10(1)	1926 (60)	9.8 (0.8)	14.4 (1.0)	**20(1)-0.6-10(2)**	2018 (67)	10.0 (0.4)	16.1 (1.4)
20(2)-0.6-20(1)	1999 (95)	9.6 (0.4)	13.9 (0.5)	**20(1)-0.6-20(2)**	2092 (49)	9.8 (0.8)	15.4 (0.3)
20(2)-0.6-30(1)	2104 (101)	9.2 (0.4)	13.2 (0.6)	**20(1)-0.6-30(2)**	2174 (136)	9.5 (0.4)	14.9 (0.5)
20(2)-0.6-40(1)	2138 (77)	9.0 (0.6)	12.6 (0.4)	**20(1)-0.6-40(2)**	2238 (50)	9.1 (0.5)	14.2 (0.5)
30(2)-0.6-10(1)	2061 (158)	9.2 (0.1)	13.0 (0.3)	**30(1)-0.6-10(2)**	2113 (91)	9.4 (0.7)	14.4 (0.2)
30(2)-0.6-20(1)	2126 (39)	9.1 (0.3)	12.4 (0.9)	**30(1)-0.6-20(2)**	2238 (174)	9.3 (0.2)	13.8 (0.1)
30(2)-0.6-30(1)	2229 (152)	8.5 (0.7)	11.8 (0.4)	**30(1)-0.6-30(2)**	2370 (126)	8.8 (0.6)	13.2 (0.8)
30(2)-0.6-40(1)	2308 (124)	8.1 (0.4)	11.2 (0.6)	**30(1)-0.6-40(2)**	2396 (188)	8.4 (0.3)	12.4 (0.8)
40(2)-0.6-10(1)	2221 (98)	8.4 (0.2)	11.4 (0.5)	**40(1)-0.6-10(2)**	2368 (201)	8.5 (0.4)	12.7 (0.8)
40(2)-0.6-20(1)	2338 (131)	8.0 (0.1)	10.8 (0.7)	**40(1)-0.6-20(2)**	2413 (73)	8.2 (0.5)	11.8 (0.7)
40(2)-0.6-30(1)	2407 (201)	7.9 (0.2)	10.3 (0.4)	**40(1)-0.6-30(2)**	2485 (131)	8.0 (0.7)	11.6 (0.3)
40(2)-0.6-40(1)	2517 (142)	7.8 (0.3)	9.5 (0.3)	**40(1)-0.6-40(2)**	2599 (179)	7.9 (0.1)	11.3 (0.6)

Numbers in parentheses are standard deviations.

The peak load of the sandwich structures are affected by skin fiber content, layer stacking, and core properties. The peak load values for the structures with 0.6% and 1.2% ACA increase with total fiber content. For instance, the peak load of 40(1)-0.6-40(2) (2599 N) is 34% higher compared to the structure 10(1)-0.6-10(2) (1934 N). Similarly, the peak load of 10(1)-1.2-10(2) increases from 1713 to 2196 N for 40(1)-1.2-40(2) (28% improvement). This behavior show that stiffer skins with low elasticity improve the peak load of the whole structure. Moreover, the

results indicate that the top skin played a more dominant role controlling the structure peak load. For instance, the peak load of structure 10(1)-0.6-40(2) is 2101 N compared to 2599 N for 40(1)-0.6-10(2).

In the case of skin thickness, the results show that a thicker bottom skin improves the peak load of the structures. As an example, the peak load of sample 10(1)-0.6-30(2) (2056 N) is about 7% higher than the peak load of structure 10(2)-0.6-30(1) (1929 N). Throne et al. [134] showed that typical structural foams fail at impact load between one and 20 times lower than their unfoamed counterparts, but skin thickness is the main parameter controlling the level.

The deflection at peak load results for sandwich panels with foam core are presented in Tables 4.2 and 4.3. Comparing the deflection at maximum force of the structures with 0.6 and 1.2% ACA shows that they are not significantly affected by the foam core. For instance, the deflection of 10(2)-0.6-10(1) and 10(2)-1.2-10(1) are 10.7 and 10.6 mm, while the deflection of 20(2)-0.6-10(1) and 20(2)-1.2-10(1) are 9.8 and 9.9 mm, respectively. This can be explained as the core density decreased, the role of the core decreases as well and the skins are governing the deflection of the sandwich structures under impact [133].

On the other hand, comparing the deflection of the structures with and without foam cores shows that structures with foam core have higher deflection. The deflection of structure 20(2)-X-30(1) for 0, 0.6, and 1.2% ACA are 8.9, 9.2, and 9.3 mm, respectively. In this case, as the structures with HDPE core are perforated, bending and stretching of the skins are not the main failure modes contrary to structures with foam core which have higher deflection due to their lower stiffness.

Table 4.3. Mechanical response of low-velocity impacted sandwich panels with a 1.2% ACA foam core.

Sample	Max. force (N)	Deflection @ max. force	Energy (J)	Sample	Max. force (N)	Deflection @ max. force	Energy (J)
10(2)-1.2-10(1)	1674 (123)	10.6 (0.4)	14.4 (0.9)	**10(1)-1.2-10(2)**	1713 (58)	10.7 (1.0)	15.3 (0.5)
10(2)-1.2-20(1)	1701 (92)	10.1 (0.2)	14.2 (1.2)	**10(1)-1.2-20(2)**	1749 (72)	10.2 (0.5)	14.8 (1.2)
10(2)-1.2-30(1)	1751 (75)	9.8 (0.5)	13.2 (0.5)	**10(1)-1.2-30(2)**	1788 (146)	10.1 (0.6)	14.6 (0.3)
10(2)-1.2-40(1)	1820 (145)	9.7 (0.6)	12.7 (0.6)	**10(1)-1.2-40(2)**	1849 (92)	9.9 (0.1)	14.0 (0.2)
20(2)-1.2-10(1)	1776 (94)	9.9 (0.1)	12.9 (0.4)	**20(1)-1.2-10(2)**	1801 (71)	10.0 (0.4)	14.2 (0.6)
20(2)-1.2-20(1)	1844 (87)	9.5 (0.4)	12.0 (0.3)	**20(1)-1.2-20(2)**	1870 (126)	9.7 (0.3)	13.5 (0.4)
20(2)-1.2-30(1)	1885 (153)	9.3 (0.4)	11.3 (0.7)	**20(1)-1.2-30(2)**	1914 (34)	9.4 (0.2)	13.0 (1.2)
20(2)-1.2-40(1)	1937 (49)	9.1 (0.3)	10.7 (1.1)	**20(1)-1.2-40(2)**	1957 (171)	9.2 (0.5)	12.2 (0.9)
30(2)-1.2-10(1)	1891 (166)	9.2 (0.7)	11.2 (0.3)	**30(1)-1.2-10(2)**	1912 (97)	9.3 (0.1)	12.6 (0.7)
30(2)-1.2-20(1)	1950 (61)	8.9 (0.2)	10.3 (0.1)	**30(1)-1.2-20(2)**	1975 (56)	9.1 (0.7)	11.9 (0.4)
30(2)-1.2-30(1)	1985 (128)	8.6 (0.7)	9.8 (0.4)	**30(1)-1.2-30(2)**	2014 (81)	8.9 (0.2)	11.2 (0.3)
30(2)-1.2-40(1)	2032 (151)	8.2 (0.1)	8.2 (0.3)	**30(1)-1.2-40(2)**	2070 (160)	8.7 (0.5)	10.6 (0.5)
40(2)-1.2-10(1)	2020 (43)	8.4 (0.1)	9.2 (0.3)	**40(1)-1.2-10(2)**	2087 (49)	8.5 (0.1)	10.9 (0.2)
40(2)-1.2-20(1)	2067 (114)	8.0 (0.1)	7.6 (0.5)	**40(1)-1.2-20(2)**	2118 (171)	8.2 (0.6)	10.1 (0.8)
40(2)-1.2-30(1)	2095 (102)	7.8 (0.7)	6.9 (0.4)	**40(1)-1.2-30(2)**	2153 (153)	7.9 (0.6)	9.3 (0.2)
40(2)-1.2-40(1)	2134 (50)	7.6 (0.4)	6.6 (0.1)	**40(1)-1.2-40(2)**	2196 (124)	7.7 (0.5)	8.3 (0.2)

As the density of the core decreases, the role of the skins on the structure deflection is more important. Therefore, the deflection of the structures with foam core is controlled by the total hemp content. As the total hemp content increases, the structure deflection decreases which is ascribed to lower elasticity of the structure. For instance, the deflection of 20(1)-0.6-20(2) (9.8 mm) is higher than the deflection of 30(1)-0.6-30(2) (8.8 mm). Moreover, the results show that skin thickness and load direction slightly influence the deflection of the structure. The deflection of 30(1)-1.2-40(2) is 8.7 mm which is 6% higher than for 30(2)-1.2-40(1) with a deflection of 8.2 mm. This indicates that thicker bottom skins improve the deflection of the structures.

Comparing the total absorbed energy indicates that the energy absorbing capacity of the structures with foam core is dependent on core density, skin type, and load direction. The total absorbed energy increases significantly with increasing core density. The total absorbed energy increases during the perforation as in denser specimens more material is available to absorb energy [49]. As seen in Tables 4.2 and 4.3, the total absorbed energy for structures with 0.6% ACA core is higher than their counterparts with 1.2% ACA core. For instance, the structure 40(2)-0.6-40(1) absorbed 9.5 J which is about 44% higher than the total absorbed energy by 40(2)-1.2-40(1) (6.6 J).

Comparing all the results with or without a foam core shows that sandwich structures with unfoamed HDPE core absorbed more energy to be perforated. As an example, the total absorbed energy of the series 10(1)-X-10(2) for 0, 0.6, and 1.2% ACA are 25.3, 16.8, and 15.3 J, respectively. These results show how the core density controls the energy absorption capacity of the sandwich structures.

Furthermore, the effect of wood content in the skin layers is studied comparing the results for total absorbed energy in Tables 2 and 3. As the total hemp content increases in the structures, the total absorbed energy decreases. For example, the total absorbed energy of 10(1)-0-10(2) is 15.3 J which is 84% higher than the 8.3 J obtained for 40(1)-0-40(2). The flexibility of the structure decreases and stiffness increases, reducing the ability to absorb energy elastically [135, 136].

Stacking sequence also influences the energy absorption properties of the structures. As the thicker skin is set as the bottom skin, the total absorbed energy increases for all specimens with foam core. For instance, the total absorbed energy of 30(1)-1.2-20(2) is 11.9 J which is higher than 10.3 J for 30(2)-1.2-20(1).

The force-deformation curves of some samples with different core density are shown in Figure 4.5.

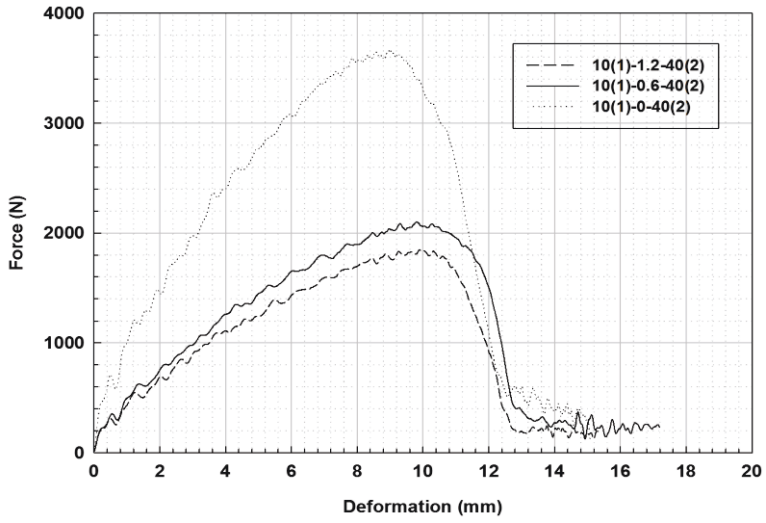

Figure 4.5. Typical force-deformation curves for selected samples.

The force response of the structures is dependent on core density and structure configuration. As the structure stiffness increases, the slope of the force-deformation curve at low deformation increases. Moreover, in structures with foam core, Hertzian failure takes place at lower deformation compared to their counterparts without foam core.

The slope of the curve at low deformation is dependent on the core. As the stiffness of the core increases, the slope of the curve increases accordingly. For instance, the slope of the energy-deformation curve of 40(1)-0-40(2), 40(2)-0-40(1), and 10(1)-0-10(2) between deflections of 2-5 mm are 1.29, 1.53, and 1.27 J/mm, while for the same deformation range, the slopes for 40(1)-1.2-40(2), 10(1)-1.2-10(2), and 10(1)-0.6-10(2) are 0.72, 0.76, and 0.83 J/mm, respectively.

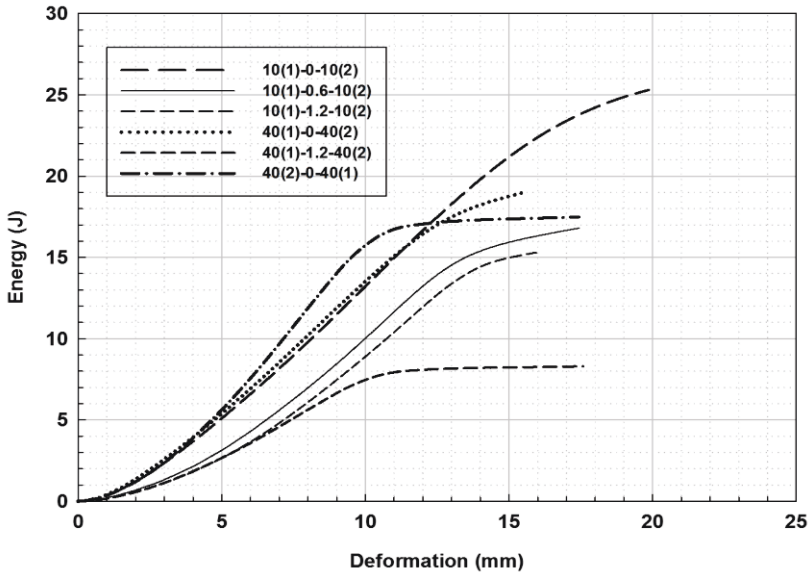

Figure 4.6. Typical energy-deformation curves for selected samples.

On the other hand, the total absorbed energy is negatively influenced by the total amount of hemp in the structures. Lower hemp content in the structures leads to higher deformability and total absorbed energy. For instance, the total absorbed energy of 10(1)-0-10(2) and 10(1)-1.2-10(2) are 25.3 and 15.3 J, while 19.0 and 8.3 J are obtained for 40(1)-0-40(2) and 40(1)-1.2-40(2), respectively.

Moreover, the total absorbed energy is dependent on the load direction as structures with thinner top skins dissipate energy better [132]. For example, the absorbed energy of 40(1)-0-40(2) with 19.0 J is higher than 17.0 J for 40(2)-0-40(1).

4.4. Failure modes

After impact testing, all the sandwich panels were carefully examined with an optical microscope to study the failure modes and then cut through the perforation

to study their cross-section. As it can be seen in Figure 4.7, the failure modes are strongly governed by the sandwich layer stacking and properties of the core. The configuration of the sandwich panels and skins thickness do not influence the failure modes.

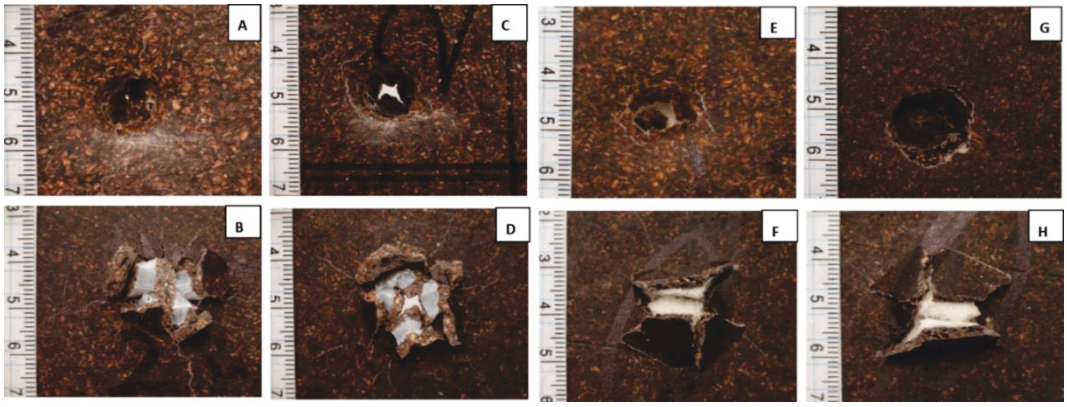

Figure 4.7. Overview images of selected samples: A, B) 10(1)-0-40(2), C, D) 20(2)-0-40(1), E, F) 10(1)-0.6-40(2), and G, H) 20(2)-1.2-40(1).

The common point between all the specimens is that damages in the bottom skin (Figure 4.7 (B), (D), (F) and (H)) are more important (severe) than for the top skin (Figure 4.7 (A), (C), (E) and (G)) as reported by Tovar-Cisneros et al. [132] The maximum perforation size in the sandwich panels with less rigid top skin (10%, 20% hemp), is similar to the impactor diameter where damages are more likely to be ductile, while the skins are deformed plastically before fracturing. In sandwich panels with high hemp content skins (30%, 40%), damages in the bottom skin are more brittle where the surface is broken into pieces with sharp edges and deep cracks in both skins.

Figure 4.7 (A) and (E) show that sandwich panels with low hemp content skins have lower damaged area and the shape of the perforation is more cylindrical, unlike sandwich panels with high hemp content skins for which the damaged area is larger with a conical shape.

The comparison between impacted specimens with different foam cores shows no difference between failure modes. All the sandwich panels with foam core (Figure 4.7 E, F, G, H) show fiber breakage, matrix breakage, and core crushing, as well as bending and shear failure. But, for sandwich panels with unfoamed HDPE core, (Figure 4.7 A, B, C, D), the samples suffer from serious damages such as bottom skin-core delamination, more severe cracks, and lower skin splitting which could be explained by higher absorbed energy and impact forces, different load transfer mechanisms between layers, as well as their tensile and shear fracture properties [119]. In these structures, the occurrence of core bending and shear failure is low, while it is more probable in sandwich structures with foam core. The failure modes in sandwich panels without foam core show that a significant amount of energy is dissipated through interlaminar damage and crack propagation. On the other hand, sandwich panels without foam core are more prone to delamination due to high core modulus [119]. As shown in Figure 4.8, the fracture angle in the sandwich structures with foam core is about 45° as reported by Throne et al. [134].

Figure 4.8. Cross-section images of the perforated sandwich structures: A) 40(1)-0-40(2), B) 10(1)-0-20(2), C) 40(1)-0.6-40(2), D) 10(1)-0.6-20(2), E) 40(1)-1.2-40(2), and F) 10(1)-1.2-20(2).

In the sandwich structures without foam core, the angle is close to 90°. Tovar-Cisneros et al. [132] also reported these differences between the impact strength of asymmetric structural foams and their unfoamed counterparts. Based on their observations, a model was proposed to relate the inside area of the fractured hole with the bottom skin thickness. The equation was then used to calculate the total area diffusing the impact energy in sandwich structures with foam core (see Figure 4.1 for parameter definition):

$$S = \pi d L_U + \sqrt{2}\pi(d + L_C)L_C + \pi(d + 2L_C)L_L \quad (4\text{-}1)$$

and the following equation was proposed for sandwich structures without foam core:

$$S' = \pi d(L_U + L_C + L_L) \quad (4\text{-}2)$$

The calculated results of S/S' (normalized area) for two sandwich configurations with L_u = 1 mm, L_C = 4 mm, L_L = 2 mm, and L_u = 2 mm, L_C = 4 mm, L_L = 1 mm are 1.67 and 1.58, respectively. The difference between the normalized areas for these two configurations shows that the perforated area depends on skin thickness. As the thickness of the top skin decreases, the interior area of the perforated hole increases accordingly, thus more energy is needed for complete perforation.

The relative absorbed energy, which is defined as the total absorbed energy of the sandwich structure with foam core compared to its counterpart without foam core, is presented in Table 4.4. As the total hemp content of the structure increases, the difference between the normalized area and the relative absorbed energy increases which can be attributed to different fracture modes depending on the skin. For example, the relative absorbed energy of 10(2)-1.2-10(1) and 40(2)-1.2-40(1) are 1.65 and 2.58, respectively.

Table 4.4. Relative absorbed energy (dimensionless) of the sandwich structures with 0.6 and 1.2% ACA compared to the structures with 0% ACA.

Sample	0.6% ACA	1.2% ACA	Sample	0.6% ACA	1.2% ACA
10(2)-X-10(1)	1.49 (0.16)	1.65 (0.13)	**10(1)-X-10(2)**	1.50 (0.13)	1.65 (0.10)
10(1)-X-10(2)	1.51 (0.14)	1.64 (0.14)	**10(1)-X-10(2)**	1.50 (0.13)	1.67 (0.15)
10(2)-X-30(1)	1.55 (0.09)	1.70 (0.09)	**10(1)-X-30(2)**	1.49 (0.08)	1.65 (0.07)
10(2)-X-40(1)	1.57 (0.13)	1.74 (0.11)	**10(1)-X-40(2)**	1.53 (0.11)	1.71 (0.05)
20(2)-X-10(1)	1.55 (0.16)	1.74 (0.10)	**20(1)-X-10(2)**	1.50 (0.17)	1.71 (0.13)
20(2)-X-20(1)	1.55 (0.09)	1.79 (0.06)	**20(1)-X-20(2)**	1.55 (0.07)	1.76 (0.05)
20(2)-X-30(1)	1.58 (0.09)	1.84 (0.11)	**20(1)-X-30(2)**	1.55 (0.07)	1.78 (0.13)
20(2)-X-40(1)	1.61 (0.10)	1.89 (0.13)	**20(1)-X-40(2)**	1.59 (0.06)	1.85 (0.11)
30(2)-X-10(1)	1.58 (0.11)	1.84 (0.05)	**30(1)-X-10(2)**	1.61 (0.06)	1.83 (0.07)
30(2)-X-20(1)	1.60 (0.10)	1.93 (0.08)	**30(1)-X-20(2)**	1.61 (0.08)	1.86 (0.04)
30(2)-X-30(1)	1.65 (0.10)	1.99 (0.07)	**30(1)-X-30(2)**	1.61 (0.12)	1.90 (0.09)
30(2)-X-40(1)	1.71 (0.10)	2.32 (0.09)	**30(1)-X-40(2)**	1.69 (0.11)	1.98 (0.11)
40(2)-X-10(1)	1.69 (0.11)	2.10 (0.08)	**40(1)-X-10(2)**	1.69 (0.12)	1.96 (0.08)
40(2)-X-20(1)	1.74 (0.16)	2.47 (0.13)	**40(1)-X-20(2)**	1.73 (0.16)	2.01 (0.14)
40(2)-X-30(1)	1.70 (0.07)	2.52 (0.10)	**40(1)-X-30(2)**	1.68 (0.05)	2.11 (0.05)
40(2)-X-40(1)	1.79 (0.07)	2.58 (0.05)	**40(1)-X-40(2)**	1.69 (0.10)	2.29 (0.08)

Numbers in parentheses are standard deviations.

Moreover, as the core density increases, the difference between the normalized area and the specific absorbed energy increases because the fracture cannot be assumed as brittle which is the main assumption to have a fracture with a 45° angle. Therefore, as the core density increases, the fracture angle increases and structures with low density foam core absorb energy by deformation, indentation, and compression, thus the impacted area absorbing energy increases [134]. For example, the relative absorbed energy of 40(1)-0.6-40(2) and 40(1)-1.2-40(2) are 1.69 and 2.29, respectively. This confirms that the core density affects the perforation mechanisms and fracture behavior of the sandwich structures.

4.5. Conclusion

The main objective of this work was to study the impact response of three-layer sandwich structures with and without foam core based on HDPE and hemp. The influence of skin fiber content, skin thickness, and core density on the low-velocity impact response of the structures was investigated. The density of the core was controlled by the foaming agent content.

For all the sandwich panels (with or without a foam core) the Charpy impact strength depended on the skin fiber content and core density. As the density of the core decreased, the energy absorption properties and specific impact strength of the structures improved. It was reported that the specific impact of 30(1)-1.2-20(2) and 30(1)-0.6-20(2) were 60% and 40% higher than the specific impact strength of 30(1)-0-20(2). On the other hand, increasing the total fiber content in the structure lowered the Charpy impact strength; i.e. the materials are more brittle.

Based on the results obtained from falling weight impact tests, core type, skin thickness, and total fiber content controlled the deformation, peak load, and total absorbed energy. In all structures with different core density, increasing total fiber content increased the load peak, while it decreased the deflection and absorbed energy. On the other hand, decreasing core density decreased the peak load and total absorbed energy. The total absorbed energy of 10(1)-X-10(2) for 0.6, and 1.2% ACA compared to structure with 0% ACA core decreased by 34 and 40% respectively, while the peak load of the same sandwich structures with foam core were reported to be 45 and 105% lower than the peak load of 10(1)-0-10(2). Moreover, the results showed that the peak load of the structures was dependent on the load direction, skin thickness, and total fiber content.

Finally, relative absorbed energy was shown to depend on failure mechanisms which were governed by the sandwich structure configuration, core density, and skin type. As the core density increased the failure was more brittle and the failure

mode switched form core crushing to interlaminar debonding. Nevertheless, the results showed that a wide range of impact responses can be expected from three layer sandwich structures depending on their design.

Acknowledgements

The authors acknowledge the financial support of the Natural Sciences and Engineering Research Council of Canada (NSERC). The technical help of Mr. Yann Giroux was also much appreciated.

Chapter 5

General conclusions and recommendations

5.1. Conclusions

Recyclable and bio-based materials have caught the attention of many people all over the world due to concerns about environmental issues such as greenhouse gas emission. Hemp fiber is widely available in Canada as an agricultural by-product. This renewable fiber has good mechanical and physical properties that can be used to produce WPC. On the other hand, sandwich structures with foam core are becoming more popular due to their low weight, high strength and flexural modulus, leading to excellent specific properties (per unit weight).

In this work, the main objective was to prepare, characterize and study the influence of different design parameters on the performance of multi-layer sandwich structures with foam core, using HDPE as the matrix and hemp as reinforcement. Compression molding was used to prepare single layers as well as three-layer sandwich structures.

Since one of the main obstacles of WPC is low compatibility between the fibers and the polymer, the first step of this work was devoted to optimize MAPE content (coupling agent) to improve adhesion and stress transfer between the phases. The mechanical properties of HDPE composites with hemp fibers prepared by extrusion and compression molding showed that MAPE addition can substantially improve the tensile, flexural, torsion and impact properties of the composites. The results also showed that an optimum MAPE amount was around 9% wt. based on fiber content. For example, composites with 10% hemp and 9% wt. MAPE exhibited improved elongation at break (24%), tensile strength (53%) and impact strength (27%), compared to its uncompatibilized counterpart. These results were confirmed by SEM observation which clearly showed the low compatibility between hemp and HDPE and how this was changed as MAPE content increased. For the composite with 9% wt. MAPE, the surface of the fiber was completely wetted by the matrix and no voids, gaps or fiber pull-out was observed. For composites with MAPE content over 9% wt. showed lower mechanical properties because extra coupling agent molecules are not located at the fiber-matrix interface (saturation) and reside in the bulk polymer acting as plasticizers.

The effect of fiber content was also studied. While some mechanical properties such as modulus and strength were found to increase with fiber content, others properties such as elongation break and impact strength were significantly reduced by fiber addition. For example, the addition of 40% hemp fiber in the composite decreased the impact strength by 8%.

After optimization of the skin layers (HDPE-hemp-MAPE composites), the layers were assembled together to produce sandwich structures composed of a foamed/unfoamed core between two composite skins. By changing skin thickness (1 and 2 mm) and hemp content in the skin (0-40% wt.) and density of core via different blowing agent concentrations (0, 0.6, and 1.2% wt.) different sandwich structures were produced and characterized in terms of morphology, density and mechanical properties under flexural and impact loadings. Based on the results obtained, the following conclusions can be drawn:

SEM micrographs of the sandwich panels showed that the produced foam core had a closed-cell structure. Density was reduced by about 18% and 27% with increasing chemical blowing agent (ACA) content from 0.6 and 1.2%, as compared to the unfoamed HDPE matrix. As the foam density decreased, cell size increased from 156 to 387 μm, while cell density increased from 4.26 x 103 to 8.88×10^4 cells/cm^3. In all cases, SEM micrographs showed that good interlaminar adhesion between the skins and the cores were obtained.

For all sandwich panels, with or without a foam core, flexural modulus and strength were dependent on the skin fiber content and skin thickness. On the other hand, with increasing hemp content, the overall deformability of the structures was decreased. Based on the results obtained, the skin layers had more influence on the flexural properties compared to core properties, but the specific flexural strength was mainly controlled by the core density. The results showed that the specific flexural strength of structures with 0.6 and 1.2% ACA foam core were 21 and 36% higher than for an unfoamed one (0% ACA). Similarly, the specific flexural moduli were mainly controlled by core density. The addition of 0.6% or 1.2% ACA in the core improved the specific flexural modulus by 21 and 29% compared to structures without a foam core.

Also, the Charpy impact strength was dependent on the skin fiber content and core density. As an example, the impact strength of sample 20(1)-0-10(2) was 89 J/m compared to 76 J/m for sample 20(1)-0-40(2) which is a decrease of 10%.

As the density of the core and total fiber content decreased, the energy absorption properties and specific impact strength of the structures were improved. For instance, the specific impact of 30(1)-1.2-20(2) and 30(1)-0.6-20(2) were 128 and 112 $J.cm^3/m.g$ which are 60% and 40% higher respectively, than the specific impact strength of 30(1)-0-20(2) which is 81 $J.cm^3/m.g$.

From the results obtained via the falling weight impact test, the core type, skin thickness and total fiber content are controlling the deformation, peak load and total absorbed energy. The results showed that the peak load of the structure was dependent on the load direction, skin thickness, core density and structure total fiber content. For instance, increasing hemp content in both skins from 10% to 40%, for the structures without foam core increased the peak load about 27%, from 3518 to 4459 N. As the density of core decreases, the peak load and total absorbed energy reduces as well. For instance, the peak load of 40(1)-X-40(2) decreased from 4459 to 2196 and 2196 N for the structures with 0%, 0.6% and 1.2% ACA, respectively.

In all the structures with different core density, increasing total fiber content increased the load peak, decreased the deflection and absorbed energy. For example, the total absorbed energy of 10(1)-0-10(2) was 15.3 J which compared to 8.3 J for 40(1)-0-40(2) was about 84% higher.

Last but not least, it can be concluded that compression molding was a proper fabrication process for multi-layer sandwich structures with or without foam core.

5.2. Recommendations and future works

In this work, several types of characterization were used to determine the effect of different design parameters on the mechanical performance of multi-layer sandwich structures with and without foam core. Although particular attention was given to perform these tests, our understanding of these complex structures is still limited. To improve our knowledge, the following suggestions are given for future investigations:

The mechanical properties of the sandwich structures with foam core are dependent on several parameters such as the type of matrix and fiber, fiber size, foam morphology, blowing agent, coupling agent, production processing, number of layers, etc. Therefore, the effects of these parameters can be investigated precisely in future studies.

In our case, the produced sandwich structures were asymmetric; i.e. the skin thickness was not similar on both side. It would be interesting to produce symmetric structures, using a limited number of design variables to give more insight regarding the influence of these parameters on the mechanical behavior of sandwich structures.

It would be interesting to have higher degree of asymmetry to study the properties which are influencing the asymmetry ratio. For this, the use of different skins with different fiber size, polymer matrices, and type of fibers can increase the final mechanical properties of the composite structures.

More experiments with different blowing agent concentration should be carried out to determine the exact relationships between morphological parameters and mechanical properties.

Some models should be developed to predict the different mechanical properties of the sandwich structures in terms of core density, skins thickness, skin fiber content and core thickness. This would also be helpful to optimize the properties for specific applications like automotive, marine and construction applications.

References

[1] Bledzki AK, Gassan J. Composites reinforced with cellulose based fibres. Progress Polymer Science. 1999; 24: 221-274.

[2] Nwabunma D, Kyu T. Polyolefin Composites. New Jersey: John Wiley. 2007.

[3] Murphy J. The Reinforced Plastics Handbook. Kidlington, UK: Elsevier Advanced Technology; 1998.

[4] Arnold CA, Hergenrother PM, McGrath JE. An Overview of Organic Polymeric Matrix Resins for Composites. Composites: Chemical and Physicochemical Aspects, TL Vigo and BJ Kinzig, Eds. 1992: 3-30.

[5] Eckert C. Proceedings of the Fifth International Conference on Woodfiber-plastic Composites Proceedings No 7263, Forest Products Society. Madison, 1999.

[6] Mohanty AK, Misra M, Drzal LT. Natural fibers, biopolymers, and biocomposites: CRC Press. 2005.

[7] Rowell RM, Sanadi AR, Caulfield DF, et al. Utilization of natural fibers in plastic composites: problems and opportunities. in Lignocellulosic-Plastic Composites. 1997: 23-51.

[8] Bledzki A, Faruk O. Injection moulded microcellular wood fibre-polypropylene composites. Composites Part A: Applied Science and Manufacturing. 2006; 37: 1358-1367.

[9] Mechraoui A. Sandwich composite de mousses polymères. PhD Thesis; Université Laval. 2010.

[10] Mishra S, Mohanty AK, Drzal LT, et al. A review on pineapple leaf fibers, sisal fibers and their biocomposites. Macromolecular Materials and Engineering. 2004; 289: 955-974.

[11]http://www.jrs.eu/jrs_en/innovative-funktionen/uebersicht-funktionen-jrs-produkte/index.php

[12] Hon DNS. Chemical modification of lignocellulosic materials: CRC Press. 1995.

[13] Mwaikambo LY, Ansell MP. Chemical modification of hemp, sisal, jute, and kapok fibers by alkalization. Journal of Applied Polymer Science. 2002; 84: 2222-2234.

[14] Kim JK, Pal K. Recent advances in the processing of wood-plastic composites: Springer Science & Business Media. 2010.

[15] Pereira PHF, Rosa M, Cioffi MOH, et al. Vegetal fibers in polymeric composites: a review. Polímeros. 2015; 25: 9-22.

[16] Krässig HA. Cellulose: structure, accessibility and reactivity: Gordon and Breach Science. 1993.

[17] Edeerozey AMM, Akil HM, Azhar AB, et al. Chemical modification of kenaf fibers. Materials Letters. 2007; 61: 2023-2025.

[18] Pracella M, Chionna D, Anguillesi I, et al. Functionalization, compatibilization and properties of polypropylene composites with hemp fibres. Composites Science and Technology. 2006; 66: 2218-2230.

[19] Dhakal H, Zhang Z, Richardson M. Effect of water absorption on the mechanical properties of hemp fibre reinforced unsaturated polyester composites. Composites Science and Technology. 2007; 67: 1674-1683.

[20] Karmaker AC. Effect of water absorption on dimensional stability and impact energy of jute fibre reinforced polypropylene. Journal of Materials Science Letters. 1997; 16: 462-464.

[21] Mukhopadhyay S, Fangueiro R. Physical modification of natural fibers and thermoplastic films for composites-a review. Journal of Thermoplastic Composite Materials. 2009; 22: 135-162.

[22] Jacob M, Joseph S, Pothan LA, et al. A study of advances in characterization of interfaces and fiber surfaces in lignocellulosic fiber-reinforced composites. Composite Interfaces. 2005; 12: 95-124.

[23] Li X, Tabil LG, Panigrahi S. Chemical treatments of natural fiber for use in natural fiber-reinforced composites: a review. Journal of Polymers and the Environment. 2007; 15: 25-33.

[24] Ahad NA, Parimin N, Mahmed N, et al. Effect of chemical treatment on the surface of natural fiber. Journal of Nuclear and Related Technologies. 2009; 6: 155-158.

[25] Nevell TP, Zeronian SH. Cellulose chemistry and its applications. Chichester: Ellis Horwood Ltd. 1985.

[26] Prasad SV, Pavithran C, Pohatgi PK. Alkali treatment of coir fibres for coir-polyester composites. Material Science. 1983; 18: 1443-1454.

[27] Suardana NPG, Piao Y, Lim JK. Mechanical properties of hemp fibers and hemp/pp composites: effects of chemical surface treatment. Materials Physics and Mechanics. 2011; 11: 1-8.

[28] Baiardo M, Frisoni G, Scandola M, et al. Surface chemical modification of natural cellulose fibers. Journal of Applied Polymer Science. 2002; 83: 38-45.

[29] Zadorecki P, Rönnhult T. An ESCA study of chemical reactions on the surfaces of cellulose fibers. Journal of Polymer Science Part A: Polymer Chemistry. 1986; 24: 737-745.

[30] Zadorecki P, Flodin P. Surface modification of cellulose fibers III. Durability of cellulose–polyester composites under environmental aging. Journal of Applied Polymer Science. 1986; 31: 1699-1707.

[31] Albano C, Gonzalez J, Ichazo M, et al. Thermal stability of blends of polyolefins and sisal fiber. Polymer Degradation and Stability. 1999; 66: 179-190.

[32] Maldas D, Kokta BV, Daneault C. Influence of coupling agents and treatments on the mechanical properties of cellulose fiber-polystyrene composites. Journal of Applied Polymer Science. 1989; 37: 751-775.

[33] Abdelmouleh M, Boufi S, Belgacem M, et al. Short natural-fibre reinforced polyethylene and natural rubber composites: Effect of silane coupling agents and fibres loading. Composites Science and Technology. 2007; 67: 1627-1639.

[34] Abdelmouleh M, Boufi S, Belgacem MN, et al. Modification of cellulose fibers with functionalized silanes: Effect of the fiber treatment on the mechanical performances of cellulose-thermoset composites. Journal of Applied Polymer Science. 2005; 98: 974-984.

[35] Valadez-Gonzalez A, Cervantes JM, Olayo R, et al. Chemical modification of henequen fibers with an organosilane coupling agent. Composites Part B: Engineering. 1999; 30: 321-331.

[36] Doan TTL. Investigation on jute fibres and their composites based on polypropylene and epoxy matrices. PhD Thesis, TU Dresden. 2006.

[37] Lu JZ, Wu Q, Negulescu I. Wood-Fiber/High-Density-Polyethylene Composites: Coupling Agent Performance. Journal of Applied Polymer Science. 2005; 96: 93-102.

[38] Anon. Silane coupling agents. Dow Corning Corporation FN.

[39] Lee LJ, Zeng C, Cao X, et al. Polymer nanocomposite foams. Composites Science and Technology. 2005; 65: 2344-2363.

[40] Lee ST, Ramesh NS. Polymeric foams: mechanisms and materials: CRC press; 2004.

[41] Gendron R. Thermoplastic foam processing: principles and development: CRC press; 2004.

[42] Chen Y, Das R, Battley M. Effects of cell size and cell wall thickness variations on the stiffness of closed-cell foams. International Journal of Solids and Structures. 2015; 52: 150-164.

[43] Martini-Vvedensky JE, Suh NP, Waldman FA. Microcellular closed cell foams and their method of manufacture. US Patents, 4473665, 1984.

[44] Shutov FA. Syntactic polymer foams. Chromatography/Foams/Copolymers. Heidelberg: Springer. 63-123, 1986.

[45] Barzegari MR, Rodrigue D. The effect of injection molding conditions on the morphology of polymer structural foams. Polymer Engineering and Science. 2009; 49: 949-959.

[46] Klempner D, Sendijarevic V. Polymeric foams and foam technology. 2nd ed. Munich: Hanser. 2004.

[47] Verdu J, Zoller A, Marcilla A. Plastisol foaming process. Decomposition of the foaming agent, polymer behavior in the corresponding temperature range and resulting foam properties. Polymer Engineering and Science. 2013; 53: 1712-1718.

[48] Landrock AH. Handbook of plastic foams: types, properties, manufacture and applications: Elsevier; 1995.

[49] Tissandier C, Gonzalez-Nunez R, Rodrigue D. Asymmetric microcellular composites: Mechanical properties and modulus prediction. Journal of Cellular Plastics. accepted, 2015.

[50] Ramesh NS, Malwitz N. Bubble Growth Dynamics in Olefinic Foams. Polymeric Foams. 1997; 669: 206-213.

[51] Yao J. Density graded LMDPE foams produced under a temperature gradient: Morphology and properties. MSc thesis, Laval University. 2011.

[52] Park CB, Cheung LK. A study of cell nucleation in the extrusion of polypropylene foams. Polymer Engineering and Science. 1997; 37: 1-10.

[53] Daniel IM, Gdoutos EE, Wang KA, et al. Failure Modes of Composite Sandwich Beams. International Journal of Damage Mechanics. 2002; 11: 309-334.

[54] Mostafa A, Shankar K, Morozov EV. Insight into the shear behaviour of composite sandwich panels with foam core. Materials and Design. 2013; 50: 92-101.

[55] Cantwell WJ, Morton J. The impact resistance of composite materials - a review. Composites. 1991; 22: 347-362.

[56] Salomi A, Greco A, Pacifico T, et al. Processing and Properties of a Polymer/Composite Double-Layer Laminate. Advances in Polymer Technology. 2013; 32: 32-43.

[57] Altenbach H. Theories for laminated and sandwich plates. Mechanics of Composite Materials. 1998; 34: 243-252.

[58] Rizov V. Elastic-plastic response of structural foams subjected to localized static loads. Materials and Design. 2006; 27: 947-954.

[59] Lakreb N, Bezzazi B, Pereira H. Mechanical behavior of multilayered sandwich panels of wood veneer and a core of cork agglomerates. Materials and Design. 2015; 65: 627-636.

[60] Smith D, Partridge PG. Flexural stiffness envelopes for planar multilayered systems containing two dissimilar materials, Proceedings of the Institution of Mechanical Engineers. 1999; 213: 1-19.

[61] Gdoutos EE, Daniel IM, Wang KA, et al. Nonlinear behavior of composite sandwich beams in three-point bending. Experimental Mechanics. 2001; 41: 182-189.

[62] Dyer SR, Lassila LVJ, Jokinen M, et al. Effect of cross-sectional design on the modulus of elasticity and toughness of fiber-reinforced composite materials. The Journal of Prosthetic Dentistry. 2005; 94: 219-226.

[63] Mechraoui A, Riedl B, Rodrigue D. Mechanical properties of polypropylene structural foams with fiber-reinforced skins. Journal of Cellular Plastics. 2011; 47: 115-32.

[64] Kazemi Y, Cloutier A, Rodrigue D. Design analysis of three-layered structural composites based on post-consumer recycled plastics and wood residues. Composites Part A: Applied Science and Manufacturing. 2013; 53: 1-9.

[65] Theulen J, Peijs A. Optimization of the bending stiffness and strength of composite sandwich panels. Composite Structures. 1991; 17: 87-92.

[66] Wang J, Waas AM, Wang H. Experimental and numerical study on the low-velocity impact behavior of foam-core sandwich panels. Composite Structures. 2013; 96: 298-311.

[67] Rizov V. Low velocity localized impact study of cellular foams. Materials and Design. 2007; 28: 2632-2640.

[68] Mines RAW, Worrall CM, Gibson AG. Low velocity perforation behaviour of polymer composite sandwich panels. International Journal of Impact Engineering. 1998; 21: 855-879.

[69] Zabihzadeh M, Dastoorian F, Ebrahimi G. Effect of MAPE on Mechanical and Morphological Properties of Wheat Straw/HDPE Injection Molded Composites. Journal of Reinforced Plastics and Composites. 2008; 29: 123-131.

[70] Raj RG, Kokta BV. Improving the mechanical properties of HDPE-wood fiber composites with additives/coupling agents. ANTEC Proc. 49th Annual Technical Conference. 1883-1885, 1991.

[71] Woodhams RT, Thomas G, Rodgers DK. Wood fibers as reinforcing fillers for polyolefins. Polymer Engineering and Science. 1984; 24: 1166-1171.

[72] Kokta BV, Maldas D, Daneault C, et al. Composites of Polyvinyl Chloride-Wood Fibers. I. Effect of Isocyanate as a Bonding Agent. Polymer-Plastics Technology and Engineering. 1990; 29: 87-118.

[73] Snijder MHB, Bos HL. Reinforcement of polypropylene by annual plant fibers: optimisation of the coupling agent efficiency. Composite Interfaces. 2000; 7: 69-75.

[74] Adhikary KB, Pang S, Staiger MP. Dimensional stability and mechanical behaviour of wood-plastic composites based on recycled and virgin high-density polyethylene (HDPE). Composites Part B: Engineering. 2008; 39: 807-815.

[75] Catto AL, Stefani BV, Ribeiro VF, et al. Influence of coupling agent in compatibility of post-consumer HDPE in thermoplastic composites reinforced with Eucalyprus fiber. Materials Research. 2014; 17: 203-209.

[76] Keener TJ, Stuart RK, Brown TK. Maleated coupling agents for natural fiber composites. Composites Part A: Applied Science and Manufacturing. 2004; 35: 357-362.

[77] Zabihzadeh M, Dastoorian F, Ebrahimi G. Effect of MAPE on mechanical and morphological properties of wheat straw/HDPE injection molded composites. Journal of Reinforced Plastics and Composites. 2008; 29: 123-131.

[78] Rana AK, Mandal A, Bandyopadhyay S. Short jute fiber reinforced polypropylene composites: effect of compatibiliser, impact modifier and fiber loading. Composites Science and Technology. 2003; 63: 801-806.

[79] Hedenberg P, Gatenholm P. Conversion of plastic/cellulose waste into composites. I. Model of the interphase. Journal of Applied Polymer Science. 1995; 56: 641-651.

[80] Sanadi AR, Caulfield DF, Jacobson RE. Agro-fiber thermoplastic composites. Paper and composites from agro-based resources. Florida: CRC Press; 1997.

[81] Leu SY, Yang TH, Lo SF, et al. Optimized material composition to improve the physical and mechanical properties of extruded wood-plastic composites (WPCs). Construction and Building Materials. 2012; 29: 120-127.

[82] Kazemi Y, Cloutier A, Rodrigue D. Mechanical and morphological properties of wood plastic composites based on municipal plastic waste. Polymer Composites. 2013; 34: 487-493.

[83] Mechraoui A, Riedl B, Rodrigue D. The effect of fibre and coupling agent content on the mechanical properties of hemp polypropylene composites. Composite Interfaces. 2007; 14: 837-848.

[84] Fan M. Characterization and performance of elementary hemp fibres: factors influencing tensile strength. Bioresources. 2010; 5: 2307-2322.

[85] Jayaraman K, Bhattacharyya D. Mechanical performance of woodfibre-waste plastic composite materials. Resources, Conservation and Recycling. 2004; 41: 307-319.

[86] Kumar V, Soragaon B. Fabrication and evaluation of multilayered polyurethane foam core sandwich panels for static flexural stiffness. Procedia Engineering. 2014; 97: 1227-1236.

[87] Dai H, Hah T. Flexural behavior of sandwich beams fabricated by vacuum-assisted resin transfer molding. Composite Structures. 2003; 61: 247-253

[88] Zenkert D, Burman M. Tension, compression and shear fatigue of a closed cell polymer foam. Composite Science and Technology. 2009; 69: 785-792.

[89] Ashby L, Ashby M. Cellular Solids: Structure and Properties. 2nd ed. Oxford: Cambridge University Press. 1997.

[90] Petras A, Sutcliffe MPF. Failure mode maps for honeycomb sandwich panels. Composite Structures. 1999; 44: 237-252.

[91] He M, Hu W. A study on composite honeycomb sandwich panel structure. Materials and Design. 2008; 29: 709-713.

[92] Yazicia M, Wrightb J, Bertinb D, et al. Experimental and numerical study of foam filled corrugated core steel sandwich structures subjected to blast loading. Composite Structures. 2014; 110: 98-109.

[93] Manalo AC, Aravinthan T, Karunasena W, et al. Flexural behaviour of structural fibre composite sandwich beams in flatwise and edgewise positions. Composite Structures. 2010; 92: 984-995.

[94] IM D, Abot JL. Fabrication, testing and analysis of composite sandwich beams. Composite Science and Technology. 2000; 60: 2455-2463.

[95] Fam A, Sharaf T. Flexural performance of sandwich panels comprising polyurethane core and GFRP skins and ribs of various configurations. Composite Structures. 2010; 92: 2927-2935.

[96] Sharaf T, Shawkat W, Fam A. Structural performance of sandwich wall panels with different foam core densities in one-way bending. Journal of Composite Materials. 2010; 44: 2249-2263.

[97] Styles M, Compston P, Kalyanasundaram S. The effect of core thickness on the flexural behaviour of aluminium foam sandwich structures. Composite Structures. 2007; 80: 532-538.

[98] Kumar V, Suh NP. A process for making microcellular thermoplastic parts. Polymer Engineering and Science. 1990; 30: 1323-1329.

[99] Kumar V, Weller J. Production of microcellular polycarbonate using carbon dioxide for bubble nucleation. Journal of Engineering for Industry. 1994; 116: 413-420.

[100] Gosselin R, Rodrigue D. Cell morphology analysis of high density polymer foams. Polymer Testing. 2005; 24: 1027-1035.

[101] Kabir MdE, Saha MC, Jeelani S. Tensile and fracture behavior of polymer foams. Journal of Materials Science and Engineering: A. 2006; 429: 225-235.

[102] Rizov V, Shipsha A, Zenkert D. Indentation study of foam core sandwich composite panels. Composite Structures. 2005; 69: 95-102.

[103] Barzegari MR, Rodrigue D. Flexural behavior of asymmetric structural foams. Journal of Applied Polymer Science. 2009; 113: 3103-3112.

[104] Tissandier C, Vazquez Fletes RC, González-Núñez R, et al. Microcellular agave fibre-high density polyethylene composites produced by injection molding. Journal of Materials and Science Engineering: A. 2012; 11: 662-677.

[105] Zhang J, Ashby M. Mechanical selection of foams and honeycombs used for packaging and energy absorption. Journal of Materials Science 1994; 29: 157-163.

[106] Foo C, Seah L, Chai G. Low-velocity impact failure of aluminium honeycomb sandwich panels. Composite Structures. 2007; 85: 20-28.

[107] Shim V, Yap K. Static and impact crushing of layered foam-plate systems. International Journal of Mechanical Sciences. 1997; 39: 69-86.

[108] Bhuiyan A, Hosur M, Jeelani S. Low-velocity impact response of sandwich composites with nanophased foam core and biaxial ±45 braided face sheets. Composites Part B: Engineering. 2009; 40: 561-571.

[109] Wang B, Yang M. Damping of honeycomb sandwich beams. Journal of Materials Processing Technology. 2000; 105: 67-72.

[110] Tan C, Akil H. Impact response of fiber metal laminate sandwich composite structure with polypropylene honeycomb core. Composites Part B: Engineering. 2012; 43: 1433-1438.

[111] Wanga J, Waas A, Wang H. Experimental and numerical study on the low-velocity impact behavior of foam-core sandwich panels. Composite Structures. 2013; 96: 298-311.

[112] Abrate S. Impact on composite structures: Cambridge University Press. 1998.

[113] Anderson T, Madenci E. Experimental investigation of low-velocity impact characteristics of sandwich composites. Composite Structures. 2000; 50: 239-247.

[114] Park J, Ha S, Kang K, et al. Impact damage resistance of sandwich structure subjected to low velocity impact. Journal of Materials Processing Technology. 2008; 201: 425-430.

[115] Mines P, Worrall C, Gibson A. Low velocity performation behaviour of polymer composite sandwich panels. International Journal of Impact Engineering. 1990; 32: 855-879.

[116] Bernard ML, Lagace PA. Impact resistance of composite sandwich plates. Journal of Reinforced Plastics and Composites. 1989; 8: 432-445.

[117] Shih WK, Jang BZ. Instrumented impact testing of composite sandwich panels. Journal of Reinforced Plastics & Composites. 1989; 8: 270-298.

[118] Zhou G, Hill M. Investigation of parameters governing the damage and energy absorption characteristics of honeycomb sandwich panels. Sandwich Structures. 2007; 9: 309-342.

[119] Hazizan M, Cantwell WJ. The low velocity impact response of foam-based sandwich structures. Composites Part B: Engineering. 2002; 33: 193-204.

[120] Lee LJ, Zeng C, Cao X, et al. Dynamic response of composite sandwich plate impacted by a rigid ball. Journal of Composite Materials. 1993; 27: 1238-1256.

[121] Zhang G, Wang B, Ma L, et al. Energy absorption and low velocity impact response of polyurethane foam filled pyramidal lattice core sandwich panels. Composite Structures. 2014; 108: 304-310.

[122] Mohan K, Yip TH, Idapalapati S, et al. Impact response of aluminum foam core sandwich structures. Material Science and Engineering: A. 2011; 529: 94-101.

[123] Kazemi Y, Cloutier A, Rodrigue D. Design analysis of three-layered structural composites based on post-consumer recycled plastics and wood residues. Composites Part A: Applied Science and Manufacturing. 2013; 53: 1-9.

[124] Kavianiboroujeni A, Cloutier A, Rodrigue D. Mechanical characterization of asymmetric HDPE/hemp composite sandwich panels with and without a foam core, Journal of Sandwich Structures and Materials. in press, 2015.

[125] Doroudiani S, Park CB, Kortschot MT. Processing and characterization of microcellilar foamed High-Density Polyethylene/Isotactic Polypropylene Blends. Polymer Engineering and Science. 1998; 38: 1205-1215.

[126] Jayaraman K, Bhattacharyya D. Mechanical performance of woodfibre-waste plastic composite materials. Resources, Conservation and Recycling. 2004; 41: 307-319.

[127] Atas C, Liu D. Impact response of woven composites with small weaving angles. International Journal of Impact Engineering. 2008; 35: 80-97.

[128] Evci C, Gülgeç M. An experimental investgation on the impact response of composite materials. International Journal of Impact Engineering. 2012; 43: 40-51.

[129] Shyr TW, Pan YH. Impact resistance and damage characteristics of composite laminates. Composite Structures. 2003; 62: 193-203.

[130] Belingardi G, Vadori R. Low velocity impact tests of laminate glass-fiber-epoxy matrix compoosite material plates. International Journal of Impact Engineering. 2001; 27: 213-229.

[131] Davies G, Zhang X. Impact damage prediction in carbon composite structures. Composite Structures. 1994; 16: 149-170.

[132] Tovar-Cisneros C, González-Núñez R, Rodrigue D. Effect of mold temperature on morphology and mechanical properties of injection molded HDPE structural foams. Journal of Cellular Plastics. 2008; 44: 223-237.

[133] Zhou J, Zaki Hassan M, Guan ZW, et al. The low velocity impact response of foam-based sandwich panels. Composites Science and Technology. 2012; 72: 1781-1790.

[134] Throne JL, Progelhof RC, Kumar S. Closed-Cell Foam Behavior Under Dynamic Loading-III. Impact Loading of High Density Foams. Journal of Cellular Plastics. 1985; 21: 123-140.

[135] Hitchen SA, Kemp RMJ. The effect of stacking sequence on impact damage in a carbon fiber/epoxy composite. Composites. 1995; 26: 207-214.

[136] Hosur MV, Mohammed AA, Zainuddin Z, et al. Impact performance of nanophased foam core sandwich composites. Materials Science and Engineering: A. 2008; 498: 100-109.